Central University of Technology, Free State

Image Learning and Correction as a Means of Evaluating and Fault-Finding Computed Tomography Scanner Image Artefacts

Benganga Joe-Herve Bonkondo

Dissertation submitted in fulfilment of the requirements for the Degree.

Master of Engineering in Electrical Engineering

in the

Department of Electrical, Electronic and Computer Engineering

of the

Faculty of Engineering, Built Environment and

Information Technology

at the

Central University of Technology, Free State

Supervisor: Prof. B Kotze: Doctor of Technologiae: Engineering: Electrical

Bloemfontein

2024

Declaration

I, Joe-Herve Bonkondo Benganga, with student number ######### and identity number **#############**, do hereby declare that this research project which has been submitted to the Central University of Technology, Free State, for the degree Master of Engineering in Electrical Engineering, is my independent work and complies with the code of academic integrity as well as the other relevant policies, procedures, rules and regulations of the Central University of Technology, Free State, and has not yet been submitted before by any person in fulfilment of the requirement of any qualification.

JHB BENGANGA:……

Date: …November 2023

Dedication

I would like to dedicate this to my daughter Mohau B. Modingwane. The most beautiful being alive. I'd like to also dedicate this to the people who got me started and who continuously motivated me: my mom, Dr K. Nabangaba, and my dad, Dr B.A. Benganga.

Lastly, this paper is dedicated to all the technicians working in the field who want to make a difference in their surroundings and work conditions.

GLORY TO YOU AND YOUR HOUSE!!!

Acknowledgements

I'm grateful to Almighty God for affording me the opportunity to study. I am sincerely grateful and would like to thank my supervisor, and mentor, Prof. Ben Kotze, who supported me during this arduous course. Prof. Kotze`s support was without a doubt crucial and invaluable in my dedication to this research study.

Sincere acknowledgement to Dr Tshepo Kukuni and Mr Lepekola Lenkoe, for their technical advice, encouragement, time, and efforts to ensure that I did not lose sight during this journey. Furthermore, I would like to send my words of gratitude to Rea Thusa Consulting Engineers (PTY) LTD for support with the utilisation of their software and the technical advice provided.

Abstract

The concept of image reconstruction modelling in both industry and academia has led to the investigation of different artefacts found in the medical fraternity. This concept is aimed at optimising the efficiency of fault-finding in the CT scanner to automatically identify artefacts without any human intervention. It is for such reasons that an automated artefact detection model based on machine learning and vision needs to be investigated, developed, and implemented to evaluate the feasibility and reliability of such a system in a live environment setup for service engineers and specialists alike. During the image acquisition process, images were taken from Toshiba medical equipment for image processing and machine learning purposes. The data collected contain a total of 170 images namely Dataset_1 with each subset dataset comprising 85 ring and 85 metal artefact images for data testing with 19 iterations. Additionally, a subset image dataset comprised of a total of 88 image dataset namely Dataset_2 with each subset dataset having 44 ring and 44 metal artefact images. This was conceptualised in this format for validation of the model results. The iteration determinant was the prerogative of the research based on the satisfactory output results. Training of the model was created utilising Keras to allow the model to learn by identifying the different features of the image.

The first test was to observe the data accuracy in terms of artefact detection and the second test was based on the overall system accuracy based on different epochs and image dataset sizes. The first model was based on a fixed 50-epoch test. The results demonstrate that the more the input dataset, the higher the accuracy with more than 90% accuracy reading. However, to prove the robustness of the model technically and scientifically, the epoch and iteration change were necessary. Subsequently, the model data loss demonstrates that the lesser the input data within the model, the higher the chances for data loss at more than 80%. The more tests and trains were conducted the lesser the data loss at below 20% for 50 epochs tests. Model two demonstrated that for 25 epochs tests based on 170 input image datasets, the test results are 87% accurate with 49% data loss from 89% accuracy and 21% data loss observed during the training phase. Subsequently, for 50 epoch tests, the results demonstrate 91% accuracy with 15% data loss, compared to 94% accuracy and 21%

loss. These results thus demonstrate the feasibility of the development of an artefact-based recognition model. Furthermore, the model based on the results was able to accurately differentiate between the metal and ring artefact without any human intervention.

Transfer learning was applied using three models namely the VGG16, Resnet50 and Inception_V3 algorithms. The results demonstrate the high loss of data on the transfer learning as opposed to the Custom CNN model. The models were then evaluated based on their efficiency and accuracy threshold, and the results demonstrate that transfer learning has higher accuracy than the custom CNN model as a result of the application of the custom CNN on an already-trained model and utilisation of that result dataset to the three evaluated transfer learning algorithms.

This research study`s primary focus was to investigate the feasibility of developing an intelligent model with the capability for automatic artefact detection and the ability to distinguish the investigated artefacts. Post the development and test stage of the initial model, an alternative model based on transfer learning was modelled using VGG16 algorithm. The results demonstrate that these models are both sustainable and reliable.

In Addition, two more models were evaluated against the two sets of “primary algorithms” namely the custom CNN model and VGG16 algorithms. The Inception_v3 and ResNet50 algorithms were added to the set of algorithms with the primary aim of comparing the results against the custom CNN and the VGG16 model. It is therefore seen that VGG16 performs better on the data accuracy aspect, where the dataset can be recognised at a higher percentage by the VGG16 model on both the test and train models as compared to the other three tested and trained models. In retrospect, the ResNet50 algorithm performs the lowest when it comes to the losses experienced by the model against the other three models.

Therefore, this study concludes that the medical fraternity must invest in the advancements of automated artefact detection models utilising this research study as a base reference model based on the results output. The results presented in this research study thus demonstrate the robustness of the model and minimal differentiation in the results outputs between two developed models of less than 2% on the 88-image and 170-image datasets.

Central University of Technology, Free State

List of Figures

List of Tables

Acronyms & Abbreviations

IP – Image Processing

CT – Computed Tomography

MIS – Medical Imaging System

MRI - Magnetic Resonance Imaging

CAD – Computer Aided Diagnosis

ML – Machine Learning

MV – Machine Vision

OpenCV – Open-Source Computer Vision Library

mA – milli Amp

mAs – milli Amps

kV – kilovolt

kVp – kilovolt peak

HU – Hounsfield Unit

SNR – Signal-to-Noise Ratio

Keywords

Artefact.

Image processing.

CT scanner.

Fault finding.

Machine Learning.

Artificial Intelligence.

Metal artefact.

Ring artefact.

Table of contents

CHAPTER I: Introductory overview of CT scanners

This chapter presents the overview of the research problem, aim, methodology, and study hypothesis. This chapter also presents the layout outlining the dissertation`s chapters detailing the expectations of the work to be done in each chapter.

1.1. Introduction.

Medical Imaging Systems (MIS) have become one of the most impressive research areas in medicine as well as the computer vision fraternity. Medical Imaging is defined as a process of concentrating captured images for diagnostic and evaluation purposes and a tool for learning about neurobiology and human behaviours [1]. Medical imaging system modalities include scanners, Magnetic Resonance Imaging (MRI) scanners, Virtual Surgical Planning (VSP) systems, and Optical Coherence Tomography (OCT) amongst a wider range of equipment used to assess the conditions of organs or tissue and monitor a patient over time for diagnostic and treatment procedures [2]. Furthermore, MIS comprises several techniques; however, every technique has different risks and benefits.

Computed tomography (CT) and MRI scanners are dominant in medical imaging because of their high resolution, good signal-to-noise ratio, and manipulation properties. Over the last almost 30 years, scanner image quality has increased considerably, with the introduction of multi-slice scanners and improved reconstruction techniques [3].

The major dominance of medical imaging systems is the visualisation aspect with the ability to detail the image data analysis and exploration for research applications.

The main application areas for medical imaging systems are highlighted but not limited to the following:

- Diagnosis.
- Treatment planning.

- Intraoperative support: 3D data-based software used in surgical rooms from preoperatively acquired images to assist surgeons during operations.
- Documentation: Reporting and other documentation tasks benefit from the incorporation of representative visualisations with labels and measurements to provide information to interpret and evaluate images.
- Educational purposes: Research reconstruction techniques and image processing algorithms to develop faster and more reliable systems for interventions on treatments.

Additionally, this research study aims at recognising different types of artefacts on the CT scanner. The automated process model for the artefact recognition and identification is presented. As a result, the CT scanner is denoted as an artificial feature that appears on the CT image [4]. Furthermore, the developments of medical imaging systems can be enhanced by utilising Artificial Intelligence (AI) algorithms and protocols. In the broader sense, AI has the potential to provide multiple industries (especially electromedical and biomedical engineering) with intelligence and prediction for future and current systems. However, this depends on image processing with “visual aid” and as a result, increases the confidence in accepting computer-aided cued results for later evaluation and analysis [5].

This research study further focuses on the artefact detection based on the CNN algorithm. The design features and the scanner-based artefacts resulting from imperfections in a scanner function will be presented [6]. Subsequently, the performance of Artificial Intelligence (AI) in medical imaging systems depends on many factors, some of which are mentioned as follows:

- Optimisation of the modality equipment, i.e. systems calibration and maintenance.
- Feature selection.
- Reference database.
- Computational efficiency.
- Relationship between industrial relevance and technical results.

AI in medical imaging systems uses machine-learning algorithms to mimic the human visual ability to perform analysis, presentation, and comprehension of complex medical data. These algorithms are in turn responsible for approximating results, based on extensive amounts of input data from a specialist. Well-defined algorithms to recognise patterns, behaviours and deep learning are used in an AI system to gather data, process it, and produce acceptable output.

Furthermore, machine learning is studied and researched within the radiology field to detect and diagnose diseases found in patients using CT and MRI images. In the years, the use of machine learning in radiology has increased. As a result, there are many opportunities and challenges for the imaging community, including the development of a common nomenclature, better ways to share image data, and standards for validating AI program use across different imaging platforms and patient populations [7]. Furthermore, the manufacturers are developing systems that can provide a trainable machine learning platform for specialists to assist in detecting a wide range of abnormalities in patients and monitoring change over time [8].

It is for such reasons that this research study will be focusing on image learning and correction measures for CT scanner image artefacts. By considering the above-mentioned factors, the benefits of this research study extend the use of Computer-Aided Design (CAD) systems, not just for detecting or tracing diseases and the like, but to assist in identifying, evaluating, and rectifying the image distortions and technical faults.

1.2. Problem Statement.

In recent years, medical imaging systems have greatly advanced in image reconstruction techniques, image restoration, and equipment evaluation. These advancements in technology have opened the playing field for further research and development in the medical research environment and have created a platform for knowledge sharing and testing. These changes have made it easier to access and learn about the concept and rectification models for image distortions currently being used in an industrial setup.

In most cases, there are standard troubleshooting procedures on how to overcome image artefacts before moving into detailed investigations and evaluation techniques. However, troubleshooting may still yield negative results, and this may be due to the evaluation or fault-finding technique/process since the troubleshooting exercise is manufacturer-specific. The said fault-finding techniques can be time-consuming and costly, which in turn is a setback for radiographers, doctors, and even patients.

1.2.1. Research question.

The investigation of a process application and recognition of artefacts without human intervention is worth investigating to optimise processes and save diagnostic time. The following research questions were set:

- Is it feasible to investigate, develop and implement an artefact-based recognition model? The feasibility in the context of this research seeks to investigate the possibility of the development of such a system “Artefact detection model”.
- Is it possible to investigate the feasibility of the comparison of the custom artefact detection model against models based on pre-trained networks with suitable transfer learning?

1.3. Objectives of study.

This research dissertation aims to investigate and develop a model prototype that can be used to identify and predict a possible solution to a 2D image representation of a CT scanner with and without artefacts.

The research design should meet the following objectives:

- Development of a custom identification artefact detection model.
- Development of an artefact detection model based on transfer learning.
- Analyse the custom artefact detection model against the transfer learning models.

In addressing these objectives, an AI artefact identifier and differentiator model was developed in Chapter III section 3.4. The results of this developed model are presented in Chapter IV.

1.4. Proposed research methodology and model design.

The process of artefact detection and image restoration in this research study will be making use of machine learning and machine vision algorithms. The custom CNN will undergo the following process:

- Image capture – The researcher will capture 50 images (the prerogative of the researcher) from the Toshiba CT scanner and place them inside a folder.
- OpenCV library will be for machine vision, and as a result, the image dataset will be filtered utilising optimised OpenCV algorithms.
- Upon filtering the dataset, the filtered and optimised dataset will be placed inside Tensorflow™ software where the machine learning process will commence.
- Once the application has been trained on the different types of artefacts (ring and metal) an unknown dataset will be entered into the system and the system will be evaluated to test if it can automatically detect the artefact and provide a possible solution for image restoration.

1.5. Limitations of this research study.

The major limitations of this research study are as follows:

- Live human patients (test subjects) were not used in the experiment due to the Personal Information Protection Act (POPIA); it is pivotal that the patient information is protected and no request to conduct such a research study was done.
- Live human patients (test subjects) were not used because one of the challenges was to avoid exposing patients to unplanned radiation exposure/dosage. The test equipment used for this experiment was the (TOS phantom).

1.6. Expected results.

- Computed tomography (CT) scanner knowledge.
- Development of an automated artefact identification model technique.
- Conference papers.
- Master's dissertation and qualification.

1.7. Hypothesis.

By making use of machine learning and machine vision applications, an automated model should be built for artefact detection and prediction of possible solutions. This model will assist in reducing the time it takes the health practitioners to identify the artefact and provide a possible solution, as this will be automatically done by the system.

1.8. Publication and presentations conducted during the study.

- J.H.B. Benganga, B. Kotze. 2022. "Image Learning and Correction as a Means of Evaluation and Fault-Finding Computer Scanner Image Artefact". International Conference on Business Management Environment and Social Science (BMESS 2022), March 2022, Bath Spa University, Academic Rak Khaimah, United Arab Emirates.
- J.H.B. Benganga, B. Kotze, T.G. Kukuni. 2022. "Application of Machine Learning for Image Artefact on Detection Based on Computed tomography Scanner". 8th International Conference on Green Computing and Engineering Technologies (ICGCET), 22-23 September 2022, Port-Louis, Mauritius.

1.9. Dissertation outline.

This research study has been organised into five different chapters, consisting of an introductory chapter (Chapter 1), literature chapter (Chapter 2), methodology chapter (Chapter 3), results chapter (Chapter 4), and finally the conclusion and future works chapter (Chapter 5).

Chapter I presents the introduction and underline the problem statement, study objectives, methodology and hypothesis for the research conducted.

Chapter II presents the different techniques relating to image processing and machine learning and their shortcomings and developments relating to artefact evaluation and identification. Furthermore, this chapter outlines the work done around this subject and ways in which the current studies can be improved.

Chapter III presents the modelling and development technique for artefact detection and artefact solution prediction. In this chapter, the image capturing process for the CT scanned image, the image processing technique, model training using machine learning techniques incorporated with the image restoration database are outlined.

Chapter IV presents the results obtained from Chapter III. Furthermore, this chapter discusses the results analysis, and evaluates the feasibility of the designed model.

Chapter V presents the research conclusion and findings with prospects for future research.

CHAPTER II: Modern CT scanner applications and data acquisition techniques.

Chapter II presents reviews on the theoretical and industrial application of the current 3rd and 4th generation (GEN) CT scans. The image processing, reconstruction models, image quality, and artefacts history are also outlined. The basic CT scanners, image presentation, and the methods used for removing artefacts in CT scan images, their types, causes, evaluation techniques, and solutions used in a medical environment setup are discussed.

This chapter will also cover the methods and techniques used to detect "abnormalities" experienced in a medical imaging system that includes methods such as the proposed methodology outlined in this research study.

2.1. Introduction: Medical technology overview.

A Computed tomography (CT) scanner is a medical imaging technique that uses computer-processed combinations of multiple measurements taken from different angles to produce images of a body, allowing radiologists and radiographers to see inside the body without cutting it [30, pp. 5 - 21]. In resonance, with the past century of technology, CT scanners have made great strides in their contribution towards medical innovative designs - including, but not limited to Magnetic Resonance Imaging (MRI). As a result in terms of the comparison between the two, MRI provides superior soft tissue contrast and is the modality of choice for evaluating neurological abdominal conditions that require detailed tissue characteristics [15], while CT scans scales in imaging bony structures and is preferred in emergencies where the diagnosis is crucial [8].This efficacy test, there has been supporting data in some meta-analyses published regarding the diagnostic accuracy of each diagnostic imaging modality [9], [10].

MRI scan is a scan that uses a strong magnetic field and radio waves to create detailed images of the organs and tissues within the body [11]. MRIs use strong magnetic field gradients, and radio waves to generate images of the organs in the body. MRI provides better contrast in images of soft tissues, e.g., in the brain or abdomen. MRI's may be perceived as less comfortable by patients, due to the usually longer and louder measurements with the subject in a long, confining tube, although "open" MRI designs mostly relieve this.

One of the most popular is ultrasound. Ultrasound is composed of sound waves with frequencies greater than 20,000 Hz, which is the upper threshold of human hearing. Ultrasonic images, also known as sonograms, are created by sending pulses of ultrasound into tissues using a probe. The ultrasound pulses echo off tissues with different reflection properties and are returned to the probe which records and displays them as an image. Additionally, the use of ultrasound technique Echocardiography, also known as cardiac ultrasound, is the use of ultrasound to examine the heart. The visual image formed using this technique is called an echocardiogram, or simply an echo.

Echocardiography is routinely used in the diagnosis, management, and follow-up of patients with any suspected heart diseases or conditions. It is one of the most widely used diagnostic imaging modalities in cardiology [12].

2.2. Review of image recognition and learning techniques for medical imaging systems.

In this study, only two medical devices are studied because of the cost associated with the CT scanners and availability of data. Medical imaging systems have made the highest advancements in medical technology both academically and for medical research purposes. Dougherty *et al.* [13] present the medical imaging systems for constructing an image in response to signals from diverse types of objects namely bodies and phantoms. Additionally, Dougherty *et al*. [13] highlight that medical imaging systems can be classified according to the radiation and academic field of use. The authors further investigated the properties of these systems, and whether the images are formed directly or indirectly.

Furthermore, equipment such as Magnetic Resonance Imaging (MRI) scanners are denoted as medical imaging techniques that produce three-dimensional anatomical images used in radiology for medical diagnosis, detection of diseases and monitoring of patient treatment. The MRI employs a complex technique by using a strong magnet that produces a magnetic field that excites and detects the changes of protons found in the water molecules that make up living tissues. A radiofrequency current is pulsed through a patient stimulating the protons which are then detected by the MRI sensors. When images are produced from this process doctors can make out the difference between the tissues based on their magnetic properties. This is one of the sophisticated physiological processes of the body scans that are currently in use [14].

2.2.1. Artefact detection in CT images using deep learning.

MRI scanners use strong magnetic fields such as 1) magnetic field gradients and 2) radio waves that generate images of organs in the body. Additionally, MRI is deemed one of the most important non-invasive imaging techniques that is currently in practice within the medical fraternity, due to its richness of attainable tissue contrast [15]. Furthermore, the Positron Emission Tomography (PET) are also used for the same principle.

The scanner is a functional imaging technique that uses radioactive substances known as radiotracers to enable the visibility of organs and measure changes in metabolic processes and other physiological activities including blood flow and absorption. PET is denoted as a method used for measuring biochemical and physiological processes in vivo in a quantitative way by using radiopharmaceuticals labelled with positron-emitting radionuclides such as ^{11}C, ^{15}O, and by measuring the annihilation radiation using a coincidence technique [16, pp. 195-207].

However, the CT scan imaging system model is covered in this research study for image acquisition and artefact detection. With this said, there are several artefacts classified in reconstruction and three-dimensional Computed Topology (3DXCT) artefacts as outlined by Amirkhanov *et al*. [17]. To demonstrate the usefulness and impact of deep learning and machine learning, both approaches were used to predict different aspects of the COVID-19 outbreak. For example, Hemdan *et al*. [18] designed COVID-19-Net with seven different models. The results demonstrate that VGG19 and DenseNet have similar performance while the f1-scores for identifying normal and COVID-19 performances are 0.89 and 0.91 respectively. Additionally, Chowdhury *et al*. proposed to use SqueezeNet to classify patients with normal chest images and patients with pneumonia and compared it with three other different deep CNN networks. It was confirmed that SqueezeNet's performance is high, reaching an accuracy rate of 98.3% [19]. In retrospect to Chowdhury`s work, Safariyan *et al*. [20] presented the use of normalised segmented lung images to aid CNN model using the k-means method.

The results observation demonstrates that the proposed method outperforms other methods in the classification of defected and non-affected lungs by any disease projected by CT images. The use of machine learning and deep learning to solve complex medical issues is further supported by Wang *et al*. [21]. These authors used a CNN-based convolutional neural network model, and the results showed that the overall accuracy for the use of CNN was 82.9%, the sensitivity 84%, and the specificity 80.5%. In addition, Yoon *et al* [22], Piao *et al* [23] presents the PET/CT visual evaluation of whether there was FDG accumulation in the lymph nodes as compared to the surrounding tissue; in cases of uncertainty, a decision was made by consulting the SUVmax, which is the maximum value of the Standardized Uptake Value (SUV) within the region of interest (threshold value: 2.5).

2.2.2. Computer-aided diagnosis.

There are many conventional techniques to identify and learn about CT images, with the most obvious technique being artefacts visible to the human eye. There are common artefacts such as the ones mentioned previously. Furthermore, some artefacts are new and are mainly caused by faulty or degrading electronic components and external factors such as room temperature and dirt, to name but a few.

The review of image recognition and learning covers the techniques and developments used in the radiology/medical field to identify lesions and cancers. Furthermore, radiologists and physicians often share and analyse similar cases with verified diagnostic results in their decision-making processes for suspected diseases and cancers. As a result, radiologists expect that Computer-Aided Diagnosis (CAD) systems can improve their diagnostic abilities based on effects between the computer and the radiologist's high abilities and medical knowledge; hence, the importance of such a model.

Generally, physicians and radiologists analyse medical images and diagnose a patient's condition, whether it be a disease or cancer, by obtaining useful images and interpreting them using their experience and knowledge. However, this method is usually not accurate and is time-consuming. Thus, it can be said that good radiologists have high and flexible abilities in learning and pattern recognition. Medical conditions are not always the same and diagnostic time is vital - hence the need to develop the proposed research model using custom CNN.

It is pivotal for physicians and radiologists to attain correct patient diagnosis. There is therefore a need for an automated artefact detection model that would assist in the identification of artefacts and provide possible solutions that will save time and are not biased.

Machine learning, including pattern recognition techniques, has become a pivotal area within machine learning and machine vision domain in developing advanced CAD systems within the medicine fraternity. Duda *et al* [24, p. 3] states that "pattern recognition is the act of extracting features from some objects in raw data and making a decision based on the classifier output such as classifying each object into one of the possible categories of various patterns". The basic concept of introducing CAD systems in medicine was proposed to provide a computer output as an alternative as well as a second opinion to assist physicians and radiologists in analysing and diagnosing patient images so that the accuracy and consistency of diagnosis could be ameliorated and the image reading time be shortened.

There are two types of CAD systems:

- CAD systems for distinguishing medical conditions into abnormal and normal conditions; and
- CAD systems for the classification of unknown cases into several types of abnormalities.

Although CAD systems have previously been developed to assist in limiting medical errors for radiographic diagnosis, these systems have not been adopted entirely in clinical practice due to performance issues such as large dataset collection. Therefore, there is an inability to detect distortions in different designs outside the design scope due to time constraints.

2.3. CT scanner basics and historical background.

The historical documentation states that the first CT scanner was established in 1972 by Hounsfield and Ambrose [25, pp. 1395-1370]. This documentation of the first CT scanner was based on their experiment of positioning a patient inside a new machine in the basement of the hospital [26, p. 3]. However, the argument has been around for decades that Damadians is the first author/developer of the CT scanner in 1977 [27]. This is contrary to statements made by different authors. It is agreed that the first functionally developed CT scanners made use of pencil-like beam sources located across from a single detector.

In former days, the scanners were identified by the generations in which they were developed. The first-generation scanners in the mid-1970s translated linearly across the field of view and projected a series of parallel beams. The top CT scanner product of the time took up to five minutes per scan to rotate between translations to acquire 180^{o} projections at 1^{0} intervals. Figure 2.1 depicts first-generation CT scanners transmitting a single-shaped beam. Thin beams passed linearly through a patient and a single detector followed on the opposite side of the patient. The tube and single detector were then rotated slightly, and the process was repeated until a 180-degree arc was covered. Although an old technique and technology the biggest advantage of the first-generation CT scanner was the reduced scatter.

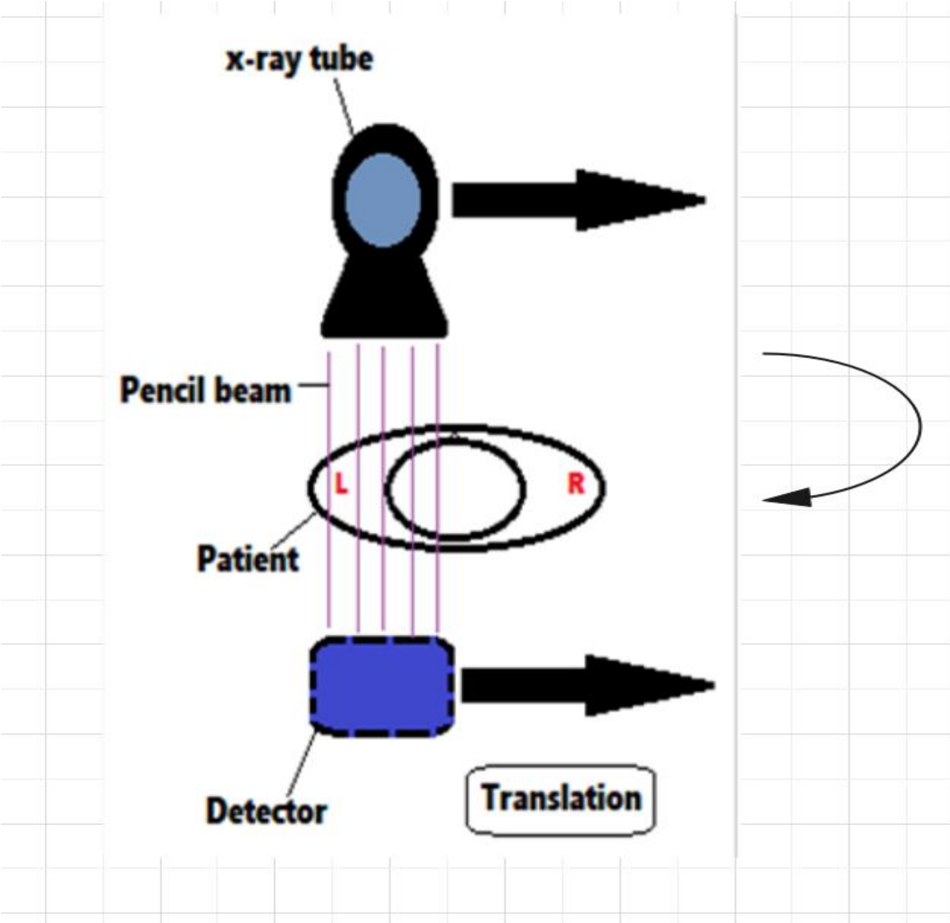

Figure 2.1: First-generation CT scanners with single pencil beam-shaped transmission [28].

The first-generation CT had the following attributes:

- Detectors: one
- Type of beam: pencil-like beam
- Tube-detector movements: translate-rotate
- Number of slices per rotation: 1
- Duration of scan (average): 25-30 minutes

Furthermore, due to technological inconsistency in the advancements of technology during the mid-1970s, the images obtained from these models had a quality issue and the scanning duration was long. However, the authors did not outline the scientific explanation towards the appropriate scanning duration bearing in mind the technology and its capabilities at that time. Table 2.1 addresses the difference in the CT scanners and gives more context to the duration aspect addressed in the previous paragraph.

Table 2.1: Different CT scanner generations [29].

Generations	First	Second	Third	Fourth
Detectors	One	Multiple	Multiple, originally 288; new scanners used over 700 detectors arranged in an arc	Multiple (more than 2 000) detectors arranged in an outer ring which is fixed
Types of beams	Pencil-like beam	Fan-shaped beam	Fan-shaped beam	Fan-shaped beam
Tube detectors	Translate-rotate	Translate-rotate	Rotate-rotate	Rotate-fixed
Duration	25-30 minutes	Less than 90 seconds	Approximately 5 seconds	A few seconds

Third- and fourth-generation scanners are currently used in the healthcare setting. Despite these two sets of generations currently used, their commercialisation into the market happened when the medical CT imaging started to take off, and as a result, the number of CT scans became enormous. Figure 2.2 illustrates the operation of the third- and fourth-generation scanners.

Figure 2.2: Test equipment being aligned (prepared for scanning) in the gantry aperture of a CT scanner.

Figure 2.2 depicts the preparatory scanning process for third and fourth-generation scanners. Third-generation scanners are still in practice in most of the medical institutions of South Africa. The CT scanner in Figure 2.2 further illustrates the classification of a digital imaging system due to its use of computers to process images. This is important as a basis for radiographers and engineers to familiarise themselves with the functions and parts involved in making a CT scanner work.

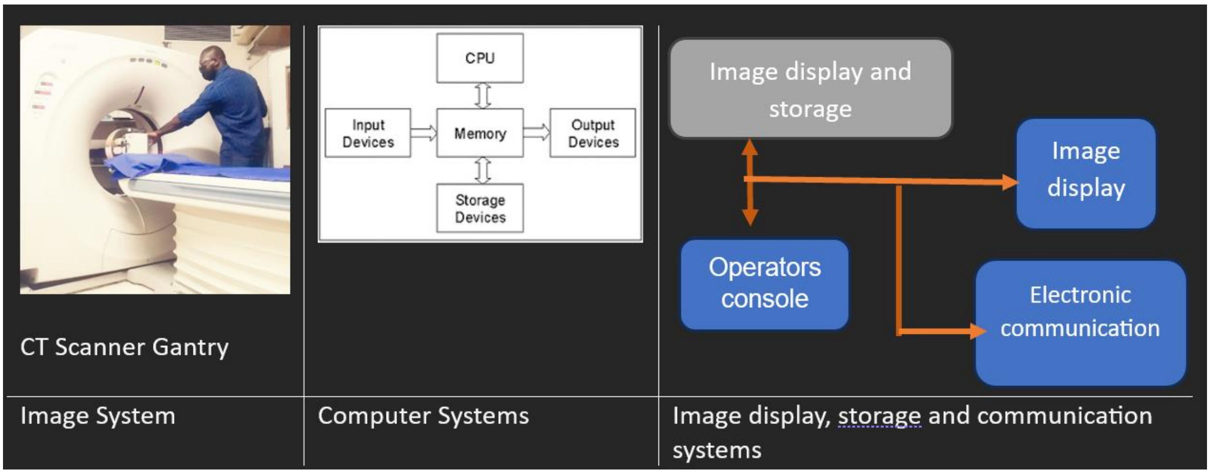

Figure 2.3: Basic equipment configuration for CT scanner.

Figure 2.3 depicts the basic equipment outlining the CT scanner and the proposal configuration model. The equipment image system comprises the following:

- Image system – this is in the scanner.
- Computer systems – this is in a computer room.
- Image display, storage, and communication [30].

In the case of evaluating image quality, it is advantageous for the technician or engineer to have prior knowledge and experience in relation to the type of CT scanner application features they are working on. This permits extra skills to aid in understanding of image processing and interpretation, which in turn is advantageous for formulating best possible solutions for removing or fixing artefacts.

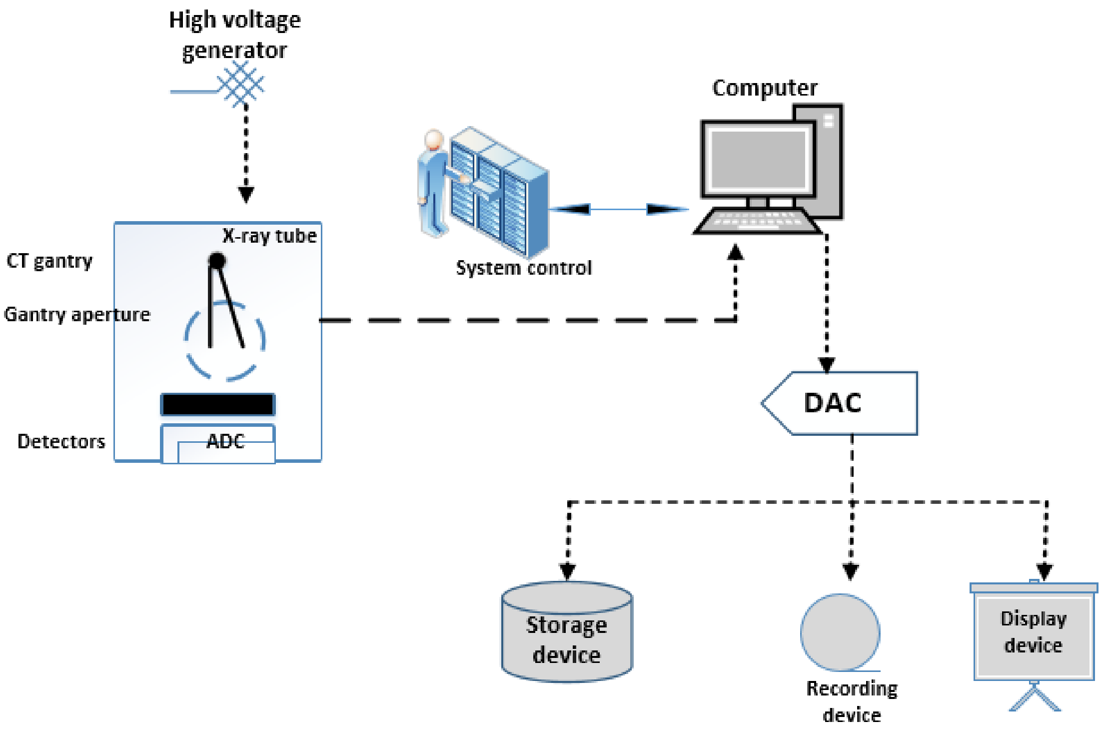

Figure 2.4: Basic flow diagram of CT scanner process [30].

Figure 2.4 depicts the basic CT scanner process consisting of a gantry, patient couch hardware equipment, operator station, and in many cases accompanying workstations provided for doctors and physicists. The CT gantry is a doughnut-shaped ring containing the tube, the detector(s), and associated equipment such as the high-voltage generator, power supplies, and control unit. The doughnut-shaped ring known as the gantry aperture accommodates the patient on a sliding couch.

The patient couch is a sliding tray on a fixed table with an adjustable height and forward motion. The tube can move 360^0 around the patient's body. As such, when X-rays pass through a patient they are attenuated and subsequently measured by the detector. The tube and detector inside the gantry rotate around a patient during scanning. The detector then converts the photons into electrical signals, which in turn must be converted into a digital signal for input into the computer. This slice represents the XY plane. X being horizontal and Y being vertical plane. The Z plane represents the patient's couch direction of movement.
The processing computer is usually located in another room or behind a lead-protected window and this is to act as a precaution that the computer processing performance

is not affected in any way. To improve the performance of the computer, it is important for the CT parts to be divided as follows: 1) reconstruction box (REC-Box); 2) console box.

The reconstruction box is where the reconstruction or image processing occurs after performing DAC (Digital to Analog Conversion) of the acquired raw data from the. The reconstructed image is then reproduced into a numeric form and converted into readable data for radiographers, doctors, and engineers to view on the display device which is the second part of the CT. At this point, the image can be recorded and stored on CDs, films, and doctor display software, for them to eventually be evaluated. Processes other than the presented processes that evaluate the artefact is represented in Figure 2.5.

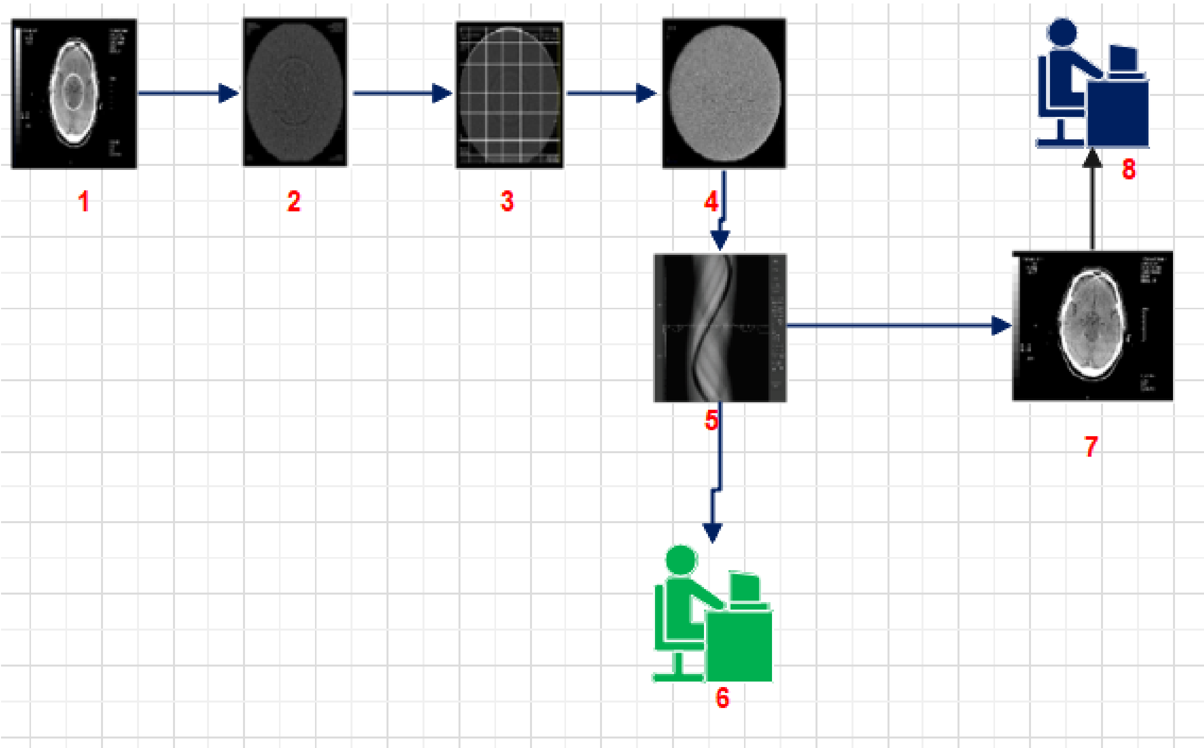

Figure 2.5: Flow diagram of research system setup.

Figure 2.5 is taken from the real-life situation where radiographers identify an artefact in an image, and the technicians are called out to be on-site and begin the fault-finding and artefact evaluation process. The layout of the research is based on the above-mentioned layout as outlined in the following steps:

- Image artefact is witnessed on a patient scan.
- The image is reproduced, and the artefact confirmation is tested on the apparatus.
- CAD is used to identify the artefact.
- Apply corrections, diagnosis, and comparative analysis to images.
- Artefact undergoes the evaluation and predictive correction process.
- The technician registers the artefact if it is new or complex. This process allows technicians to plan if the physical CT scanner needs to be attended to. This also gives engineers and technicians the chance to improve and strengthen preventative measures if or when an artefact reappears or appears on another machine.
- Image corrections and model algorithms (manufacture-specific) are applied to the initial image.
- The corrected image is shared with technicians and engineers to further analyse, diagnose, and improve the scheme techniques or principles.

2.4. CT image processing techniques.

CT image processing is not a single-step process as briefly explained in the previous section. This is a long and complex process that has its advantages and disadvantages in allowing data to be extracted for observations and analysis. Image processing refers to the use of various techniques (image processing software or algorithms) that modify the reconstruction images displayed for viewing and interpretation [30]. The processing of CT images involves multiple steps, namely data acquisition, reconstruction techniques, image display, manipulation, storage, and communication, as outlined in Figure 2.6. However, this does not imply that this is the only technical process for acquiring image manipulation, but it is deemed as the basic procedure.

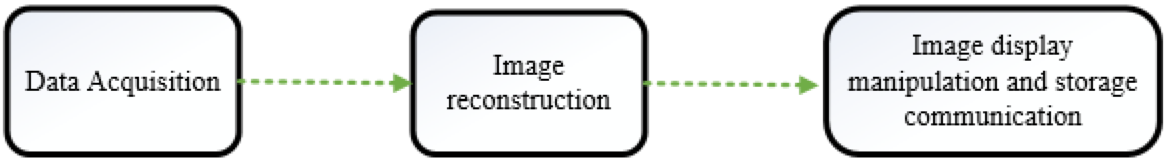

Figure 2.6: Steps in the production of the CT scanner images.

The process outlined in Figure 2.6 is as follows:

- Data acquisition refers to the collection of transmission measurements from the patient. This data is then recorded to meet the requirements of the reconstruction process.
- Image reconstruction from projection is the process of producing images of a two-dimensional distribution from estimates along a finite number of lines of known locations.
- CT scanner images are displayed on monitors built into the system that allow radiographers and doctors to view and diagnose.
- CT scanner images can also be manipulated to make the images useful and readable for patients. These manipulation operations include image smoothing, enhancement, greyscale manipulation and 3D processing (known as MPR-Multiplanar Recon in Toshiba/Canon CT scanners).
- CT images can be stored in many available formats for temporary or permanent read/write options. In Toshiba/Canon CT scanners raw data and reconstructed images can then be displayed and recorded for viewing and storage for further in-depth analysis until the parts of the system are replaced and reconfigured.

Communication in CT scanners refers to the transmission of text data and images from the system to other devices such as printers, diagnostic workstations, display monitors, trauma rooms and computers outside the hospital via network communication or the internet. This section of the image processing for CT scanners is relatively new to the basic functions. Subsequently, the image processing producer depends on the equipment configuration for the CT scanner as illustrated in Figure 2.3. The basic configuration outlined in Figure 2.6 aligns with the configuration model that is utilised in this research study.

2.5. CT scanner image presentation.

The third-generation CT scanners have designed systems that allow radiologists to use software instead of the conventional light boxes and films to evaluate and diagnose images. This allows monitoring of the scanners with a sufficient resolution for greyscale/CT values and spatial resolution as an essential prerequisite for the clinical application of image analysis and reconstruction techniques. This often allows for the convenient interpretation of images even if the data acquisition process is not at its best.

Furthermore, the CT scanner image presentations have varying explanations suited to their purpose or point of analysis. A convention of CT scanner measurement is directly related to the local attenuation coefficients of the tissue volume elements. Equation (2.1) depicts the attenuation coefficients translation into grayscale values known as CT numbers. Hounsfield unit scale is a linear transformation of the original linear attenuation coefficient measurement into one in which the radiodensity of distilled water at standard pressure and temperature is defined as 0 Hounsfield unit, while the radiodensity of air at standard temperature and pressure is defined as -1000 HU [31]. The calibration tests of HU with reference to water and other materials may be done to ensure a standardised response. Additionally, variation in the measured values of reference materials with known composition, and variation between and within slices may be used as part of test procedures as later covered and explained in Chapter 3.

$$\mathrm{HU} = 1000X\,\frac{[\mu-\mu_{water}]}{\mu_{water}-\mu_{air}} \qquad (2.1)$$

Where:

μ = linear attenuation coefficient

μ_{water} = water attenuation coefficient

μ_{air} = air attenuation coefficient

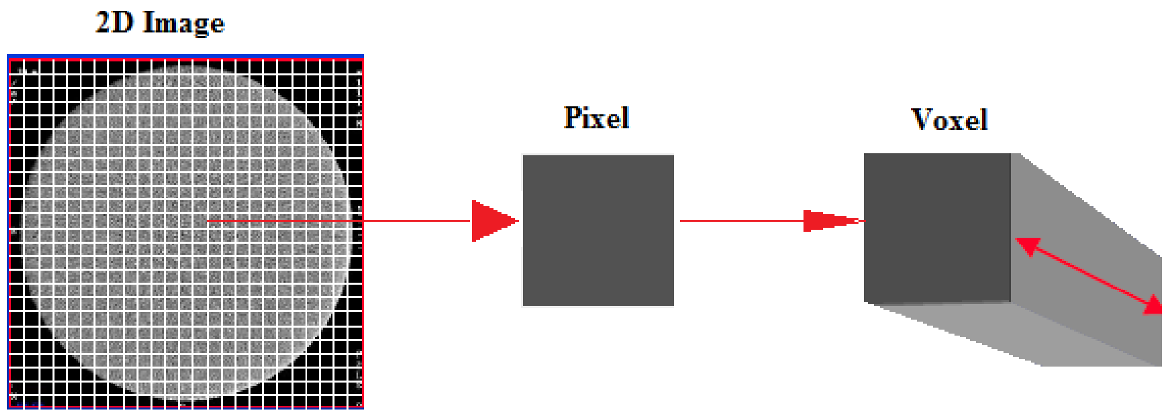

Figure 2.7: 2D image of a medium water phantom

Furthermore, Figure 2.7 depicts the 2D image model for the phantom. This model is built utilising third-generation scanners. Therefore, the third-generation scanners determine u_{water} from periodic calibration scans of water or water-equivalent phantoms. This is due to attenuation coefficients that are affected by the beam energy. Proper generator calibration is necessary for accurate and reproducible and acceptable Hounsfield/greyscale values.

Additionally, the last phase in the creation of the CT image is that of the display. Image display includes all the system components necessary to convert the digital data created from the reconstruction process to electrical signals needed by the CT display monitor. The display system also includes the ability to display patient information and scan protocol data and provides many graphic aids designed to assist in image interpretation.

2.5.1. Window level.

The window level selects the centre CT value of the window width. The window level selects which Hounsfield numbers are displayed on the image. The window level selects which Hounsfield values are displayed as shades of grey.

2.6. Principal evaluation techniques for CT image quality.

The principal evaluation technique covers the characteristic properties that influence the image quality of CT scanners. The CT scanner degrades over time producing images with artefacts. Fundamentally, the CT image quality is dependent on many factors most common being noise, spatial resolution, image contrast resolution and artefacts. Zarb *et al*. [32] outline the objectivity for measuring the image quality physically. However, each of these characteristics is then influenced by several other factors such as data acquisition, etc.

There are several methods outlined by Lin *et al*. [33] such as:

- scan localisation light accuracy,
- alignment of Gantry table; and
- slice localisation from radiographic (scout) image. This is a historical reference; however, it is deemed relevant for this subject despite many improvements that have been attained in this subject.

Additionally, Jackson *et al*. [34] outline the procedure for using a Konica Minolta CT system for the measurement of a CT radiation profile width and compare this method to conventional film measurements [34]. However, the evaluation of this method cannot be compared to the current study as the objectives and testing pieces of equipment differ.

2.7. Types of noise found in CT images.

Noise in CT refers to the degree of uncertainty in the measurement of the attenuation of the beam passing through the patient [32]. Plainly explained, noise is defined as the grainy appearance on the cross-sectional image because CT noise appears as fluctuations in HU.

Image noise can be defined as a measure of fluctuations that can be made using the region of interest as illustrated in Figure 2.8 below.

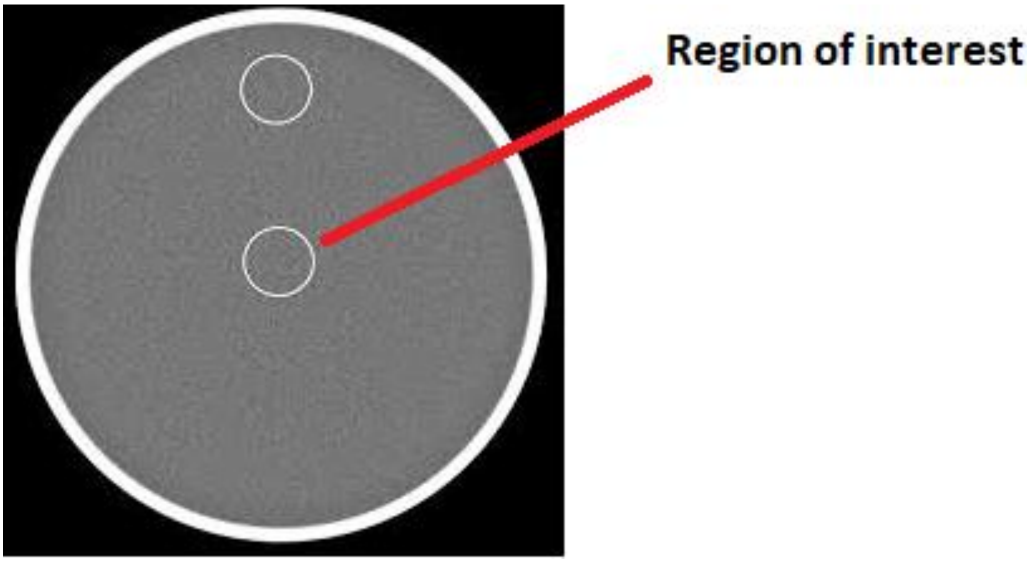

Figure 2.8: CT medium water Phantom used for the assessment of noise.

The noise level can be stated as a percentage of contrast or in CT numbers. For example, if 3 is the standard deviation for a CT unit with a CT number range of +-1000.

The noise produced in a CT image is a combination of noise sources that may not be entirely easy to identify separately. However, noise in CT is mainly related to several factors that influence the final image, including the following:

- Quantum noise
- Algorithm – reconstruction filter changes the viewability of the images.
- Electronic noise – LEDs and component nose frequencies affect CT performance.
- Scattered radiation.
- Scan parameters (mAs, kVp, scan time) - changing the mA values changes the beam intensity.

2.7.1. Noise uniformity.

Noise uniformity represents a certain amount of noise that is always present in an image. In most cases, this type of noise increases gradually up to a certain level where it is not necessary to even be perceived or impaired for diagnosis. As such, in CT scanners this type of process requires a process known as image quality optimisation. Noise on a cross-sectional image will equal a decrease in the image quality and inadvertently will hinder the contrast resolution, whilst improving the Signal-to-Noise Ratio (SNR) decreases the spatial resolution. However, Duan *et al*. [35] depict the method for the reduction of image noise by integrating phantom size, tube potential and tube current. Duan and co-authors outline that this method reduced the noise level by up to 40% for a 30cm phantom scanner using 80 kV. Nonetheless, this section is used as a knowledge contributing factor indicating the impact of noise in an image. For the current study, the noise is not accounted for as the study focuses on the identification of artefacts and proposing a solution.

The uniformity in relation to the values of the pixels in the reconstructed images means that they should be constant at any point in the image of the appropriate test phantom as indicated in Figure 2.9. The common size of the phantom, like the one presented in Figure 2.9, is 30 cm in diameter and each area to be measured is 5 cm in diameter [36].

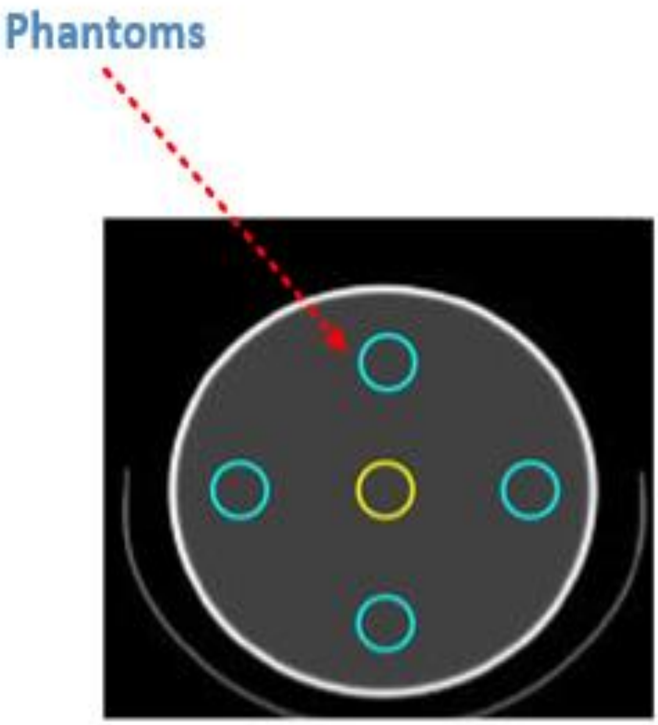

Figure 2.9: Scanned image of a medium water phantom used for assessment of CT number uniformity.

Maximum deviation of the CT number: If the scans are justified for diagnosis or treatment evaluation, there is no set number. Even two or more scans in a week or four in a month could be appropriate depending on your disease management. Regarding this research study, the deviation mentioned in this research is specific to the equipment used namely the Toshiba CT Scanner. The maximum deviation of the CT number should not exceed 2 HU from the baseline value measured at acceptance. (CT water must not be greater than ± 5 HU from the centre of the phantom to the periphery) [37].

2.7.2. Gaussian noise.

Gaussian noise is amplifier noise with the primary cause occurring at the acquisition stage [38]. However, image noise is not limited to the above mentioned; there are other noises such as the outlined indicated by [39]:

- Gamma noise – this noise refers to the mean and variance of density and this can be obtained through mean variance.
- Exponential noise – an unwanted change in pixel values in an otherwise homogeneous image.
- Salt and pepper noise - this noise is also called shot noise, impulse or spike noise and is usually caused by faulty memory locations, malfunctioning pixel elements in the camera sensors or timing errors in the process of digitalisation.

2.8. Types of artefacts.

Artefact is a name given to a ‘distortion’ or errors that occur in reconstructed CT images. The CT scanner image artefact may in most cases have a discrepancy between the reconstructed CT image number and the attenuation coefficient. This is due to the CT numbers that are represented in the greyscale values. The incorrect measurements produce CT numbers that do not represent the attenuation coefficient of a patient or object. One of the many other causes relating to this challenge is the CT scanner that degrades over time making it more likely to experience the appearance of artefacts within the scanned images. In practical experience relating to this research study, the users need to ensure that the CT scanner is well-calibrated to produce good-quality images for medical use.

In most cases, to resolve the degradation or image artefact, restoration can be conducted by radiographers by reconstructing raw image data, re-exposing patients that move during scanning, or increasing the current to remove unwanted image noise.

Additionally, CT image artefacts have different causes and appearances, with the equipment including old or faulty High Voltage (HV) generators, incorrectly set air-conditioning temperatures, patient movement and/or new or untrained radiographers. Furthermore, every section of the CT scanner influences image quality and causes artefacts. Table 2.2 provides a list of artefacts mainly experienced in CT scanners, including but not limited to causes and correction techniques.

Table 2.2: Artefact causes and corrective measures.

Artefacts	**Causes**	**Correction Techniques**
Patient Motion Artefact 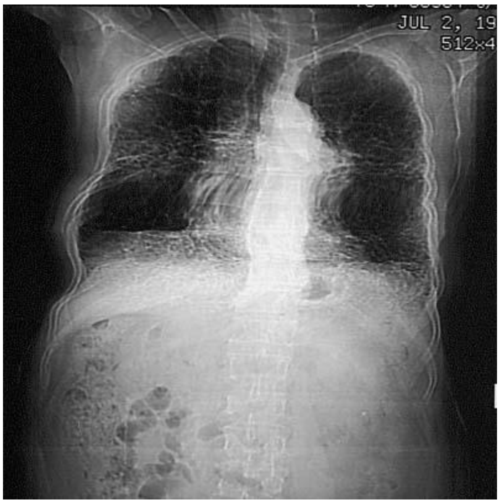	Patient motion can be voluntary or involuntary movement	Positioning aids to make patients comfortable and to ensure that they understand the importance of remaining perfectly still during scanning. Shorten the scan time of examinations
Streak Artefact	Streak Artefact. – The presence of metal on the patient such as jewellery, clothing items,	Remove all metal objects on the patient and avoid metal being in the

	removal dentures; or dried up patient contrast on the equipment and bed as well as other solid objects on or around the patient. These give rise to the lines distorting the image and almost appearing like metal artefacts.	scan field
Beam Hardening Artefact 	Beam hardening - A beam is composed of individual photons with a range of energies. As the beam passes through an object, it becomes “harder,” that is to say its mean energy increases because the lower-energy photons are absorbed more rapidly than the higher-energy photons [40].	Filters such as bowtie ensure the uniformity of the beam at the detectors
Partial Volume Artefact [41].	When a dense	Scan patient in thin

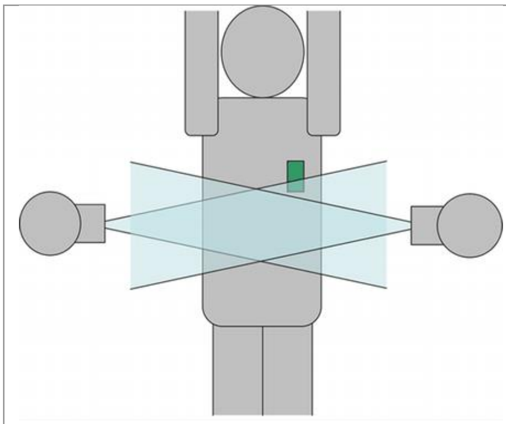	object lying off-centre protrudes partway into the width of the beam that yields a CT number representative of the average attenuation of the materials within a voxel.	slice sections
Equipment-Induced Artefact 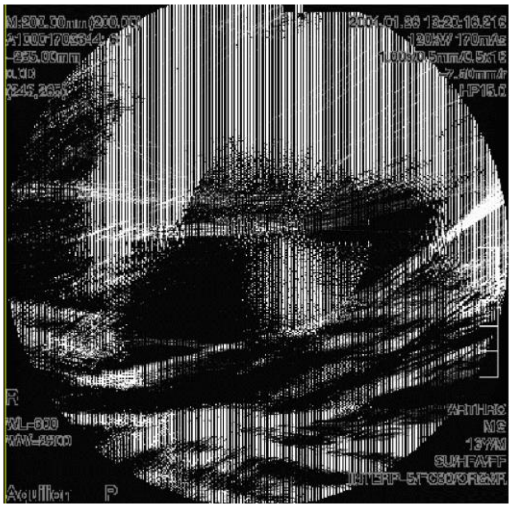	Streaks caused by mechanical failure or imperfections such as poor gantry rigidity or tube misalignment and poor sampling of the detector signals	Balancing algorithm that corrects the raw data during acquisition or after scanning
Noise-Induced Artefact	Poor selection of exposure techniques such as scan rotation speeds resulting in fluctuation of HU between uniform material points	Adaptive filtering algorithm that dynamically adjusts the amount of smoothing operation based on the flux level at each projection channel.

		

Table 2.2 further outlines the CT image artefacts that are common and can occur for various reasons. Additionally, the knowledge of these artefacts is important because they degrade image quality to non-diagnostic levels**.** Furthermore, the design features are incorporated into modern third- and fourth-generation scanners, as highlighted earlier.

There are many instances where patient positioning and best scan parameters are selected to fix or alleviate the artefacts. Subsequently, there are many instances where the artefact is attended to by engineers who are required to have added understanding of electronics, image evaluation techniques and some knowledge or training on the specific manufacturer's product and reconstruction processes. Loosely expressed, manufacturers have different definitions for CT image quality, as well as which equipment and scan parameters are more important compared to others.

As outlined earlier, this research study utilises 2D CT images obtained from Toshiba manufacturing noise with the artefact reduction techniques for the different CT manufacturers as follows:

- Toshiba – offers three quality settings for standard deviation image noise.
- General Electric - makes use of noise indexing based on standard deviation CT value for a specific water phantom.
- Siemens – makes use of reference 4D mAs standard adult image quality with 70 kg body weight.
- Philips – Utilises reference image.

Based on the already outlined literature, it is important to optimise and augment image quality for better image processing results. However, it is necessary to understand why some of the artefacts occur and how they can be prevented or suppressed. Amongst others, this can be accomplished by high radiation dose or the use of perfect detectors.

Several artefacts are not commonly known. In most cases, this is due to faulty or degraded electronics, incorrect patient planning and external factors, or a combination of these faults. Such malfunctions cause multi-sectional artefacts, which are produced by incorrect image reconstruction processes and incorrect CT scanner functions. Multi-sectional artefacts mostly appear to have multiple artefacts in one image.

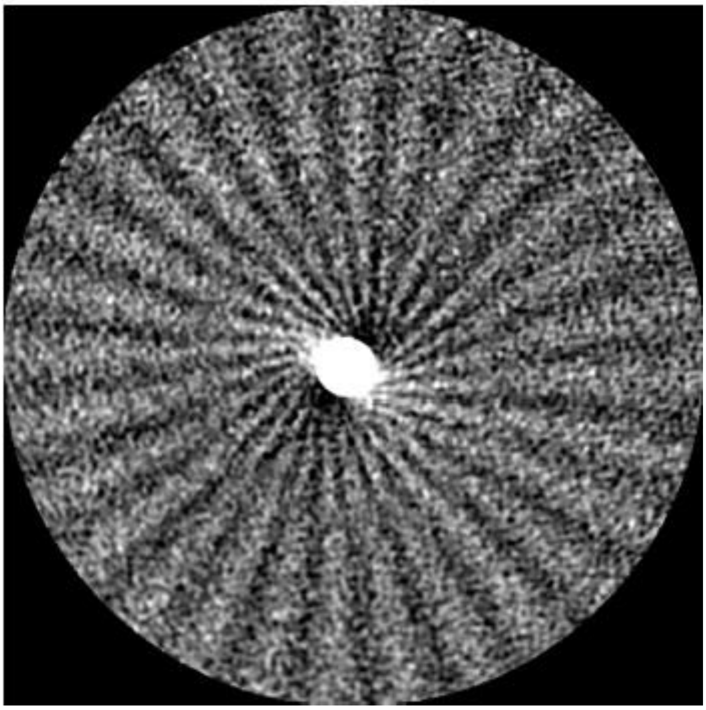

Figure 2.10: Windmill artefact, metal, and staggered artefact on a medium water phantom [42].

It is important to note that some artefacts are deemed as "normal artefacts". Other objects such as metal objects, bone and soft tissue, and bone-to-air transitions can cause image distortion during reconstruction and produce artefacts such as the streak artefact.

However, there are several PET/CT artefacts as well; with their appearances being different than those seen on dedicated PET scanners, and therefore several new artefacts that are unique to combined PET/CT scanners [43]. Additionally, the design features incorporated into modern CT scanners minimize some types of artefacts, and some can be partially corrected by the scanner software. In many instances, careful patient positioning and optimum selection of scanning parameters are the most important factors in avoiding CT artefacts [44]. This would contribute to the remodelling and parameter adjustments in future CT scanner designs. Nonetheless, the challenge for metal artefacts in most cases is the input image with metal artefacts. However, this challenge was addressed by Zhang et al. [45], who used CT images without metal to simulate images with metal and metal artefacts, and images with metal but without metal artefacts [45, 46].

2.9. Review on correction techniques used for CT image artefacts.

Although in its simplest of definitions, not all artefacts are the same and as a result, they should all be approached differently. Several techniques are used to evaluate and correct the different artefacts accordingly. In most instances, the evaluation is made by identifying the size and shape.

Furthermore, citing the historical background, the review will be based on two of the most common artefacts experienced by radiographers and engineers, namely those produced by third- and fourth-generation CT scanners.

Figure 2.11 outlines an example of different ring artefact statuses from severe, subtle to circular types of ring artefact with a defective detector element that creates a bright or dark ring centred on the centre of rotation [47]. Furthermore, the ring artefact is immediately visible and comes in various forms. However, in most cases, if not all, the ring artefact would point to a damaged or faulty detector element that needs replacement or adjustment and a broken power supply. The induced artefact in many documented field experiences about ring artefacts was caused by degraded electronics, and as a result, the avoidance and software corrections include selecting the correct scan details and protocols of the full system calibration and having knowledge of anatomy.

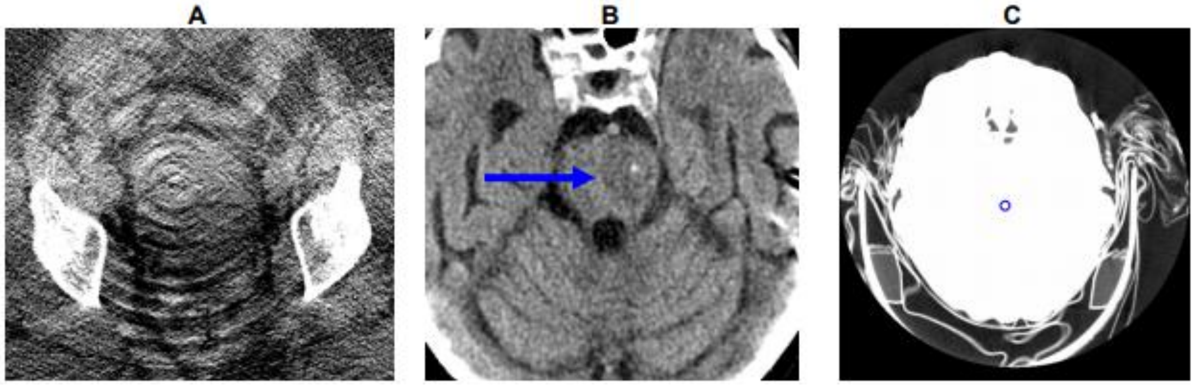

Figure 2.11: Ring artefact. A. Severe ring artefact B. Subtle ring artefact C. Circular reconstruction region [38].

Eldib *et al*. [48] proposed a corrective method for a cone-beam CT by correcting the defective pixels whose values are close to zero or saturated in a projection domain. Subsequently, Salplachta *et al*. [49] introduced a new ring artefact reduction procedure that combines several ideas from existing methods into one complex and robust approach. The procedure was implemented in the scope of lab-based nano CT with detection based on charge-coupled devices. Liang *et al*. [50]. proposed a novel ring artefacts reduction approach that integrates the benefits of an efficient iterative framework with the Relative Total Variations (RTV) algorithm for texture extraction. The iterative framework with RTV relates to a method that makes use of simple mean values analysis to detect and correct artefacts. It is argued that despite the results being positive for any type of detector, the results are much more effective on flat-panel detectors.

Metal artefacts are artefacts caused by the presence of metal objects in the scan field, and in most cases the scanned field of metal objects can lead to severe streaking artefacts. However, metal artefacts are caused by multiple mechanisms, some of which are related to the metal itself, and some to the metal edges. Additionally, the reconstruction in certain parts of the image for which many high-count measurements of features dominate higher in the identification as opposed to the under-determined parts of the image. De Man *et al*. [51] outline the use of posterior algorithm for the reduction of metal streak artefacts. Moreover, De Man and co-authors present the use of Markov random algorithm for image reconstruction.

A major CT manufacturer, Toshiba, designed Single Energy Metal Artefact Reduction (SEMAR) for use on non-removable items such as dental fillings, prosthetic devices, and surgical clips, without the need to tilt the gantry. SEMAR can uncover bone and soft tissue structures normally distorted by beam hardening. SEMAR was designed using data segmentation, forward projection, and interpolation to complete the algorithm for removing metal artefacts. The algorithm uses the image-based metal segmentation methods, in which the metal region is segmented in the reconstructed images and forward-projected to localise the projection data that have been contaminated by the metal.

2.10. Application of Computer-Aided Diagnosis in medical technology.

Scrutinisation and analysis of medical images where physicians often compare similar diagnostic cases with verified diagnostic results are a result of the evolution in digital technologies in clinical practices [52]. Furthermore, in certain applications, CAD is used to diagnose a plethora of diseases and medical conditions of the human body. [53]. CT uses radiations that have a negative effect on organisms, especially for their ability to cause genetic mutations. In MRI screening, the patient may feel claustrophobic due to the enclosed space inside the magnetic tube. Ultrasound screening is recommended for women with dense breasts, but it has a high false positive rate [54].

The Content Based Image Retrieval (CBIR) scheme includes the following components and steps [55], which serves as a historical reference due to its importance towards the study objectives:

- Step 1: The system accepts an input query of a suspected Region of Interest (ROI) identified by a physician.
- Step 2: From the detected query, the CAD system applies a region growth algorithm to segment the suspected mass in the ROI. The efficiency of the suspected region segmentation directly influences the accuracy of extracted and computed features in images used in the CBIR algorithm.
- Step 3: The system then extracts and computes a set of image features from the segmented ROI and its surrounding background. The objective of this

process is to identify ineffective and adequate image features that aid in reducing the gap between computer vision and human vision (i.e., the physician).

- Step 4: The CBIR system discards a small number of images stored in the reference image database. Although the capability of CAD systems depends on the size and heterogeneity of reference databases, the above-mentioned CAD system using the CBIR algorithm employs an adaptive method in which only a small number of references have an explicit influence on the detection of the specifically queried ROI. This inadvertently means that discarding reference ROIs with lower impact on the input ROI is an important aspect of improving the computational efficiency of the CAD system.
- Step 5: The system applies an algorithm to analyse and obtain a set of K reference images that is considered like the input ROI.
- Step 6: Based on the comparisons of the obtained reference ROIs to the inputted ROI and their established outcomes - positive or negative, the CAD system computes a likelihood score of the inputted ROI being associated with a positive ROI.

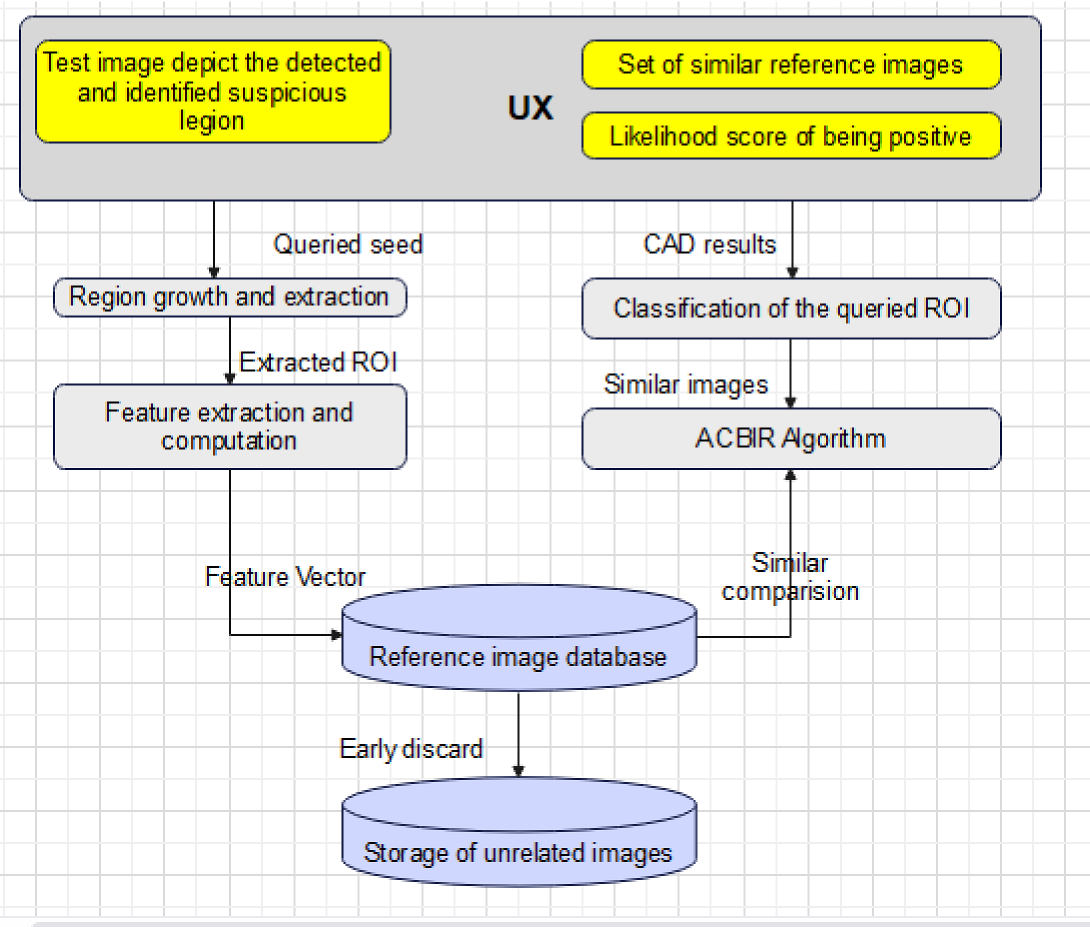

Figure 2.12: CAD scheme using Content-Based Image Retrieval (CBIR) approach [5].

Although the CBIR approaches provide physicians with visual assistance, developing this type of CAD system concept is arduous and highly challenging. However, the performance and accuracy of this CAD system would depend on several components to consider such as the high-level performance of segmentation, feature selection, dataset collection and size, and the relationship between the clinical applicability and visual similarity of the CAD system results and similar proposed research. Subsequently, Chi-Tung Cheng *et al*. [56, pp. 1-11] depict the development of a deep learning model that can detect most types of trauma-related findings on pelvic scans. This model uses an algorithm that identifies hip fracture, pelvic area fracture, and dislocations amongst other scan diagnoses. Furthermore, the system called PelviXNet uses classification confidence scores and class activation heat maps to indicate and localise fractures in scans.

Additionally, in mid-2019, the Society for Imaging Informatics in Medicine (SIIM) developed an Artificial Intelligence (AI) algorithm that can accurately detect lung nodules on CT scans by analysing the reconstructed images and the raw sinogram data. Furthermore, sinogram is the visual representation of the raw projection data produced during CT image acquisition. Subsequently, the CAD system was developed to reduce radiologists' workload and to help them efficiently diagnose lung cancer.

In this research study, the researchers first extracted suspicious nodule candidates from the CT images using their previously developed vector quantisation technique. After the nodule candidate was projected to the sinogram domain, the researchers applied a deep-learning model on the sinogram data to reduce false-positive results. However, nodules can vary significantly in size from 4 x 4 pixels to 75 x 75 pixels. As a result, small nodules may wind up being just a tiny fraction of the patch. Another issue experienced in this research is the resizing and conversion of images, which processes introduced new artefacts.

More recently, a CAD system was developed using deep learning to differentiate between COVID-19 and other pneumonia. This CAD system uses ResNet50. ResNet-50 is a convolutional neural network that is 50 layers deep. A pre-trained version of the network trained on over million images from the ImageNet database can be loaded on this system [57].

The aforementioned-trained network can arrange and analyse images into 1000 object categories, such as keyboard and mouse. As a result, the network learns feature representations for an extensive spectrum of images. As with most studies involving deep learning the collection of datasets taking time and some being unnecessary were some of the problems experienced in this research. The researcher also admits that in the early stages of the coronavirus, it was difficult to discern between viral pneumonia and COVID-19.

2.11. Transfer learning.

In most machine learning-based applications, the on-trained data are compared to the unknown data. Some applications to a certain degree do not provide comfortability mainly around the results. In a research study such as this one, it is crucial to investigate the impact of data transferred from the "transfer learning" approach against the existing results. Transfer learning is defined as a specific kind of machine where just a portion of the test data is utilised for producing another test data [58]. Mostly aligned with the medical fraternity, Kong et al. [59] outline the importance of utilising and developing automated techniques to assist in bad locks due to the high number of demands experienced in the field.

Figure 2.13 depicts the difference between traditional learning and transfer learning.

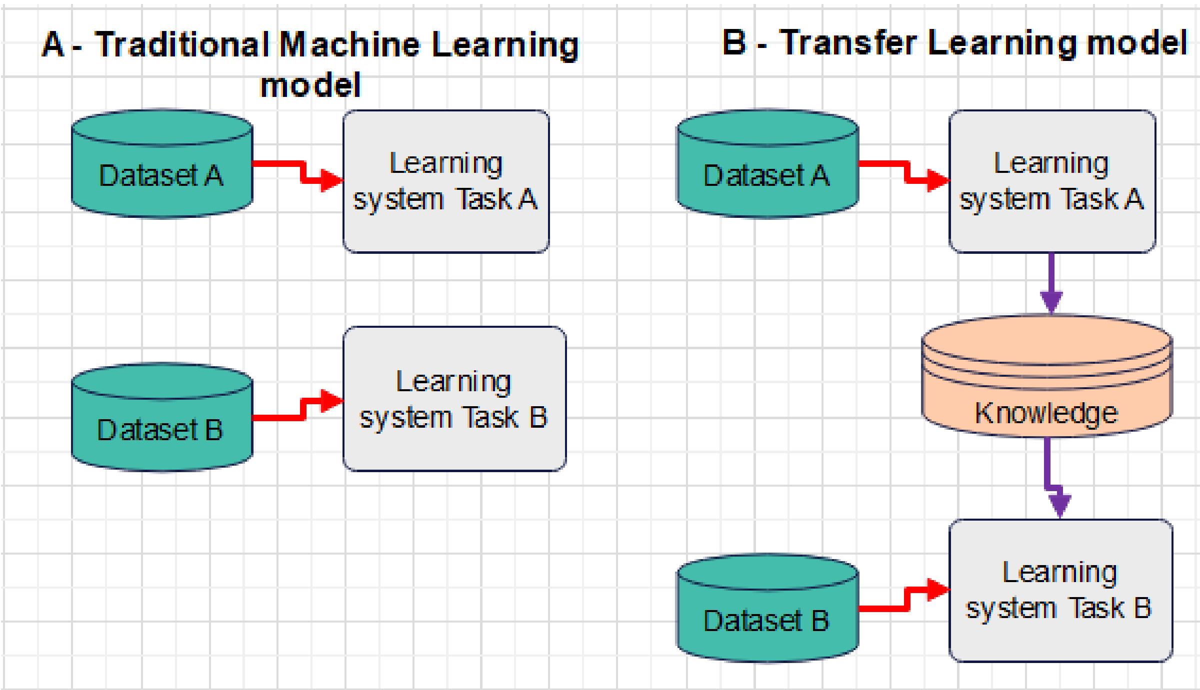

Figure 2 13: Traditional machine learning model vs. transfer learning [60].

In Figure 2.13, a distinct comparison is made between a traditional ML model and transfer learning. Figure 2.13 (A) section depicts the Traditional Learning (TL) approach against the Transfer Learning approach. As depicted in Figure 2.13, traditional machine learning focuses only on the isolated task without any knowledge or information retention, while transfer learning relies on variables from the completed machine learning tasks such as features, labels etc. which enable further data training.

2.12. Chapter summary.

Over the years medical imaging analysis software has been used by medical practitioners and they have shown great improvement. The improvement entails the quality of these software, performance and functionality that offers more for evaluation and diagnosis for students and researchers alike to focus on the problems of specific application areas. If taken advantage of, these additional tools for evaluation could further encourage the value of CT scans for the benefit of specialists, patients, and future research.

This chapter has presented the work done in CT scans and its applications in the radiography sector. Furthermore, this chapter also appraises the currently utilised medical devices for CT scanning. The types of noise that are seen in CT scans are also identified. Additionally, the types of artefacts and the work or methods from previous authors are depicted. However, the literature does support the conduction of such a research study for the utilisation of both image processing and artificial intelligence techniques to identify and detect artefacts without any human intervention.

This chapter further made mention of the transfer learning approach. This approach is investigated against the literature and its possible contribution towards the study's objectives.

CHAPTER III: Development model for artefact detection and identification from CT scanner datasets.

This chapter outlines the methodological approach for artefact detection and the process for identifying the possible artefact solution. This process makes use of an artificial model that compares the raw data datasets against the processed datasets. Upon the system rectifying the artefact, a possible solution is indicated to the user or technician. This model operates without any human intervention through model artefact learning and restoration utilising AI and image processing techniques.

3.1. Introduction: Artefacts identification and processing developments.

In the early days of image processing development, linear filters were used as the primary tools for image enhancement and restoration. However, due to the advancements in technology, other algorithms such as supervised learning multi-class classification logistic regression algorithm and linear regression algorithm are currently in use in the market.

3.1.1. Toshiba Phantom.

Toshiba phantom otherwise known as a TOS phantom, is a specially designed apparatus that is scanned or imaged in a Canon/Toshiba CT scanner. The phantom is used to evaluate, analyse, and verify calibration data and the performance of the scanner. The TOS phantoms are readily available with the installation of the CT scanner as an accessory and provide consistent results as opposed to a living subject or cadaver.

Likewise, as briefly mentioned in section 1.5 Limitations of this research study, using the TOS phantom avoids subjecting patients to direct and unsafe radiation exposure and risks. The phantoms' basic design consists of an outer plastic shell. The shell is filled with water and has a compartment that houses imaging inserts that represent different densities of the human anatomy for calibrating X-rays and ensuring regulatory radiation; a dosimetry insert in the air gap.

The TOS phantom is created out of hard and soft materials that mimic the responses of human anatomy under specific conditions for specific organs, such as tissue, lungs, bone etc. The phantom used for this research is covered in detail in section 3.3.2 accompanied by figures and tables.

3.1.2. Dataset creation and data acquisition process method

The image model technique was developed by utilising the CT scanner to acquire images from the Canon, Aquilion Prime CT scanner which were then formulated to two set of datasets namely Dataset_1 and Dataset_2. Dataset_1 is an image dataset that comprises of 85 ring images and 85 metal images, while Dataset_2 is an image dataset that comprises of 44 ring images and 44 metal images. In the acquisition process of this images, a set of procedures as described below were followed based on the manufacturer scan protocol settings:

- The CT scan was first set at 120kV.
- 50mA (lowest mA to create high noise levels) and 350mA (for tube reservation and radiation scatter and leakage).
- Small and large Field of View (FOV).
- 4 mm x 4 slice thickness.
- 1-second scan rotation speed.
- FC70 filter kernel. FC70 is the reconstruction filter for system performance evaluation.
- Metal artefacts were created using metal rods, aluminium sheets and work tools placed in and around the TOS phantom.
- Ring artefacts were produced by loosely disconnected detector boards, adjusted power detector power supplies, work tools, tape and office stationery placed in the field of view.
- Images were retrieved from the console using a USB.

- Images were opened, converted, and renamed using MicroDicom software.

Based on the manufacturer recommended settings, the image quality and reconstruction speeds of this system produce the desired images and results. Figure 3.1(a-b) presents the CT scanner and the computer system software.

(a)  (b) 

Figure 3.1(a): Canon Aquilion Prime CT Scanner workstation; (b)Canon Aquilion Prime CT scanner scan room.

Figure 3.1(a) presents the actual CT scan machine, while in Figure 3.1(b) computer on the right is used to perform the actual scanning and acquiring of the images. The computer on the left is then used as a display console that allows the user to verify image quality and diagnostic features used by doctors and radiographers.

In the initial algorithm modelling of custom CNN, Dataset_1 and Dataset_2 was taken from Toshiba CT scanner equipment for both ring and metal artefacts in a stage called collect and prepare data. The images were then cleaned to optimise their light intensity utilising the convolution algorithm.

3.2. Algorithm modelling technique.

This section of the study presents the algorithm modelling approach. In modelling the algorithm, certain sections and data flow must be abided to have non-biased data.

Figure 3.1 depicts the data flow approach to be utilised in this research study, mostly with the focus on feature extraction and classification based on the convolution model.

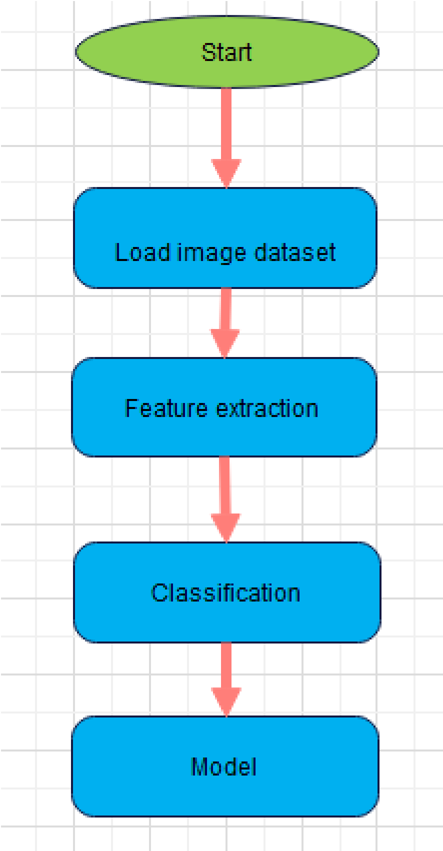

Figure 3.2: Algorithm model flowchart.

In Figure 3.2 the two datasets are loaded into the model. Once this has been completed, it is of paramount importance to augment the training dataset artificially by applying image augmentation to ensure stable results [*Annexure H*].

3.2.1. CNN architecture.

Image dataset augmentation in this model is accomplished by defining image data generator parameters within the algorithm. The parameter settings are set as follows:

- Rescale —This process entails the use of digital images to create pixel values between 0 and 255 (0 in black, 255 in white). Rescale makes use scale array of the initial image pixel values to be between [0,1] to ensure lower losses; hence, the proposition for the use of a lower pixel range.

- Shear_range — Image transformation takes place. The shape of the image is the transformation of the shear. Shear_range re-arranges one axis and distorts the image by stretching the image at a specific angle known as the angle of the shear.
- Zoom_range — The image is zoomed to 0.2 which is a value that is still within the image frame range, as images larger than 1.0 are deemed out of the picture.
- Horizontal_flip — A few images are horizontally inverted at random; however, this depends on the research objectives.

Furthermore, an approach making use of Convolution Neural Networks (CNN) is applied. CNN is designed for images that contain convolution layers that compare overlapping rectangular patches of the input to small learnable weight metrics "kernels/ filters" that encode features.

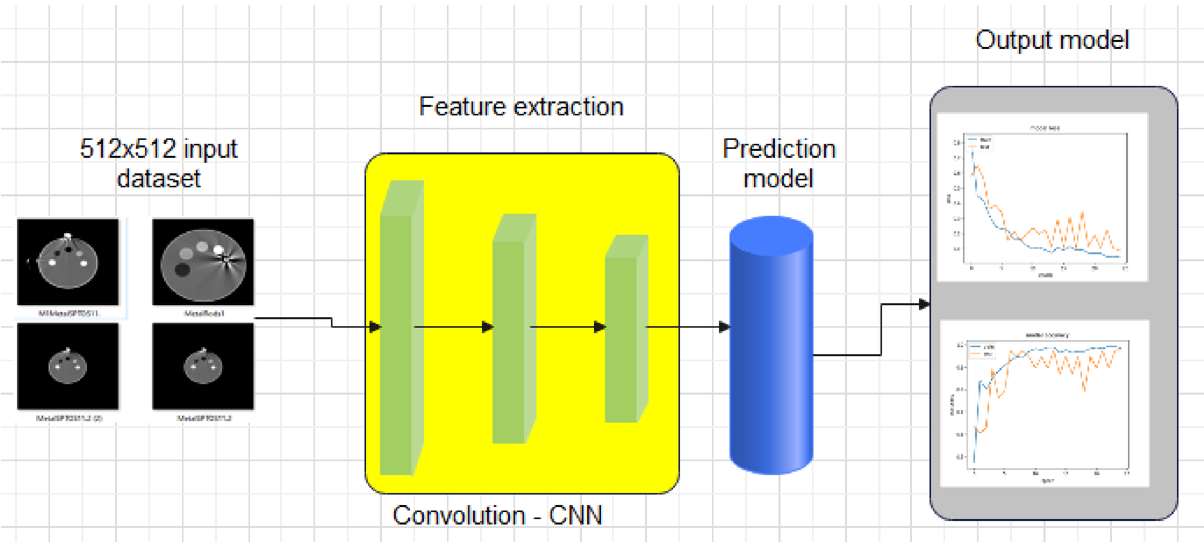

Figure 3.3: Convolution neural network output.

Figure 3.3 depicts the convolution neural network. In the context of the convolution in this research study, the input dataset for both artefacts is placed in the convolution model for feature extraction. This occurs after the model has been trained with 88 input image datasets. Upon completing this task, the results are transferred to the prediction model and the system automatically produces the output results.

The full convolution network comprises the input dataset (metal and/or ring artefact). CNN architecture in the context of this research study is based on the application of the convolution model on the input dataset. The convolution structure as presented in Figure 3.3 comprises the input dataset that is transformed and passed to the feature extraction layer. In this layer, features such as edges, texture and colour are detected. However, the input matrix dimension utilised in this algorithm is a 3x3 matrix that is applied on the image dataset.

In the convolution algorithm, stride is applied in the input dataset as follows: When the stride is 1, the filter is moved one pixel at a time. When the stride is 2, the filter is moved two pixels at a time, and so on. However, in the context of this algorithm, larger filter sizes and strides were used to reduce the size of a large image to a moderate size based on the 3x3 image dataset matrix.

However, it is critical to note the steps described below before a CNN model can be constructed as follows. However, the below process depicts the process conducted in this research study and not the generic application of the CNN algorithm:

- Commence the model filtering by utilising lower filter values such as 32 and begin to increase it layer wise.
- Construct the model with a layer of Conv2D.
- Apply MaxPooling.
- Use kernel_size based on an odd number, i.e. 3x3 matrix as per the above algorithm.
- Use the rely activation function.
- Input shape takes in image width and height with the last dimension such as colour channel.
- Flattening the input after CNN layers and adding ANN layers.
- Use of softmax activation function.

The following pseudocode conversion of the 2D image dataset was used as follows:

```
# Hyperparameters of Conv2D
Conv2D (
   filters,
```

```
    kernel_size,
    strides= (1, 1),
    padding="valid",
    activation=None,
    input_shape=(height,width,color channel)
    )
# Hyperparameters of MaxPooling2D
MaxPooling2D (
    pool_size=(2, 2), strides=None, padding="valid"
    )
```

Furthermore, a 2D CNN architecture was implemented by designing a 22-layered 2D CNN that consists of five 2D convolution layers. The reason for the utilisation of a 22-layered 2D CNN is to ensure that the model stability is high, which constituted the use of 32 filters, of which three consisted of a 64-layers filter based on a 3x3 kernel size. In the convolution (Conv) layer as outlined earlier.

ReLu activation layer and max-pooling (MAXPOOL) layer with a stride of two are applied sequentially. The feature extraction block consists of both CONV (ReLu and MAXPOOL) modules. In obtaining the output results, the extraction block is flattened and passed to a fully connected layer with 475,746 parameters, which are feature parameters that are extracted from the input dataset. Furthermore, for purposes of providing the context of the algorithm setup based on Figure 3.2, the two-step approach is as follows: 1) Mirror padding operation and 2) use of softmax function. In the application of the softmax function, the function is used to find the parameters in the maximum of the connected layer. The approach makes use of the conditional probabilities of the softmax function. Probability theory states that the output of the softargmax function can be used to represent a categorical distribution, that I s the probability distribution over K different possible outcomes as presented in equations 3.1.

$$p(\mathrm{y} = \mathrm{j}|\mathrm{x}) = \frac{e^{x^T w_j}}{\sum_{k=1}^{K} e^{x^T w_k}} \qquad 3.1\ [61]$$

The model calculation based on the 2D-CNN model makes use of equation 3.1.

Where: J = sample vector of X and a weighing vector W;

$x^T W_j$ = inner product of X and W;

The 2D CNN algorithm used in this research study is based on the 3x3 kernel filter [*Annexure G*].

3.3. Raw CT scanner output image acquisition process for artefacts detection.

This section presents the output CT scanner image acquisition process based on the metal and ring artefacts obtained from the Toshiba medical equipment. The assumption is that the process applied in the Toshiba-based equipment can also work with the other types of medical equipment. However, the focus of this research study is on the Toshiba equipment, and the application of such a model on other medical equipment remains a window for further research.

3.3.1 Imaging acquisition process.

The image acquisition process requires both capturing and storage of images, and in this research study this process was conducted on Toshiba medical equipment. Figure 3.4 depicts the initial images taken for image processing and machine learning purposes. However, two phantoms were used to evaluate the artefact mitigation methods. Additionally, after the data were collected, a model was developed to enable data training, and the same data were then fitted into the same data training model for evaluation and model training purposes.

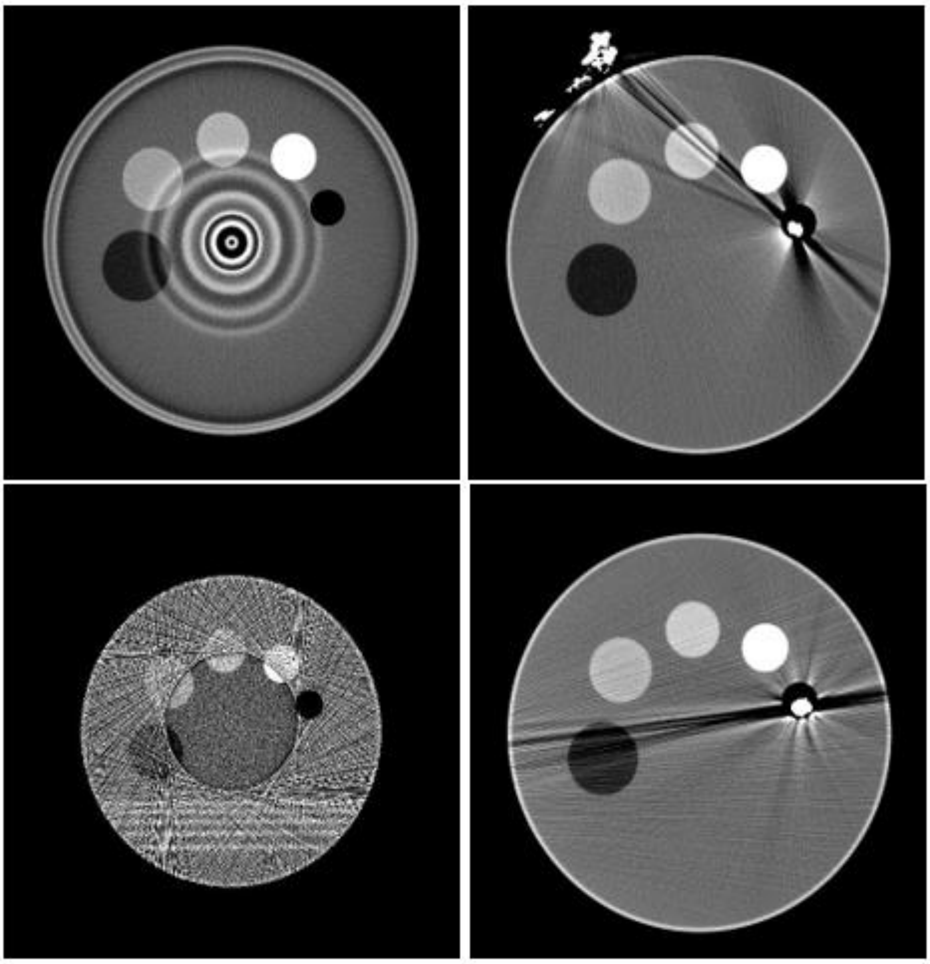

Figure 3.4: Image samples taken from a Toshiba CT scanner.

Figure 3.4 outlines the image quality, reconstruction speed, and installation procedures from the images obtained from the CT scanners to produce favourable results. It is, however, seen that the artefacts get rigid due to patient motion, and this often significantly degrades image quality [62]. Additionally, the images outlined in Figure 3.4 were acquired without metal or distortions ("baseline images"), with metal and hard material distortions, disconnected detector boards, and/or disconnected power supplies to create visible artefacts ("artefact images").

3.3.2 Toshiba (TOS) phantom identification.

The TOS phantom is a testing apparatus that measures the Hounsfield Units (H.U or CT number) of the different density representations in the human body, standard deviations, and in some instances, linearity. The various materials representing the human body include air, representing air, Delrin representing bone, acrylic representing new blood, nylon representing old blood, polypropylene representing lungs, and water representing water.

The TOS phantom is ideal for use to evaluate artefacts, especially their features that closely represent clinical conditions. This is true because, in many instances, artefacts are visible in conditions outside the clinical aspect for which engineers are responsible for fault-finding and evaluation purposes, as outlined in Figure 3.5.

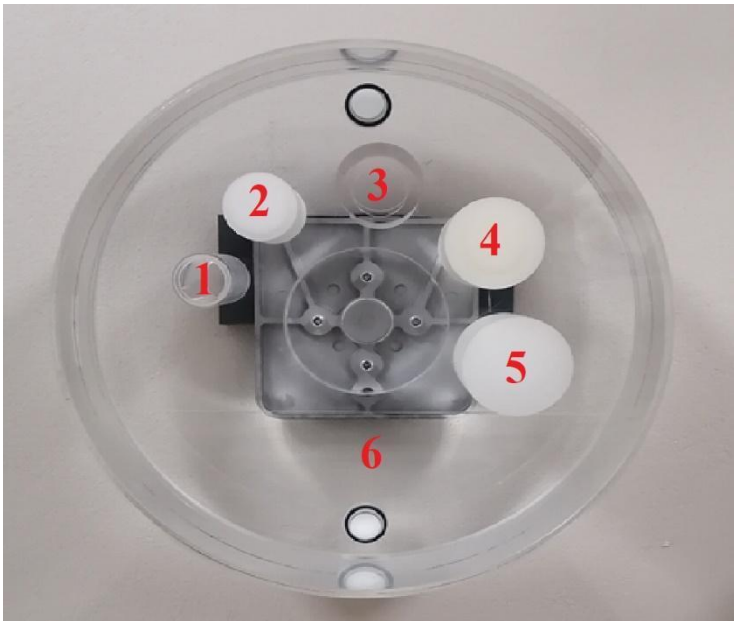

Figure 3.5: TOS phantom. The numbers represent the Region of Interest (ROI) to measure the CT number/HUs, standard deviation. ROI 6 has a wide range to measure the HU, uniformity, and linearity [63].

The CT number/HUs ROIs: 1 to 6, range between the following values as presented in Table 3.2.

Table 3.2: Material ROIs representation.

ROI (Region Of Interest) Material	**Anatomical Representation**	**Range of CT Number/HU values**
1. Air	Air	-1020 to -975

2. Delrin	Bone	330 to 350
3. Acrylic	New blood	115 to 135
4. Nylon	Old blood	90 to 110
5. Polypropylene	Lungs	-115 to -95
6. Water	Water	-5 to 5

The TOS phantom was scanned with and without metal and other hard materials in peripheral locations to create three types of artefacts: 1) ring artefacts; 2) metal artefacts and 3) streak artefacts. All the scans were repeated multiple times to investigate the reproducibility of artefact creation methods as well as for having a dataset for the process of machine learning and image corrections.

The TOS phantom images (baseline and artefacts) were analysed for the following evaluation criteria: CT number accuracy and severity of artefacts meaning noise, contrast, linearity, and uniformity for three states: baseline images, artefact images (metal artefacts, ring artefacts, and streak artefacts) and corrected images. Figure 3.6 gives more context on the scanned TOS phantom representing four of the five eventual cases for this research study relating to Figure 3.1 namely: a) a baseline image, b) metal artefact, c) ring artefact, and d) a streak artefact.

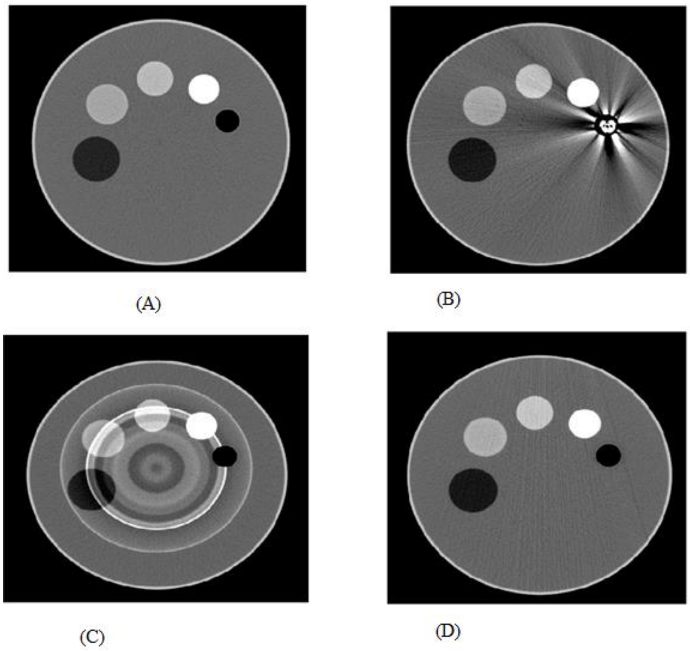

Figure 3.6: Illustration of TOS phantom under research conditions (A) Baseline image of TOS phantom (B) Metal artefact caused by iron rods in the air space (C) Ring artefacts (D) TOS phantom showing streak artefact.

3.4. System modelling and data acquisition process.

After the data were collected as outlined in section 3.3, the machine learning algorithm was implemented using Python programming language integrated with machine learning and computer vision-based algorithms and libraries such as: a) TensorFlow; b) OpenCV; and c) Keras.

- Tensorflow™ – this software is utilised as a machine learning software.
- OpenCV – utilised for image processing and detection.
- Keras library – a library interface for Tensorflow™ and is utilised as a supporting library for machine vision.

These algorithms utilise a CUDA-based Graphical Processing Unit (GPU) that allows for parallel computing provided by the GPU. The system implementation algorithm relied on the following hardware system parts:

- AMD Ryzen 5 1600 3.4 GHz six-core processor
- NVIDIA GeForce GTX 1660 Ti 1.86GHz, 6 GB GPU

- 16GB DDR4 RAM

Furthermore, the system model setup is outlined providing the following as presented in Figure 3.7:

- image data collection and preparation.
- data creation and model training.
- image testing; and
- model evaluation.

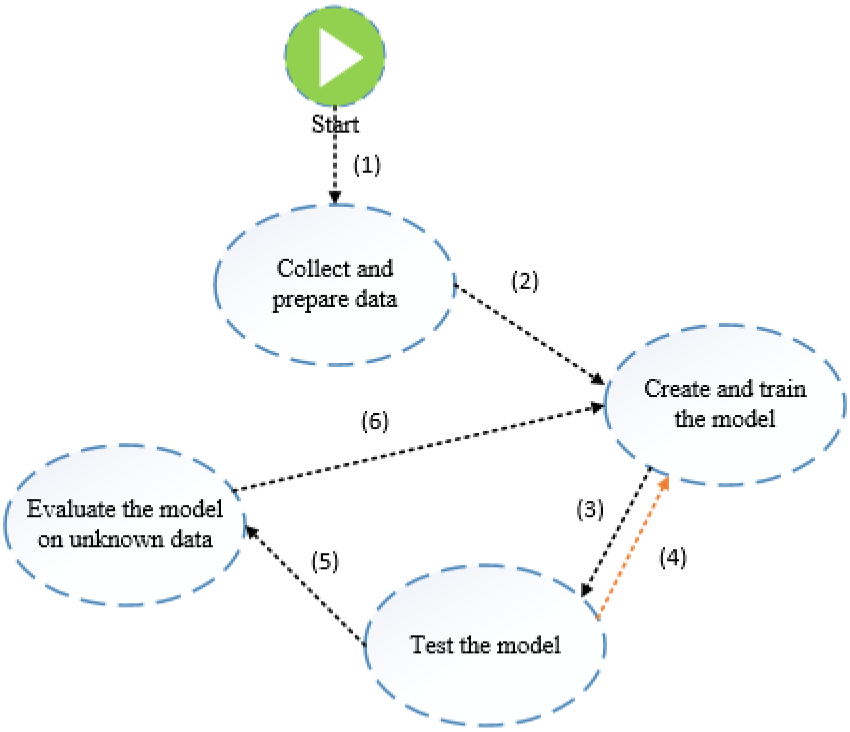

Figure 3.7: Model setup framework.

Figure 3.7 presents the model framework by outlining the start of the project and how the data were collected for the model. The data were collected by scanning an image with Toshiba equipment and manually checking the image against the scanner datasheet to identify the type of artefact. Upon noting the type of artefact, a folder was created, and images were multiplied to reach 85 image samples. They were then copied into the folder per artefact type (i.e. metal artefact and ring artefact). In this research study, the researcher took 88 image samples per investigated artefact as an input dataset. However, no scientific model or principle was utilised for image sampling size, and it was the prerogative of the researcher to estimate the image sample number.

From the different image datasets, a model was created where the system was trained and tested as per the algorithm setup (2, 3, 4, 5, 6) as depicted in Figure 3.7. The initial process flow was to collect and prepare data. The images of the different artefacts were taken and placed into a folder, and the folder was labelled per artefact, i.e. ring artefact. The model algorithm was created based on the convolution model and the input datasets were trained. The model training took 50 iterations and post the iterations, the model was tested, and the output evaluation and the system resilience and accuracy were also tested.

The system was trained and tested against a set of reconstructed image datasets and solutions. The system was trained with 50 iterations using machine learning techniques. Upon the completion of the iteration, the system or model was tested and evaluated against the unknown data. The system model was evaluated based on the Figure 3.7 design model on the unknown data, and this data was then used to determine the artefact type and possible solution(s).

Additionally, Figure 3.7 explains the “collect and prepare data” phase, with reference to the image size. The image size used was 512X512 pixels per image, with the image dataset only focusing on metal artefacts and ring artefacts as outlined in Figure 3.8.

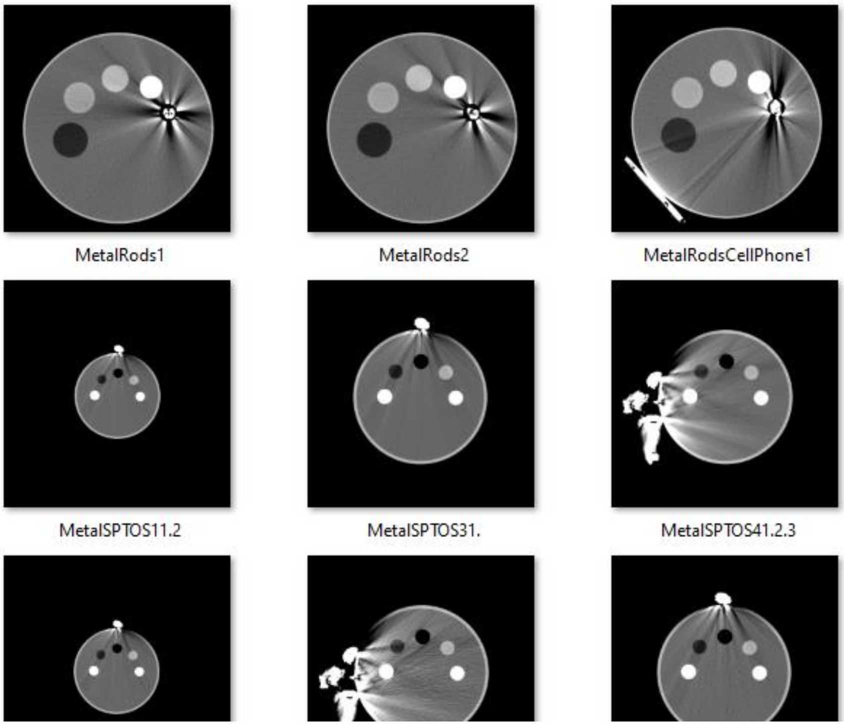

Figure 3.8: Metal artefact images 512X512 pixels.

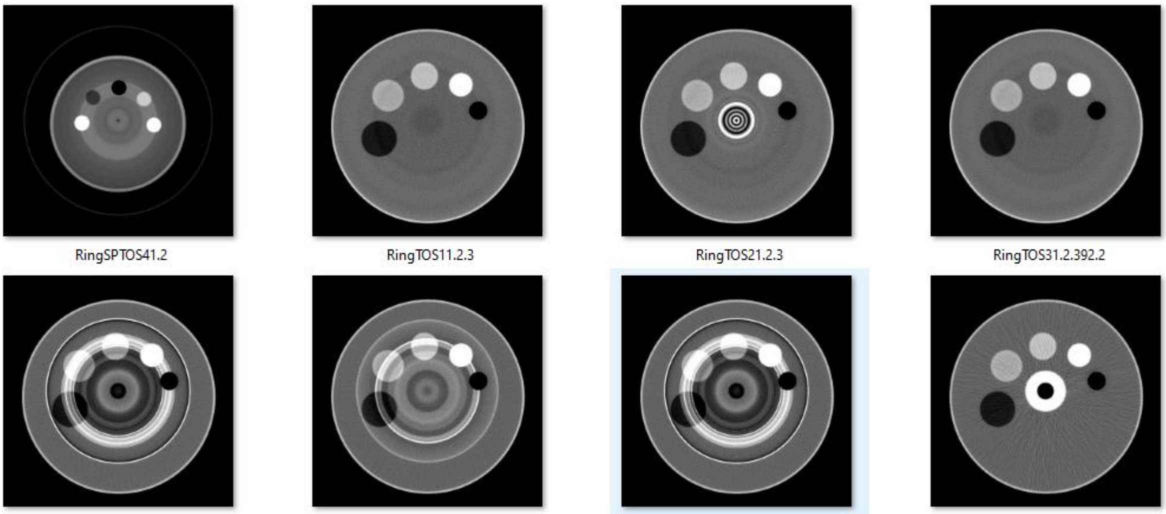

Figure 3.9: Ring artefact images 512X512 pixels.

In the collect and prepare data phase, the two images as outlined in Figures 3.8 and 3.9 were copied into a single folder to create an image dataset. This image dataset comprises raw data, as a result, the enhancement of the datasets was accomplished by utilising and applying filters to allow for machine vision application to detect artefacts without any system optimisation. However, this approach is not scientific, has not been confirmed, and was conducted on a trial-and-error basis. Furthermore, this does not contribute to the significance of this research study.

Figure 3.10 Data organisation structure.

Figure 3.10 presents the data organisation structure. This structure is saved in a directory and split into different datasets for testing, training and evaluation, and these folders are pulled into Tensorflow^{TM} software. The results of the datasets are then transposed into a graphical format.

The data collected contain 85 images in the dataset that are organised as follows:

- ring artefact - training with a maximum of 85 images for data testing with 19 iterations.
- metal artefact - training with a maximum of 85 images for data testing with 19 iterations.

The model training is created in figures 3.9 and 3.10 to allow the model to learn by identifying the different features within an image and to automatically detect the artefacts and present the type of artefact that is identified. Figure 3.10 outlines the feature detection for a metal artefact, while Figure 3.11 outlines the feature detection for the ring artefact.

The trained model construction makes use of the convolution neural networks as indicated in Figure 3.11. However, before the input dataset can be added to the model, the dataset height and width in terms of images are adjusted as follows:

```
img_width,img_height=512,512
```

Following this process, the convolution is applied to the model as indicated in Figure 3.11.

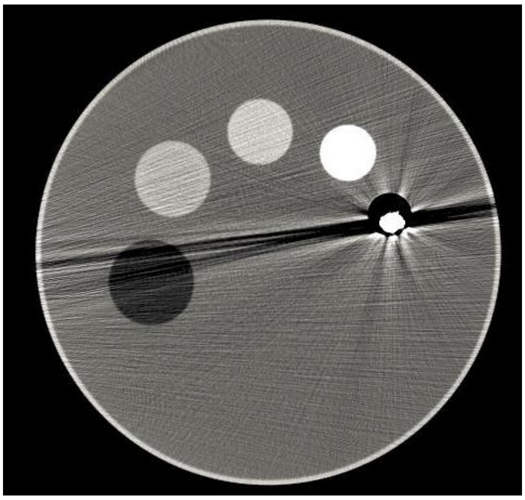

Figure 3.11: Trained image model.

Figure 3.11 depicts the trained image model through the operations as follows: a convolution operation is applied to the input dataset that then passes the results to the next layer. The reason for applying convolution in this context is to convert all pixels in its receptive field into a single value. Upon the successful application of convolution, max pooling is applied to the pixel value of the dataset. Max pooling is an operation that calculates the maximum value for patches of a feature map and uses it to create a down-sampled (pooled) featured map.

Furthermore, the activation function is then applied, with the Relu function as indicated in the algorithm model setup for the activation function that overcomes the vanishing and the image gradient problem, allowing models to learn faster and perform better. The high-level code was implemented for locating the images in the datasets for both the training data and the validation data. Upon locating the data, the feature learning model is applied to the data by first resizing the image's width and height before the convolution is applied.

The application of convolution is to differentiate the two artefacts based on their features. The system is trained and tested against a set of reconstructed image datasets and solutions. The system is trained with 85 images using machine learning techniques. Upon the completion of the iteration, the model is tested and evaluated against the unknown data to test for accuracy. The system model is evaluated (5) on the unknown data, and this data is then used to determine the artefact type and possible solution.

(a)  (b) 

Figure 3.12: (a)-(b): Metal artefact detection.

Figure 3.12 (a-b) depicts the metal artefact detection in a model after applying convolution into the dataset. Convolution is defined as a process for adding each element of the image to its local neighbours weighted by the kernel filter. Metal artefacts are seen by an organogram-like model.

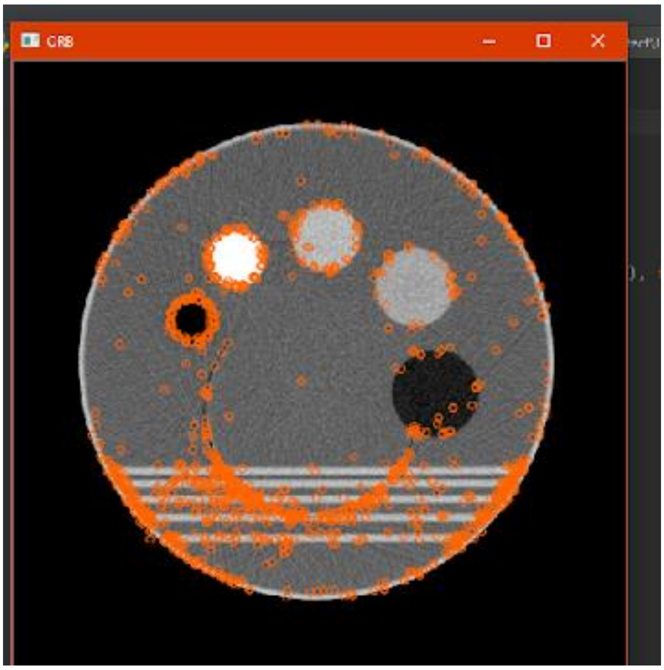

Figure 3.13: Ring artefact detection.

Figure 3.13 depicts the metal artefact detection in a model after applying convolution into the dataset where the neighbours are weighted by the kernel filter. The ring artefact is seen by circles that formulate a smile-like face.

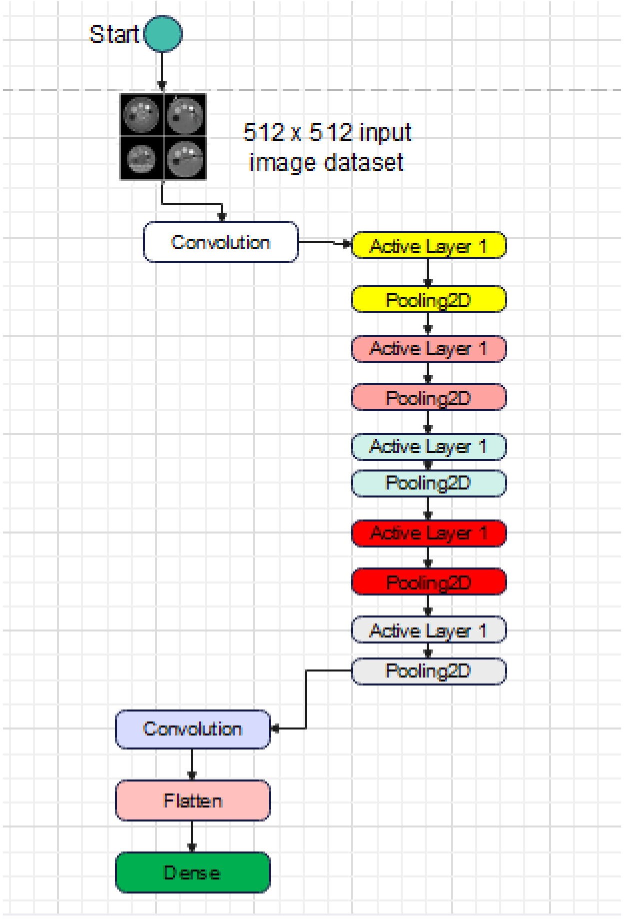

Figure 3.14: Model flow diagram.

Figure 3.13 depicts the data collection and data preparation model. The input dataset is applied to the model in the convolution layer. Upon the successful application of the convolutions, the process is highlighted at the activation layer and Pooling2D. Additionally, the features are also applied in the convolution layer and the layer is placed in flattening and dense mode, and as a result, the modelling is achievable. Furthermore, Figure 3.14 presents the model sequencing approach based on the architectural summary where the layer types, output shape and the model sequential output depict the linear model execution.

3.5. Database modelling and transfer learning implementation.

Data modelling is a critical part of a dataset as the data must be captured, compiled, and stored in a dataset. In the previous subsections, the data modelling has been completed and simulated. It is crucial to incorporate transfer learning in such a research study to have conclusive results. Figure 3.15 depicts the sequential model approach for transfer learning.

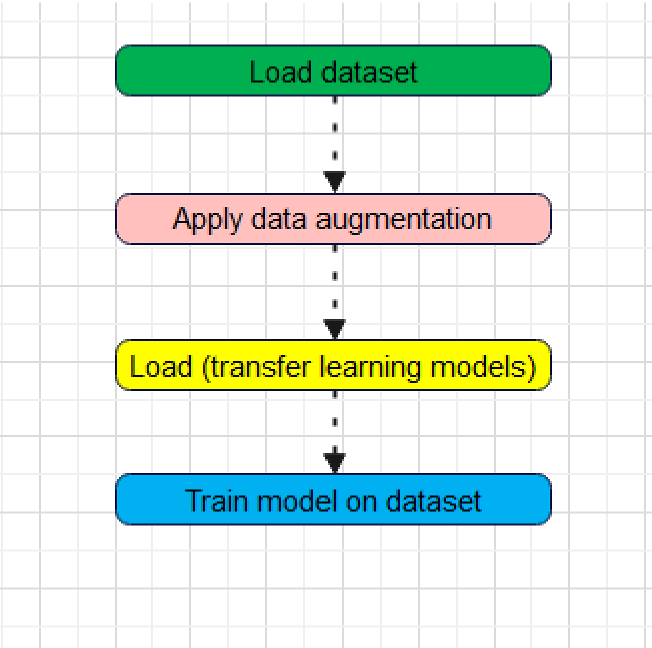

Figure 3.15: Transfer training process.

Transfer learning in this research study was carried out by applying the process model outlined in Figure 3.16. The actual processed dataset from the initial captured and processed dataset was loaded into the transfer model. The dataset upload was conducted as follows:

```
train_data_dir='Dataset/train'
validation_data_dir='Dataset/test'
```

Two test datasets were placed on two different directories, namely 1) a train dataset, and 2) a test dataset, to have a distinction between a trained dataset and a test dataset. The dataset was split into two different folder structures as indicated in Figure 3.15.

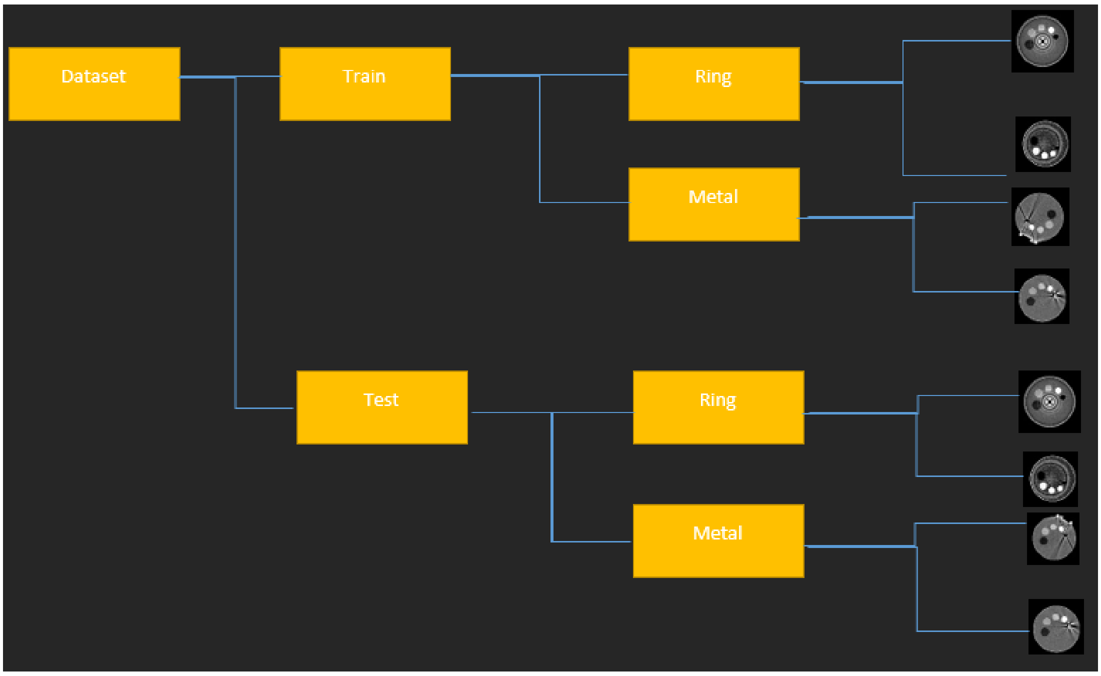

Figure 3.16: Dataset arrangement folder structure.

The data from the dataset were split into two datasets both having ring and metal artefacts. In splitting the datasets, the image data generator automatically labels all the data inside the ring folder as “ring folder”, and the data in the metal folder as “metal folder”. This allows data to be passed easily to the neural network. Furthermore, the model summary presents the Tensorflow^{TM} output based on the model construction. The model construction correlates with the reference to Figure 3.16 post the simulation.

3.5.1. Data augmentation.

Data augmentation is the process of artificially generating new data from existing data, primarily to train new machine learning (ML) models. Data augmentation artificially increases the dataset by making small changes to the original data [64]. The main objective relates to the use of augmented data as an equaliser to reduce the potential overfitting of the trained models. The use of this technique was to primarily handle two problems that may cause poor model performance hence the optimisation was conducted on all the four tested algorithms. The reason behind the use of data augmentation is due to a low number of initially trained datasets which in the context of this research study is 85 and 88 samples respectively intending to increase the model accuracy [*Annexure F*].

The utilisation of the image data generator is to easily import data with labels into the model. It is a useful class with many functions such as rescale, zoom, flip, and rotate, and as such the application of this class does not affect the data stored on the disk. This class's advantage is to further alter data on the go while passing data parameters into the model.

The code below outlines the data flow in this class:

Data augmentation is a statistical technique which allows for maximum likelihood estimation from incomplete data [65]. In the context of this research study, data augmentation is constructed in a way that the model should not overfit. Overfit is when the model gives accurate prediction on training data but gives inaccurate prediction on new data. Two methods of data augmentation are used;

- The first method is to transform the original data and store both original and transformed data in a folder.
- The second method is to use the Image Data Generator class to transform data, this generates data on the fly, which means it generates new instances of data each epoch, which allows the network to better generalize.

In addition, the second method was applied in the algorithm of this research study.

Data augmentation in this research study consists of the following transformations:

- Rescale the data.
- Vertical and horizontal shift.
- Image shearing.
- Image zooming.
- Horizontal flip.
- Vertical flip.

Code for augmentation of trained data [*Annexure H*].

Code for augmentation of testing/validation data.

Augmentation on the testing/validation data has only rescaling.

```
test_datagen = ImageDataGenerator(rescale=1. / 255)
```

Generating data with augmentation of trained data

```
train_generator = train_datagen.flow_from_directory(
    train_data_dir,
    target_size=(img_width, img_height),
    subset='training',
```

```
    batch_size=batch_size,
    class_mode="categorical")
```

vgg16 takes an image size of **224** width and **224** height.

```
img_width,img_height=224,224
```

```
batch_size=32
```

The batch size is 32, which means that every epoch generates 32 instances of the original image.

The dataset consists of 85 images of ring artefacts, which means that having $85 \times 32 = 2720$ instances, and 88 images of metal which adds up to $86 \times 32 = 2752\ instances$.

3.5.2.VGG16 data loading model.

VGG16 is a sequential model that is for transfer learning in the context of this research study.

```
model=Sequential()
```

This model consists of two convolution layers of 64 channels of 3X3 kernel with three convolution layers of 256 channels. Furthermore, three convolution layers of 512 channels of 3X3 kernel of 512 channels were also used with one maxpool layer of 2X2 pool size and 2X2 stride.

```
model.add(Flatten())
model.add(Dense(4096))
model.add(Activation('relu'))
```

After this code has been applied, the rectified linear unit activation was added to each layer to filter negative values so that they are not passed to the next layer, as follows:

```
model.add(Dense(2))
model.add(Activation('softmax'))
```

Furthermore, the dense layer of about 4 096 units and one dense softmax layer of two units were added to the model. Softmax has two layers to predict both ring and metal artefacts, and the results are based on “0” and “1” output based on the confidence “pf” of the model at each class.

To contribute to the loss and accuracy results, the determination was conducted by applying the “Loss function” where the categorical cross entropy was calculated as indicated in equation 4.1.

$$CE = -\sum_{i}^{c} t_i \, log(s_i) \qquad (3.2)$$

Where:

CE = Cross-Entropy loss

t_i = truth label

S_i = ground-truth

The accuracy results are as follows:

$$A(\%) = \frac{yPrediction}{yTime} * 100 \qquad (3.3)$$

```
from keras.optimizers import Adam
opt=Adam(lr=0.001)
```

Adam optimiser is also used to reach the global minima while training the model. This gives a learning rate of approximately 0.001. This learning rate decreases if the training bounces a lot on the epochs so that it can reach global minima.

Additionally, VGG16 model is loaded as follows:

```
from keras.applications import VGG16
```

then, the VGG16 pre-trained model is loaded as indicated below:

```
vgg16_base=VGG16(weights='imagenet',include_top=False,input_shape=(224,224,
3))
```

also, to make the model non-trainable, the following code is used;

```
vgg16_base.trainable=False
```

Addition of the last code into the last layer of the VGG16 model.

```
model=models.Sequential()
model.add(vgg16_base)
model.add(layers.Flatten())
model.add(layers.Dense(50,activation='relu'))
model.add(layers.Dense(20,activation='relu'))
model.add(layers.Dense(2,activation='softmax'))
```

3.5.3. Dataset train model

The data training and data testing are based on the below code snippet, and this evaluates the accuracy of the model detection between the trained model dataset and test model dataset.

```
model.compile(loss='categorical_crossentropy',
          optimizer=opt,
          metrics=['accuracy'])
```

```
history=model.fit_generator(
    train_generator,
    steps_per_epoch=nb_train_samples // batch_size,
    epochs=epochs,
    validation_data=validation_generator,
    validation_steps=nb_validation_samples // batch_size)
classes=train_generator.class_indices
```

The comparative analysis when investigating the model accuracy. The two tests' datasets were placed on two different directories, namely 1) a train dataset; and 2) a test dataset to have a distinction between a trained dataset and a test dataset. The reason for the introduction and presentation of figures is for the visual overview of the model structure design and its impact. Furthermore, in processing the convolution model, the data size acted as the basis for utilisation of 50 epoch, which demonstrates the system's resilience and model accuracy – hence, no need for epoch testing optimisation based on the study objectives and research question.

3.6. Chapter Summary.

In this chapter, the process for image training and learning utilising image processing and machine learning techniques and algorithms were presented. Based on the initial algorithm of utilising the custom CNN algorithm, Dataset_1 and Dataset_2 was formulated from Toshiba CT scanner equipment for both ring and metal artefacts in a stage called collect and prepare data. The model approach for code optimisation and training based on the epoch sizes for utilising machine learning and image processing techniques by identifying the features from the images and allowing the model to learn by itself for 19 iterations, was used based on the custom CNN algorithm. The model iteration value size was based on the system accuracy on the 25 and 50 epochs which resulted in 19 iterations being sufficient for such a model. In developing the system model, TensorFlow™ software was utilised for machine learning where the system was trained and deployed, with the functionality for image dataset processing and artefact detection, while Keras software was used for machine learning interface.

The results were obtained and evaluated. To have a comparison results model, a new model-based on transfer learning was developed. The transfer learning model was based on three models namely, a) VGG16 algorithm, ResNet50 algorithm and inception_V3 algorithm were developed through data augmentation. Two sets of datasets “train and test” were simulated, and the results were produced.

CHAPTER IV: RESULTS AND DISCUSSION.

This chapter presents the results obtained from the model developed in Chapter III. Firstly, the results are compared against the study objectives and the research question, and an analysis matrix is developed to test if the results correlate with the study's objectives. Secondly, the results are analysed based on the developed model and they are uniformly presented for both ring and metal artefacts.

4.1. Introduction: The formulation of results analysis.

This chapter outlines the results of the two artefacts, namely ring and metal artefacts. The experiments were conducted by developing a machine-learning model that was trained and evaluated. The simulation output results are evaluated based on the number of images used in this research study. Chapter 1 (section 1.4) outlines the use of 85 input images. However, this number was the prerogative of the researcher, and based on the preliminary results the number can increase to evaluate the accuracy of the system.

This chapter further presents the results evaluating if the research study objectives are met, citing the feasibility (possibility) for the development of an AI artefact identifier and differentiator.

4.1.1. Experimental results.

There were three different experimental results performed in this research study each was performed independently and upon getting the results, the consolidated results comparison section was formulated.

4.1.1.1. Experiment 1 results.

Experiment 1 results look at the modelling of both Dataset_1 and Dataset_2. Upon the creation of the two datasets, a custom CNN machine learning algorithm is developed, and the initial simulation is based on the training of the two datasets in the model. Once the researcher was satisfied with the training model results based on 19 iterations, test model was then simulated with both datasets and the results are presented in Figures 4.1 (a and b) based on the 25 epoch. However, the results were tested for 25 and 50 epochs for both Dataset_1 and Dataset_2.

4.1.1.2. Experiment 2 results.

Experiment 2 results look at the modelling of transfer learning. Upon obtaining the results from Experiment 1, a learning transfer model was developed for three different algorithms namely, VGG16, ResNet50 and Inception_V3. These three algorithms were evaluated independently and upon obtaining the results, the VGG16 was compared against the custom CNN as indicated in Table 4.2. Once this experiment results were completed, a comprehensive comparison between the three transfer learning models and custom CNN were presented as depicted in Table 4.3. The performance of these models were evaluated both examining the loss and the accuracy of the models.

4.2. Preliminary accuracy testing results.

Based on the model output sequencing and accuracy testing, Dataset_1 was tested, and both the accuracy and loss were determined. The preliminary results are outlined as indicated in Figures 4.1 (a) and (b). Furthermore, the model summary indicates that the testing comprises a sequence that evaluates each iteration and produces an output loss and accuracy per test.

Once the test is complete, a summary percentage of the losses vs. accuracy is compiled as indicated in Figures 4.1 (a) and (b).

The results below present the model test based on the epoch test out of 50 tests. During simulation of these results, the duration it took for the execution of each epoch is presented as well as the accuracy and losses of data. The total summation of accurate and lost data is then translated into graphical output results for the 50 epochs as presented in Figures 4.1 (a-b).

(a)

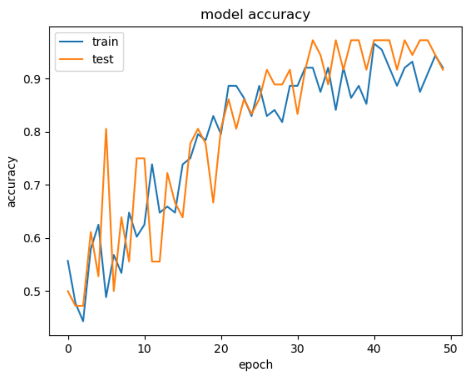

(b)

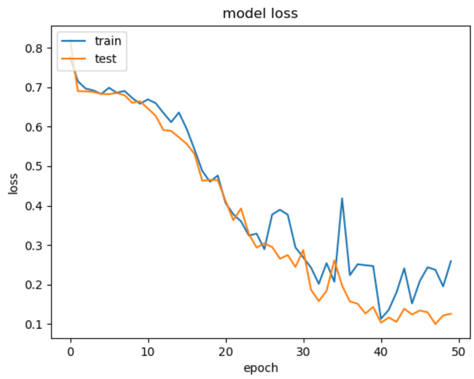

Figure 4.1: (a) Custom CNN model accuracy (b) model loss.

Figures 4.1 (a) & (b) depict the model output accuracy and loss graphs. The tests were conducted and based on the epoch results of the 88 images utilised for machine learning. Subsequently, the model evaluates how close and accurate it is to predicting the correct output - in the context of this study being the correct artefact and solution prediction. Furthermore, the epoch depicts the number of times the model goes through test data. Additionally, the model accuracy depicts how close the model is to predict the correct output in a percentage per image dataset, noting that this research study comprises of two datasets namely Dataset_1 and Dataset_2. This enables accurate differentiation between artefacts.

4.3. Transfer learning modelling results.

The reuse of dataset results within this research study has been very impactful towards the conclusion of the results. The results outlined depict the image classification utilising transfer learning. The reason for image classification is to solve pressing issues of identification and recognition accuracy. As a result, transfer learning was used to evaluate the accuracy of the results against the author model results. The VGG16 model comprises 25, 30, 35, and 40 epoch tests.

Layer (type)	Output Shape	Param #
input_1 (InputLayer)	[(None, 224, 224, 3)]	0
block1_conv1 (Conv2D)	(None, 224, 224, 64)	1792
block1_conv2 (Conv2D)	(None, 224, 224, 64)	36928
block1_pool (MaxPooling2D)	(None, 112, 112, 64)	0
block2_conv1 (Conv2D)	(None, 112, 112, 128)	73856
block2_conv2 (Conv2D)	(None, 112, 112, 128)	147584
block2_pool (MaxPooling2D)	(None, 56, 56, 128)	0
block3_conv1 (Conv2D)	(None, 56, 56, 256)	295168
block3_conv2 (Conv2D)	(None, 56, 56, 256)	590080
block3_conv3 (Conv2D)	(None, 56, 56, 256)	590080
block3_pool (MaxPooling2D)	(None, 28, 28, 256)	0
block4_conv1 (Conv2D)	(None, 28, 28, 512)	1180160
block4_conv2 (Conv2D)	(None, 28, 28, 512)	2359808
block4_conv3 (Conv2D)	(None, 28, 28, 512)	2359808
block4_pool (MaxPooling2D)	(None, 14, 14, 512)	0
block5_conv1 (Conv2D)	(None, 14, 14, 512)	2359808
block5_conv2 (Conv2D)	(None, 14, 14, 512)	2359808
block5_conv3 (Conv2D)	(None, 14, 14, 512)	2359808
block5_pool (MaxPooling2D)	(None, 7, 7, 512)	0

Based on the convolution parameters outlined, Table 4.1 depicts the transfer learning results. The results presented outline the accuracy and data loss from the initial model that is now used in transfer learning. The test epoch correlates with the initial model tested epochs to have balanced evaluation criteria and results.

Table 4.1: VGG16 experimental output results.

Number of images in dataset	**Accuracy**	**Loss Graph**	**Results**
Dataset_1	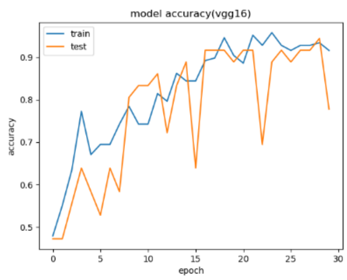	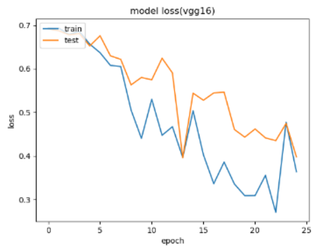	**Trained Model** 93% accuracy 43% loss **Testing model on test data** 91% accuracy 41% loss Number of epochs is 25
Dataset_1	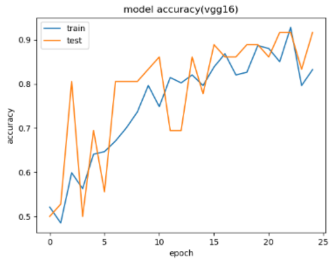	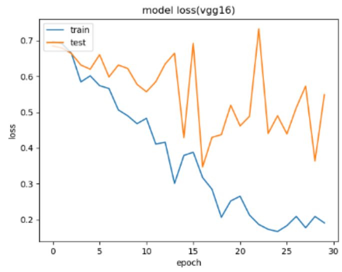	**Trained Model** 90% accuracy 20% loss **Testing model on test data**

			91% accuracy 53% loss Number of epochs is 30
Dataset_2	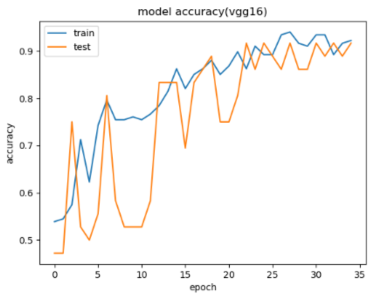	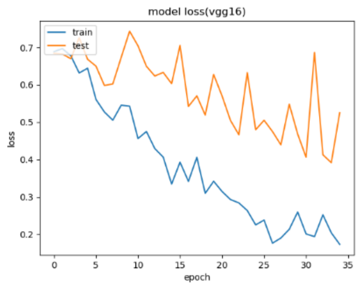	**Trained Model** 90% accuracy 22% loss **Testing model on test data** 90% accuracy 54% loss Number of epochs is 35
Dataset_2	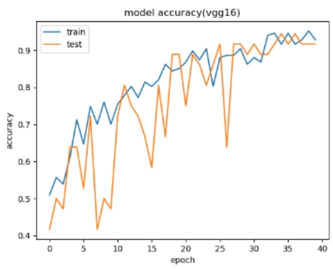	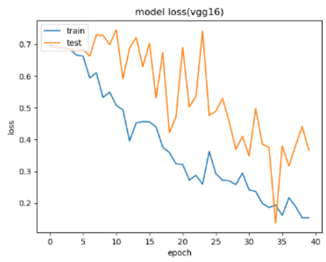	**Trained Model** 96% accuracy 15% loss **Testing model on test data** 91% accuracy

			45% loss Number of epochs is 40

The results from Table 4.2 demonstrate the research findings as follows: Firstly, the two sets of image datasets namely Dataset_1 and Dataset_2 were evaluated with 25 epochs up to 40 epochs respectively for both the trained model and the testing model.

The results demonstrate that the more images contained in the dataset, the higher the accuracy. However, the resilience of the algorithm is critical. For example, for Dataset_2 at 40 epochs the model accuracy is high with a threshold of a successful model at 75%, but the model losses are more than 40%.

Furthermore, Table 4.2 presents the comparison between the VGG16 against the author model.

Table 4 2: Model comparison between VGG16 and custom CNN model.

Custom CNN model accuracy	VGG16 model accuracy	Model results

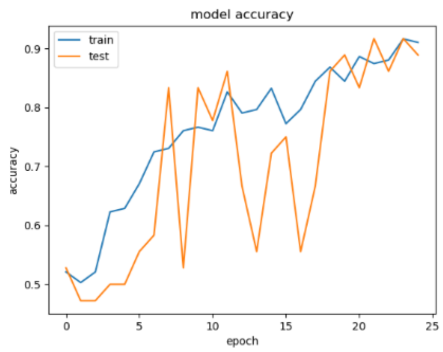	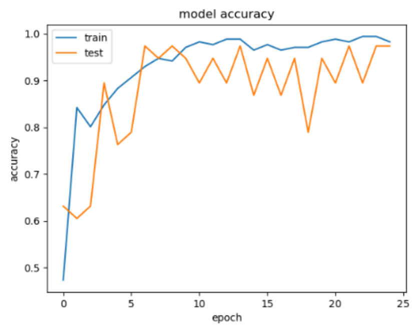	**Trained Model** 92% accuracy custom CNN 94% accuracy VGG16 **Testing model on test data** 91% accuracy custom CNN 90% accuracy VGG16 Number of epochs is 25
Custom CNN model loss	**VGG16 model loss**	**Model results**
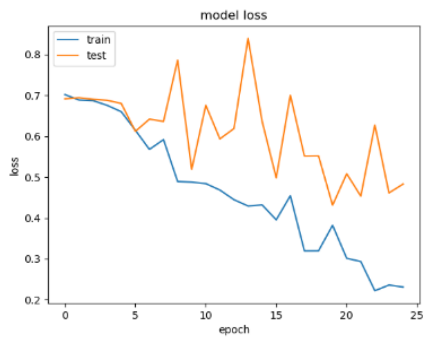		**Trained Model** 25% loss custom CNN 16% loss VGG16 **Testing model on test data** 61% loss 18% accuracy Number of epochs is 25

Table 4.3 demonstrates the losses and accuracy between research and the VGG16 model. Based on the data provided, the VGG16 experienced a loss lower than 20% both on the trained and testing data against the 18 & 25% of the custom CNN model. This is due to the stability of the model as VGG16 presents the secondary model. Additionally, VGG16 further demonstrates stability with 94 and 90% concurrently with the custom CNN model demonstrating 92 and 91% accuracy.

Two additional models were further added as indicated in Table 4.3 as presented. Table 4.3 demonstrates that the VGG16 is performing better than the three models on the training results, while the inception_V3 performance is better on the test model accuracy. Furthermore, ResNet50 experience high number of losses on the trained data as opposed to the other three model. Additionally, the ResNet50 model has shown a lower level of loss amount in the test data.

Table 4.3: Model comparison results output between c *r learning models.*

Custom CNN model accuracy	VGG16 model accuracy	Inception_v3 accuracy	ResNet 50 model loss
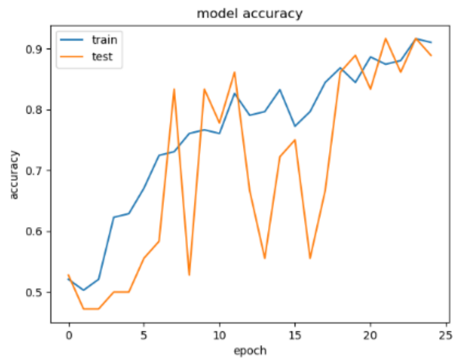	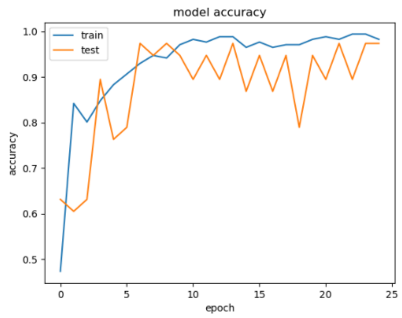	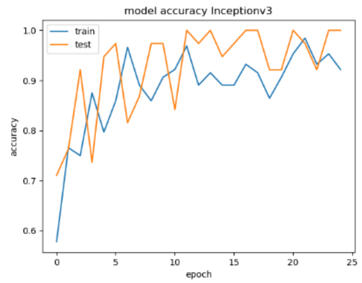	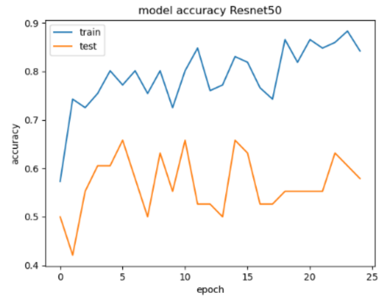
Custom model loss	VGG16 model loss	Inception_v3 model loss	ResNet 50 model loss
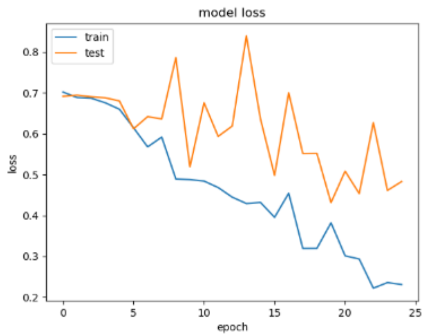	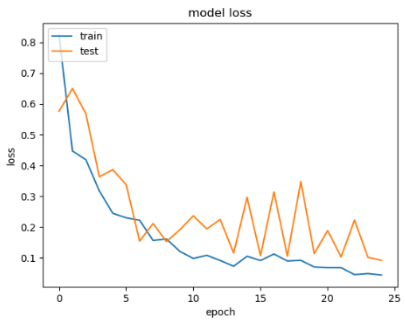	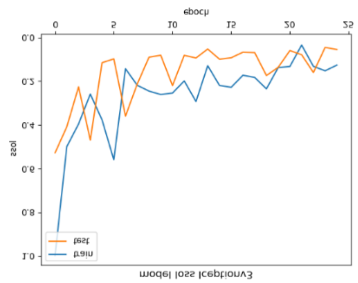	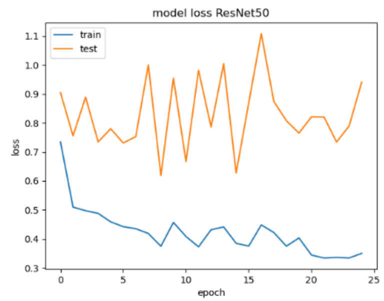

4.4. Comparative analysis against the study objectives.

Artefacts can seriously degrade the quality of CT images - in some instance to the point of making diagnostics unusable. However, to optimise image quality, it is necessary to understand why artefacts occur and how they can be prevented or suppressed. CT artefacts originate from a range of sources. CT image artefacts are plenty, and the same should be said for their fault-finding techniques. There are many different types of CT image artefacts, including noise artefacts, beam hardening, scatter, motion, metal and ring artefacts.

The general approach in artefact evaluation makes use of analytic clinical data (patient scan). This approach is recommended to try to reproduce the artefact using a test phantom or just air in the scan field. However, this approach has led to the conduct of this research study, which aimed to develop an automated model that can be used to identify different artefacts without any human intervention.

Table 4.4 depicts the output results obtained during the testing phase.

The tested results in Table 4.4 are results that are obtained from both experiment 1 and 2 between the custom CNN and VGG16. The reason for this presentation of custom CNN and VGG16, is that the custom CNN is treated as the author primary model design with VGG16 as the primary transfer learning model.

Table 4.4: Custom CNN study results output based on different epoch tests.

Number of images in dataset	**Accuracy**	**Loss Graph**	**Results**

Dataset_ 1	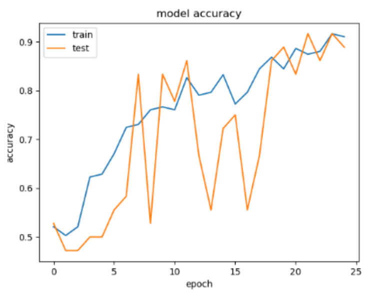 	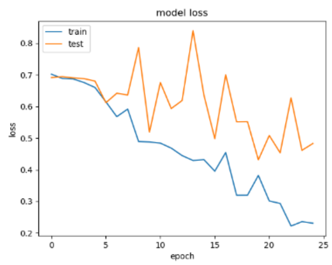 	**Trained Model** 89% accuracy 21% Loss **Testing model on test data** 87% accuracy 49% loss Number of epochs is 25
Dataset_ 1	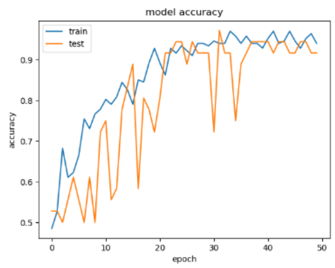 	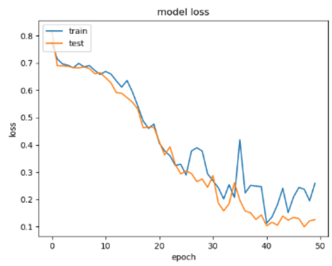 	**Trained Model** 94% accuracy 21% Loss **Testing model on test data** 91% accuracy 15% loss Number of epochs is 50
Dataset_ 2	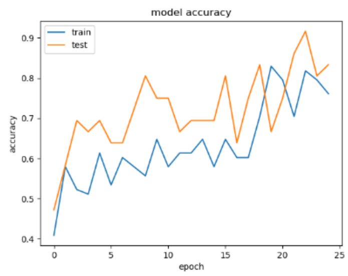 	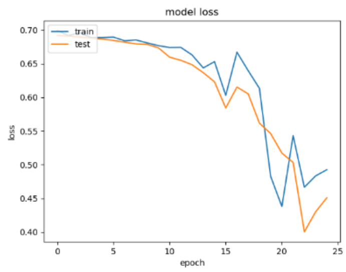 	**Trained Model** 75% accuracy 47% Loss **Testing model on test data** 80% accuracy 45% loss

			Number of epochs is 25
Dataset_ 2	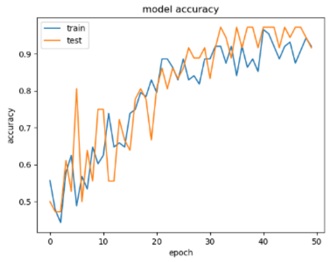	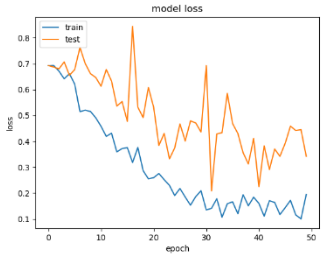	**Trained Model** 91% accuracy 21% Loss **Testing model on test data** 90% accuracy 31% loss Number of epochs is 50

Table 4.4 depicts the research findings as follows: Firstly, Dataset_1 with 25 epochs and Dataset_2, with 50 epochs respectively. Table 4.4 presents both the trained model and the testing model.

For Dataset_2 with 25 and 50 epochs, the results demonstrate that Dataset_2 with both ring and metal artefacts were trained, and for 25 epochs the data accuracy was 75% with 47% loss, while for 50 epoch the data accuracy was 94% with approximately 21% loss. When these results were translated to the actual tested model, the accuracy was 90% with approximately 31% loss. This demonstrates the stability and reliability of the model beyond 90% between the trained and the tested data. Furthermore, for 25 epochs the results demonstrate the decline in the model accuracy for trained input datasets at 89% accuracy, which is 1% lower than the 50 epochs. However, the losses remain the same at 21% for both epochs. Additionally, for the tested model, the model accuracy is reduced to 87% with approximately 49% accounting for the losses for the 25 epoch, representing a 4% decline in the accuracy results and a 6% improvement in the loss area.

4.5. Chapter summary.

In this chapter, the detailed analysis of the developed model was discussed. The initial model results demonstrate the robustness of the model testing. Dataset_1 and Dataset_2 were compared against each other based on the different model setups. The distinction of the image dataset was to evaluate the contribution of the image dataset size against the results both for the initial model and the transfer model. In this model the results were evaluated based on the accuracy and losses. The losses were evaluated independently of the overall model operation. The results demonstrate that the algorithm robustness does not depend entirely on the image number and size but is inclusive of the test image brightness. The initial model demonstrates the high accuracy of detection and differentiation of the different artefacts (ring and metal).

This chapter further presented the results obtained from the transfer learning model. The test results demonstrate higher data losses experienced as opposed to the initial model. This is due to the recycling of data that occurs during the use of transfer learning because of certain image features getting lost in the model. However, this does not affect the model detection and differentiation accuracy; hence, the model passed the set 75% threshold.

Additionally, two more models were evaluated namely the Inception_v3 and ResNet50 and were compared against the custom CNN model and the VGG16 model. It is seen that VGG16 performs better on the accuracy data both the test and train while the ResNet50 performs below par on the loss encountered against the other three models.

CHAPTER V: CONCLUSION AND FUTURE WORK

This chapter presents the conclusion of the research study and summarises the research findings and recommendations. The study's contributions to the broader science ecosystem and recommendations towards future research.

5.1. Summary of the research study.

Artefacts in CT images can stem from various sources and impact on quality to varying degrees. Modern scanners incorporate design features that mitigate certain types, and some can be partially positioned to adhere to best practices in scanning protocols, which remains crucial in avoiding image artefacts, particularly metal artefacts. It is worth noting that the progression toward harnessing machine learning and the broader utilisation of advanced technology in radiology is driven not only by the need to bolster diagnostic confidence, but also by the potential emergence of new clinical applications, benefiting technicians and service engineers alike.

Nonetheless, it is imperative to recognise that CT image quality comprises several components influenced by technical parameters as discussed in Chapter II. While image quality has always been a concern in radiology, achieving technically acceptable image quality discrepancies grow alongside technological advancements and the growing demand for technology such as AI in radiology. There are many trade-offs in CT image quality such as the interplay between noise, spatial resolution, and radiation dosage. Methods aimed at reducing radiation dose may entail trade-offs in image quality, including an increase in noise or a decrease in low contrast resolution. In this context, technicians and engineers can develop Computer-Aided-Diagnosis simulators for images and artefact evaluation.

The primary objective of this research study was to create an automated machine-learning-based model capable of detecting artefacts by comparing data from the trained model against actual data from the testing model. This model was developed using Dataset_1 and Dataset_2 captured from a Toshiba CT scanner. Subsequently, a Python-based machine learning model was developed for each image with dimensions of 512x512 pixels.

Based on the evidence presented in Chapter 4, this research study concludes that the model is efficient, achieving an accuracy of 87% and 91% for 25 and 50 epochs, respectively with the Dataset_1. Additionally, for Dataset_2, the model exhibited an accuracy of 80% and 90% for 25 and 50 epochs, respectively. These results align with the research hypothesis and objectives. In summary, this Chapter affirms the achievement of the study's objectives, namely:

- Demonstrating the feasibility of developing an automated artefact differentiator model with accurate results.
- Assessing the model's efficiency using an existing model and utilising the model results through transfer learning.
- Establishing the feasibility of developing and implementing an artefact-based recognition model.

5.2. Efficiency and effectiveness of the designed model - learning transfer vs. designed model.

Model efficiency was assessed based on both the losses and accuracy of the designed model and transfer learning. Both models employed an equal number of images for ring and metal artefacts. Alterations in epochs were reduced in the transfer model but did not significantly affect the output results. Efficiency was evaluated against a 75% accuracy threshold. Results indicated that both models are accurate, but the transfer model experiences higher losses due to feature losses occurring after applying linear regression and simulating the initial model.

5.3. Development of an automated artefact differentiator model.

The model was created to automatically differentiate two artefact types – ring and metal without any human intervention. The results demonstrate an accuracy rate exceeding 75%. This confirms the model's ability to identify these artefacts without human involvement. Furthermore, these results underscore the necessity for such models in medical facilities to enhance efficiency and reduce human error.

5.4. Implementation of artefact-based recognition model.

The implementation of an artefact-based recognition model is crucial in both the initial and transfer learning models. After rigorous testing at different epochs, the results affirm the conclusiveness and real impact of such a model in a medical environment.

5.5. Study limitations to images of phantoms.

What would be needed to have the model detect artefacts in CT images of head scans would be to design and fabricate a head phantom. The phantom used in the research study has 6 ROIs containing materials representing what is found in the human body from head to toe.

- The phantom is the primary equipment used to fault-find and troubleshoot real-time artefacts by technicians/engineers on a machine. Once an artefact is removed from the system, the same phantom is used for QA by the technicians and radiographers to affirm that the system is ready and good enough for medical use.
- Secondly, what would be needed to have the model detect artefacts in the CT images are real-life scans of patient scans. Obtaining these would have gone against the rule and regulation brought up by Canon/Toshiba of sharing images of patients as these images would contain personal information.

In addition to that matter, the artefacts collected for this paper were collected on the condition that the CT scanner was fully calibrated and reproducing artefacts that wouldn't affect the state of the system. In all cases, if an artefact appeared on a patient's head scan radiographers are asked to reproduce the reported artefact using the phantom in question.

For this research, the researcher focused on these two artefacts because they were reproducible without affecting the state and integrity of the CT scanner. Another factor that was considered about these two artefacts is that although they are two types (ring and metal), they do appear in other forms such as hard and soft rings, single rings, multiple rings, and those mentioned in Figure 2.12. The other artefacts as mentioned in Table 2.3 are solvable by application knowledge which the radiographers have and can repair without technical intervention such as ensuring the patients are still during scan, filter and balancing algorithms built into the system and slice selections. More artefacts could have been included however it is these two artefacts used in the research paper that will always require a technician to go to the site to fault-find and troubleshoot. The ones that would require a little extra knowledge for the engineering part of totally fixing the artefacts.

5.6. Contribution to human knowledge.

This research study has contributed to advancing human knowledge in the field of AI and machine learning by:

- Developing an automated artefact differentiator model capable of identifying metal or ring artefacts without human intervention.
- Investigating the application of machine learning algorithms to enhance operations in the medical field, particularly for technical or engineering support.
- Designing and developing an automated image-based artefact differentiator model.

5.7. Suggested future works.

While the primary research objectives were achieved, the study had limitations due to its scope and focus. As a result, the following avenues for future research are suggested:

- Comparison of images from various CT scanner manufacturers rather than just one.
- Examination of nonuniformity within images and its impact on the detection model.
- Application to real-life CT patient images.
- Development of wider detectors covering a broader range of anatomy, accompanied by advancements in technologies such as graphic card processing speed and reconstruction techniques.
- Exploration of CAD scheme design and evaluation within this model setup.

References

[1] H. Kasban, M. El-Bendary and D. Salama, “A Comparative Study of Medical Imaging Techniques,” International Journal of Information Science and Intelligent System, vol. 4, no. 2, pp. 37-58, 2015.

[2] S. Scheidegger. [Online]. Available: https://home.zhaw.ch/~scst/Biomedtec-Dateien/MedIma_Intro.pdf. [Accessed 14 01 2023].

[3] M. Tan and J. Rego, “The changing environment for imaging specialists,” The permanent journal, Advances in Imaging, 2006.

[4] H. Novak, B. Runge, Z. Keran and M. Orosnjak, “Image Artefacts in Industrial Computed Tomography,” Technical Journal, vol. 14, no. 4, pp. 434-439, 2020.

[5] Z. B, “Computer-Aided Diagnosis in Mammography Using Content-Based Image Retrieval Approaches,” pp. 829-849, 4 June 2009.

[6] J. Barrett and N. Keat, “Artifacts in CT,” Recognition and Avoidance, p. 1679, 22 June 2004.

[7] J. Thrall, X. Li, Q. Li, C. Cruz, S. Do, K. Dreyer and J. Brink, “ORIGINAL ARTICLEArtificial Intelligence and Machine Learningin Radiology: Opportunities, Challenges,Pitfalls, and Criteria for Success,” Journal of the American College of Radiology, vol. 15, no. 3, pp. 1-5, 2018.

[8] D. Umar, “MRI vs. CT Scan: A Comparative Study in Radiology Diagnosis,” Cambridge, 2023.

[9] Kim SJ, Pak K, Kim K. Diagnostic accuracy of F-18 FDG PET or PET/CT for detection of lymph node metastasis in clinically node negative head and neck cancer patients; A systematic review and meta-analysis. Am J Otolaryngol. 2019 Mar-Apr;40(2):297-305. doi: 10.1016/j.amjoto.2018.10.013. Epub 2018 Oct 23. PMID: 30473166.

[10] S. Tang, X. Tang, Y. Yang and C. Zhang, “18FDG-PET/CT for the detection of regional nodal metastasis in patients with head and neck cancer: A meta-analysis.,” Oral Oncol, vol. 51, pp. 314-320, 2015

[11] J. Marcin and P. Lam, “Medical News Today,” 8 June 2023. [Online]. Available: https://www.medicalnewstoday.com/articles/146309. [Accessed 12 March 2024].

[12] “Medical Departments & Centers,” 17 January 2024. [Online]. Available: https://www.mayoclinic.org/departments-centers/echocardiography-laboratory/overview/ovc-20442326. [Accessed 11 March 2024].

[13] D. G, “Digital Image Processing for Medical Applications,” pp. 1-459, 2007.

[14] D. A. Pollaco, "Magnetic Resonance Imaging," p. 1, 22 March 2016.

[15] K. Mollenhoff, A. Oros-Peusquens and J. Shan, "Introduction to the basics of magentic resonance imaging," pp. 1-25, 2012.

[16] "Positron emission tomography: the conceptual idea using a multidisciplinary approach," vol. 27, no. 3, pp. 195-207, August 2002.

[17] A. Amirkhanov, C. Kuhn, J. Kastner, P. Elsinga, T. Willemsen and W. Vaalburg, "Fuzzy CT Metrology: Dimensional Measurement on Uncertain Data," in 29th Spring Conference on Computer Graphics, 2013.

[18] E. Hemdan, M. Shouman and M. Karar, "COVID-19 Screening on chest images using deep learning classifiers to diagnose COVID-19 in images," 2020.

[19] M. Chowdhury, T. Rahman and A. Khandakar, "Can AI help in screening viral and COVID-19 pneumonia?," 2020.

[20] "Application of Statistical Machine Learning and Deep Learning in Diagnosis of COVID-19 through CT Images," in in 4th International Conference on soft Computing, 2021.

[21] S. Wang, B. Kang and J. Ma, "A deep learning algorithm using CT images to screen for Corona Virus Disease (COVID-19)," 2020.

[22] D. Yoon, H. Hwang, S. Chang, Y. Rho, H. Ahn, J. Kim and I. Lee, "CT, MR, US, 18F-FDG PET/CT, and their combined use for the assessment of cervical lymph node metastases in squamous cell carcinoma of the head and neck," EUR Radiol, vol. 19, pp. 634-642, 2009.

[23] "Evaluation of 18F-FDG PETCT for diagnosing cervical nodal metastases in patients with oral cavity or oropharynx carcinoma," Oral Surg. Oral Med. Oral Pathol. Oral Radiol. Endodontol., vol. 19, pp. 933-938, 2009.

[24] R. Duba, P. Hart and D. Stork, "Pattern Classification," in Pattern Classification, p. 3., 2013

[25] G. Friedland and B. Thurber, "The birth of CT," 1996.

[26] A. Filler, "The History, Development and Impact of Computed Imaging in Neurological Diagnosis and Neurosurgery: CT, MRI and DTI," p. 3, 2009.

[27] Wikipedia, Wikipedia, [Online]. Available: https://en.wikipedia.org/wiki/Raymond_Damadian. [Accessed 09 July 2024].

[28] Z. Cho, "Physical Science and Technology," pp. 843-877, 2003.

[29] B. Botz and A. Shetty, "CT scanner evolution," 2021. [Online]. Available: https://radiopaedia.org/articles/ct-scanner-evolution. [Accessed 13 July 2021].

[30] E. Seeram, “Computed Tomography,” in Physical Principles, Clincal Applications, and Quality Control, St Louis, Missourl, ELSEVIER, 2016.

[31] Wikipedia, Wikipedia, 6 May 2024. [Online]. Available: https://en.wikipedia.org/wiki/Hounsfield_scale. [Accessed 2 July 2024].

[32] F. Zarb, L. Rainford and M. McEntee, “Image quality assessment tools for optimization of CT images,” vol. 16, pp. 147-153, May 2010.

[33] P. Lin, T. Beck, C. Borras, G. Cohen, R. Jucius, R. Kriz, E. Nickoloff, L. Rothenberg, K. Strauss and T. Villafana, “Specification and accpetance testing of computed tomography scanners,” American Association of Physicist in Medicine , 1993. [Online]. Available: https://www.aapm.org/pubs/reports/detail.asp?docid=38. [Accessed 20 August 2024].

[34] S. Jackson, S. Ahmad, Y. Hu and C. Ruan, “Evaluation of different techniques for CT radiation profile width measurement,” Applied clinical medical physcics, vol. 14, no. 4, pp. 227-237, 2013.

[35] X. Duan, J. Wang, S. Leng, B. Schmidt, T. Allmendinger, K. Grant, T. Flohr and C. McCollough, “Electronic Noise in CT Detectors: Impact on Image noise and artifacts,” Medical Physics and Informatics, vol. 201, pp. 626-632, 2013.

[36] P. Chu, S. Yu, Y. Wang, A. Seibert , L. Cervantes, N. Kasrale, C. Chu and R. Smit-Bindman, “Phantom selection in pediatric computed tomography using data from large multicentre registry,” 2021.

[37] Toshiba, “Operation manual for toshiba scanner, aquilion prime, 2014-2016 noise, mean ct number and uniformity,” 2016.

[38] A. Rashid and M. K. Rahim, “Extensive Experimental Analysis of image statistical Measures for Image Processing Appliances,” Signal Processing, Image Processing and Pattern Recognition, vol. 9, no. 3, pp. 49-60, 2016.

[39] M. Sontakke and M. Kulkami, “Different types of noises in images and noise removing technique,” International journal of Advanced Technology in Engineering and Science, vol. 03, no. 01, pp. 102-115, 2015.

[40] Toshiba, “Toshiba technical training notes for CT artifacts,” 2016.

[41] Jiang Hsieh, "Partial volume artifact reduction in computed tomography," Proceedings of 3rd IEEE International Conference on Image Processing, Lausanne, Switzerland, 1996, pp. 567-570 vol.3, doi: 10.1109/ICIP.1996.560558.
keywords: {Computed tomography;X-ray imaging;Head;Error correction;Attenuation;Image reconstruction;Object detection;X-ray detection;X-ray detectors;Laboratories},.

[42] G. Dougherty, “Digital Image Processing for Medical Applications,” 2007, pp. 1-459.

[43] T. Blodget, A. Mehta, A. S. Mehta, C. Laymon, J. Carney and D. Townsend, “PET/CT artifacts,” pp. 49-63, January 2011.

[44] J. Barrett and N. Keat, “Artifacts in CT: Recognition and Avoidance,” RadioGraphics, vol. 24, no. 6, p. 1, 2004.

[45] Y. Zhang and H. Yu, “Convolutional neural network based metal artifact reduction in,” IEEE Trans. Med, vol. 37, pp. 1370-1381, 2018.

[46] M. Selles, J. van Osch, M. Maas, M. Boomsma and H. Wellenberg, “Advances in metal artifact reduction in CT images: A review of traditional and novel metal artifact reduction techniques,” European Journal of Radiology, vol. 170, p. 8, 2024.

[47] J. Hsieh, “Computed tomography: Principles, design, artifacts and recent advances. SPIE,” 2003.

[48] M. Eldib, M. Hegazy, Y. Mun, M. Hye, M. Cho, M. Cho and S. Lee, “A Ring Artifact Correction Method: Validation by Micro-CT Imaging with Flat-Panel Detectors and a 2D Photon-Counting Detector,” p. 269, 30 January 2017.

[49] J. Salplachta, T. Zikmud, M. Zemek, A. Brinek and Y. Takeda, “Complete Ring Artifacts Reduction Procedure for Lab-Based X-ray Nano CT System,” p. 238, 1 January 2021.

[50] X. Liang, Z. Zhang, T. Niu, S. Yu, S. Wu, Z. Li, H. Zhang and Y. Xie, “Iterative image-domain ring artifact removal in cone-beam,” CT. Phys. Med. Biol, vol. 62, pp. 5276-5292, 2017.

[51] B. De Man, J. Nuyts, P. Dupont, G. Marchal and P. Suetens, “Reduction of metal streak artifacts in x-ray computed tomography using a transmission maximum a posteriori algorithm,” p. 1, July 2000.

[52] B. Zheng, “Computer-Aided Diagnosis in Mammography Using Content-Based Image Retrieval Approaches:,” pp. 829-849, 4 June 2009.

[53] J. Yanase and E. Traintaphyllou, “A systematic survey of computer-aided diagnosis in medicine: Past and present developments,” vol. 138, p. 4, 2019.

[54] C. Kaushal, S. Bhat, D. Koundal and A. Singla, Recent Trends in Computer Assisted Diagnosis (CAD) System for Breast Cancer Diagnosis Using Histopathological Images, vol. 10, no. 4, pp. 211-227, 2019.

[55] Y. Zhang, “An overview of content based images retrieval techniques,” in 18th International Conference on Advanced Information Networking and Application, 2004.

[56] C.-T. Cheng, Y. Wang, H.-W. Chen, P.-M. Hsiao, C.-N. Yeh, C.-H. Hsieh, S. Miao, J. Xiao, C.-H. Liao and L. Lu, “A Scalable physician-level deep learning algorithm detects universal trauma on pelvic radiographs,” pp. 1-11, 2021.

[57] M. Rahimzadeh and A. Attar, “A modified deep convolutional neural network for detecting COVID-19 and,” Informatics in Medicine Unlocked, vol. 19, pp. 1-9, 2020.

[58] M. Barwary and M. Abdulazeez, “Impact of deep learning on transfer learning: A review,” International journal of Science and business, vol. 5, no. 3, pp. 201-214, 2021.

[59] L. Kong, C. Li, F. Zhang, Y. Feng, Z. Li and B. Luo, “Leveraging multiplefeatures for document sentiment classification,” Information science, vol. 518, pp. 39-55, 2020.

[60] D. Sarkar, “A comprehensive hands-on guide to transfer learning with real-world applications in deep learning,” 2018. [Online]. Available: https://towardsdatascience.com/a-comprehensive-hands-on-guide-to-transfer-learning-with-real-world-applications-in-deep-learning-212bf3b2f27a. [Accessed 10 01 2022].

[61] Wikipedia. [Online]. Available: https://en.wikipedia.org/wiki/Softmax_function. [Accessed 10 July 2024].

[62] Y. Zhang and L. Zhang, “A rigid motion artifact reduction method for CT based on blind decovolution,” vol. 12, no. 8, p. 1, 2019.

[63] P. Seslija, Y. thakur and D. Tso, “Scanner and kVp dependence of measured CT number in the ACR CT phantom,” Applied Clinical Medical Physics, vol. 14, no. 6, pp. 342-345, 2013.

[64] “AWS,” https://aws.amazon.com/what-is/data-augmentation/, [Online]. Available: https://aws.amazon.com/what-is/data-augmentation/. [Accessed 20 01 2024].

[65] W. Data, 10 march 2024. [Online]. Available: https://en.wikipedia.org/wiki/Data_augmentation. [Accessed 14 March 2024].

Annexure

The annexure section presents the information that was not included in body of the dissertation. The annexure section comprises four annexures presenting the ring and metal artefact in Annexure A, followed by two articles that were produced flowing from this research (Annexure B and Annexure C). Annexure D presents the algorithms utilised in this research study. Annexure E presents the Toshiba/Canon causes of, and solutions for metal and ring artefacts.

Annexure A: Artefact datasets

Article Annexure B: https://www.neuroquantology.com/article.php?id=5859

Article Annexure C: https://www.webology.org/abstract.php?id=3114

Annexure D: Code algorithm

Annexure E: Toshiba/Canon causes of, and solutions for metal and ring artefacts.

Annexure F: Code transfer learning code

Annexure G: Algorithm 2D CNN

Annexure H: Code setup

Annexure I: Data Augmentation

Annexure J: Output prediction code

Annexure A: Ring and metal artefact datasets

The metal artefact dataset contained in this research study, comprises of both 85 and 88 image dataset and Annexure A presents an example of few images.

Metal artefact dataset

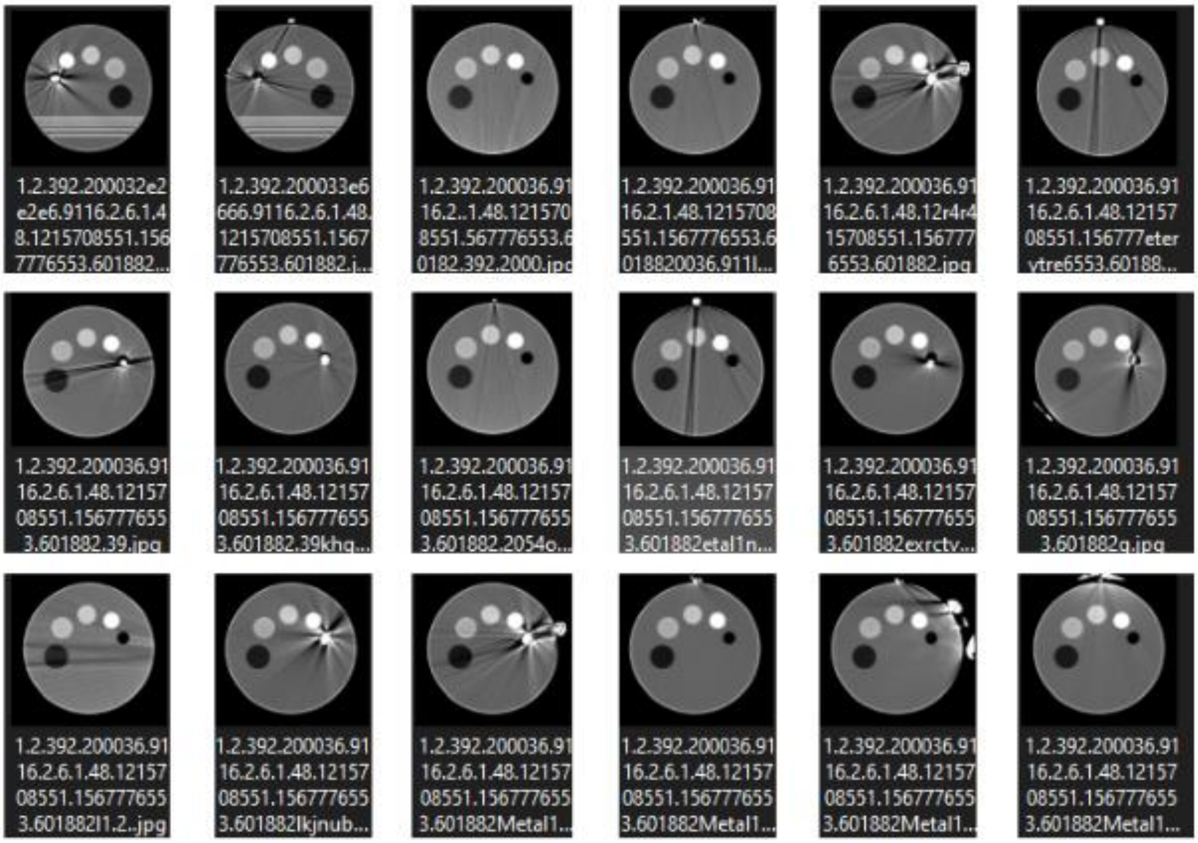

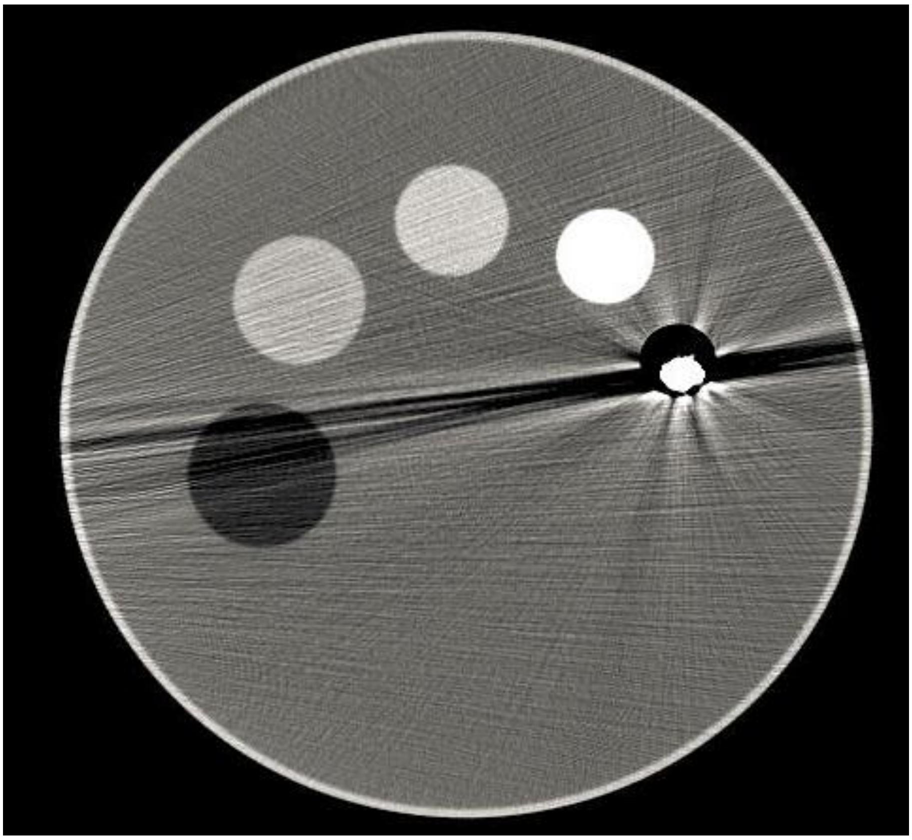

The metal artefact dataset contained in this research study, comprises of both 85 and 88 image dataset and Annexure A presents an example of a few images.

Ring artefact dataset

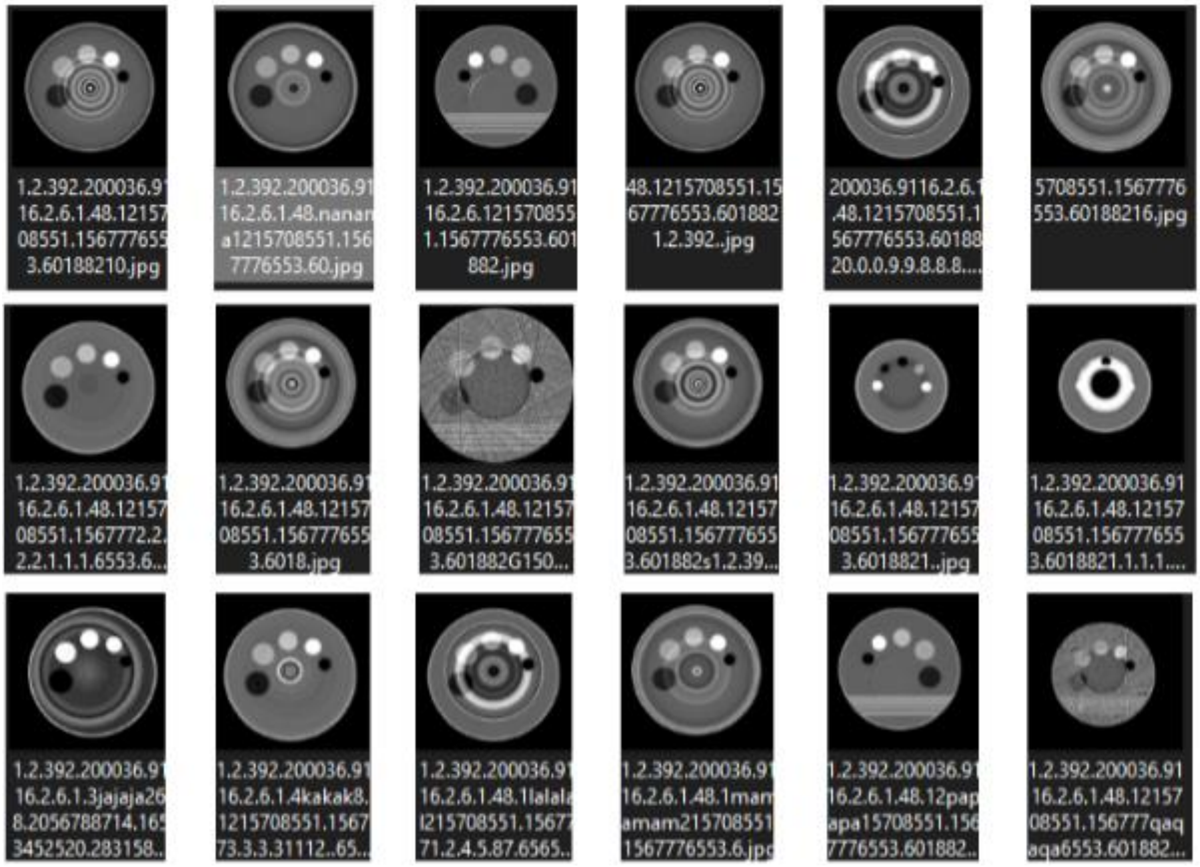

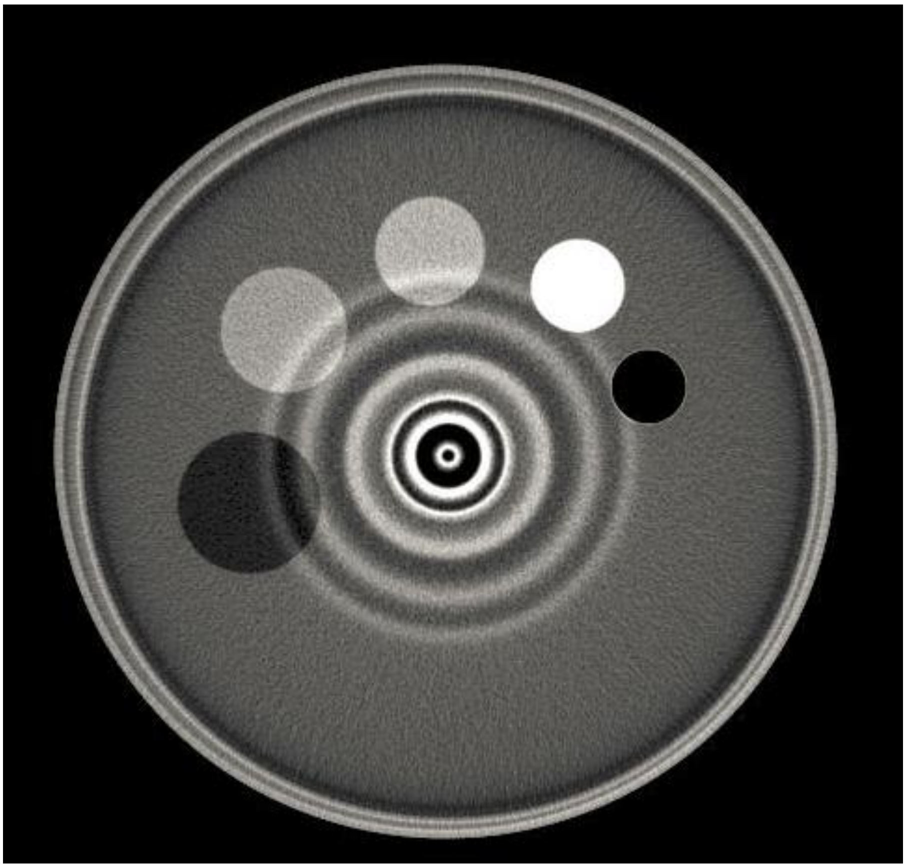

Annexure B: Image Learning and Correction As A Means of Evaluating and Fault-finding Computed tomography Scanner Image Artefacts

At The 2nd International Conference on Business, Management, Environmental, and Social Science

Image Learning and Correction as a Means of Evaluating and Fault-Finding Computed tomography Scanner Image Artefacts

J.H.B Benganga[1#], B. Kotze[1*]

[1]*Department of Electrical, Electronic and Computer Engineering*

Central University of Technology, Free State

Bloemfontein, South Africa

[#]*hervebenganga@gmail.com, *bkotze@cut.ac.za*

Abstract

The concept of image reconstruction modelling in both the industry and academia has led to the investigation of different artefacts found in the medical fraternity. This concept is aimed at optimising the efficiency of fault-finding in the CT scanner. It is for such reasons, that an automated artefact detection model with capabilities for artefact image restoration and solution prediction model needs to be investigated, developed, and implemented to evaluate the feasibility and reliability of such a system in a live environment setup for service engineers and specialist alike. During the image acquisition process, images were taken from Toshiba medical equipment for image processing and machine learning purposes. The data collected contains 100 images in the dataset comprising of 50 ring and metal artefact images for data testing with 19 iterations. Training of the model is created to allow the model to learn by identifying the different features. This paper demonstrates the consistency of the model in distinguishing between the ring and the metal artefact. However, the model accuracy inconsistency and required data augmentation to stabilise the system, hence the need for algorithm optimization to accurately detect and distinguish the artefacts despite the image sample number.

Keywords: *Artefact, Image Processing, CT scan, Artificial Intelligence, OpenCV, Machine Learning.*

1. Introduction

Image Processing (IP) has become one of the most vivid research areas in Computer Vision, especially in Medical Imaging (MI) sector. Medical imaging system in certain instances makes use of captured images for diagnostic and monitoring purposes.

This is because of Computer-Aided Diagnostic (CAD) schemes and Artificial Intelligence (AI), which has shown the CAD potential in providing multiple industries that are image processing dependent with the “visual aid” and increase confidence in accepting computer-aided-cued results in the decision making [44]. Medical imaging system modalities include s scanners, Magnetic Resonate Imaging (MRI) scanners, Virtual Surgical Planning (VSP) systems, and Optical Coherence Tomography (OCT) amongst a wider range of equipment used to assess the conditions of organs or tissue and monitor a patient over time for diagnostic and treatment procedures.

Furthermore, medical imagining systems comprises of several developed techniques, and each technique has different risks and benefits. The risks associated with medical imaging are similar risks that are found in every image processing-based application such as light intensity [54]. However, in the context of computer vision, Computed tomography (CT) and MRI scanners are dominant applications in medical imaging because of their high resolution, good signal-to-noise ratio, and manipulation properties.

Furthermore, despite the risks associated with image processing, medical imaging has been seen to have major risks such as the visualisation that details the image data analysis and exploration for research applications. The concept of image reconstruction and modelling is introduced to allow for instant processing of 2D signals to create 3D images to reduce data collection time [55]. Additionally, digital image processing software is designed to automatically identify and analyse what might not be apparent to the human eye.

This paper focuses on implementing image correction measures for a CT scanner to affect the outcome of an image and to fault find image distortions utilising machine learning applications. The final objective of this study is, therefore, to; 1) To present a method for artefact detection and reconstruction; 2) To develop a method that can distinguish between metal and ring artefacts and provide a possible solution matrix using machine learning techniques. To summarise, this article proposes an automated model for artefact analysis, detection, and provision of possible solutions.

The remainder of this paper is as follows. Section 2 provides the problem statement elaborating on the research question. Section 3 provides a discussion on the literature around medical devices, corrective techniques, and the application of CAD in the medical environment. Section 4 outlines the systems modelling technique utilising image processing and machine learning techniques for data training, data identification, data training, and provision of a possible solution. The results are outlined in Section 5 with the paper concluded in Section 6.

2. Problem statement

Currently, there are standard troubleshooting procedures that are used in practice to overcome image artefacts in the CT scanners. However, troubleshooting may still yield negative results, and this may be due to the evaluation or nonuniform fault-finding technique since the troubleshooting exercise is manufacture-specific. However, the said fault-finding techniques can be time-consuming and costly, which in turn is a setback for radiographers, doctors, and even patients.

It is for such reasons, that an automated artefact detection model with capabilities for artefact image restoration and solution prediction model needs to be investigated, developed, and implemented to evaluate the feasibility and reliability of such a system in a live environment setup for technical representatives and service engineers.

3. Literature review

MI systems have made the highest advancements in medical technology both academically and for medical research purposes. Dougherty et al. [9] present the medical imaging system for constructing an image in response to signals from diverse types of objects namely bodies and phantoms. Additionally, Dougherty highlights that medical imaging systems can be classified according to the radiation, and academic field of use. Dougherty further investigative the properties of whether the images are formed directly or indirectly.

A Computed tomography (CT) scanner is a diagnostic imaging procedure that uses s to build cross-sectional images of the body [56]. Each time the source completes one full rotation, the CT computer uses sophisticated mathematical techniques to construct a 2D image slice of the patient or object, producing signals that are processed by the machine's reconstruction component to generate cross-sectional images (slices) of the patient or object. These slices contain more detailed information than conventional s. Once several successive slices are collected by the CT scanner, they are digitally stacked to form a final three-dimensional image of the patient that allows for easier identification and location of basic structures as well as possible tumours or abnormalities.

Furthermore, equipment such as Magnetic Resonance Imaging (MRI) which is a medical imaging technique that is used in radiology to form pictures of the anatomy and the physiological processes of the body [10] is currently in use. MRI scanners use strong magnetic fields, magnetic field gradients, and radio waves to generate images of organs in the body. MRIs are deemed as one of the most important non-invasive imaging techniques in medicine not only due to the non-invasiveness of the method but due to its richness of the attainable tissue contrast [11].

3.1. Historical background on CT scanner

CT scanners are ideally set to be established in 1971, citing Hounsfield and Ambrose positioning a patient inside a new machine in the basement of the hospital. However, the argument has been around for decades that Damadians is the first author/developer of the CT scanner technology in 1977 [20]. However, this is contrary accordingly to different authors. It is, however, agreed that the first functionally developed CT scanners made use of pencil-like beam sources located across from a single detector.

The first-generation scanners were published in the mid-1970s, and it was translated linearly across the field of view and was projected as a series of parallel beams. Figure 1 depicts first-generation CT scanners transmitting a single-shaped beam.

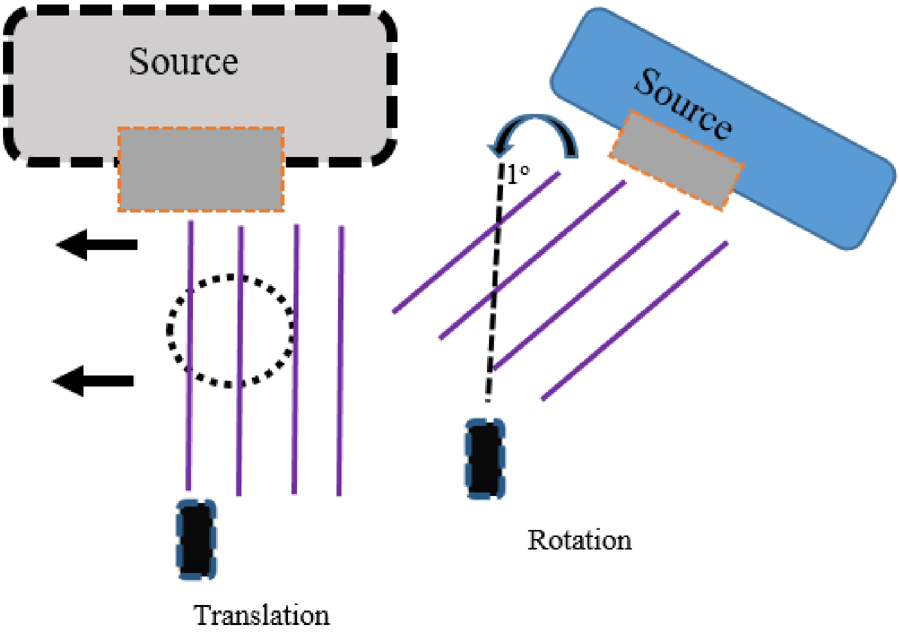

Figure 1. First-generation CT scanners single pencil beam-shaped transmission

Figure 1 depicts the first-generation CT scanner. The source in the translation model is placed parallel to the beam-shaped transmission. For the additional test model, the source is rotated 1° to evaluate the best optimal model.

3.2. Review on correction techniques used for CT image artefacts

The induced artefact in many documented field experiences ring artefacts caused by degraded electronics. As a result of the degraded electronics, the avoidance and software are implemented for the selection of the correct scan details and protocols of the full system calibration and knowledge of anatomy.

In retrospect, Eldib et al. [38] proposed a corrective method for a cone-beam CT by correcting the defective pixels whose values are close to zero or saturated in a projection domain. Subsequently, Salplachta et al. [39] introduce a new ring artefact reduction procedure that combines several ideas from existing methods into one complex and robust approach.

3.3. Review of image recognition and learning techniques for medical image systems

There are several types of conventional techniques used to identify and learn about CT images, with the most obvious one being visible to the human eye. However, these methods are aligned with certain types of artefacts. Some artefacts are new and are mainly caused by faulty or degrading electronic components and external factors like the room temperature and dirt, just to name a couple.

In retrospect for pattern recognition, machine learning techniques have become instrumental in the development of CAD systems. Duda et al. [57] state that pattern recognition is the act of extracting features from some objects in raw data and making a decision based on the classifier output such as classifying each object into one of the possible categories of various patterns. However, the basic concept of introducing

CAD systems in medicine was proposed to provide a computer output as a second opinion to assist radiologists in interpreting images, so that the accuracy and consistency of radiological diagnosis could be improved, also that the image reading time could be reduced. [https://pubmed.ncbi.nlm.nih.gov/15917443/]

4. Methodology

The system development model comprises of data acquisition, data testing, data modelling, and the application algorithm for data training and provision of a possible solution. The data is collected by taking pictures of different artefacts namely ring, and metal artefact and convert them to a listed dataset.

During the image acquisition process, the images are taken from Toshiba medical equipment and are saved into a folder, which is then converted into a listed dataset. Figure 2 depicts the initial images taken for image processing and machine learning purposes. However, the two phantoms were used to evaluate the artefact by physically comparing each image with an artefact against an image without an artefact. Additionally, after the data was collected, a model was developed to create an enabling environment for data training and to allow the same data to be fitted into the same data training model for evaluation and model training purposes. Figure 2 further depicts the ring and metal artefact that are investigated in this article.

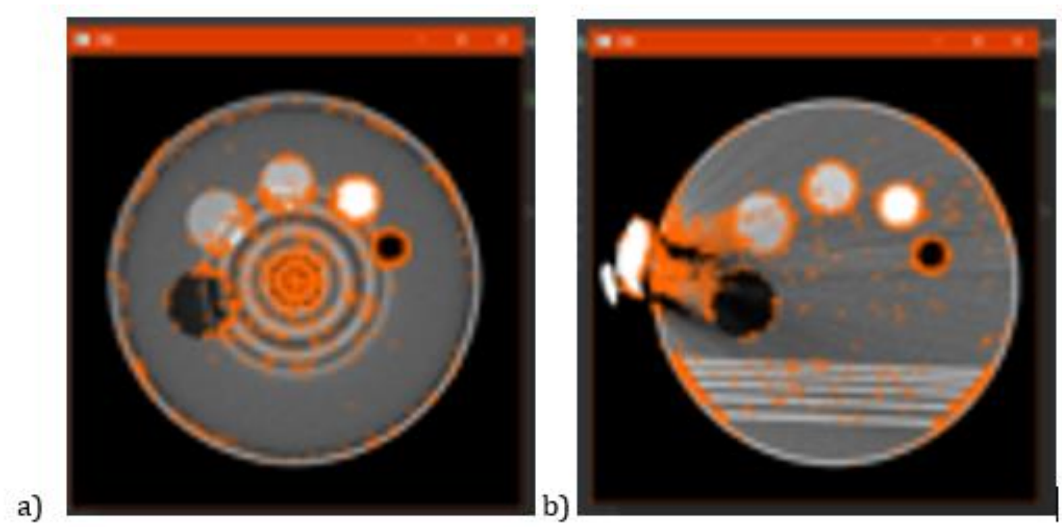

Figure 2. Image sample of both a) ring artefact; b) metal artefact taken from Toshiba equipment.

Figure 2 depicts the image samples obtained from a Toshiba CT scanner. Each image represents a type of an artefact in this instance a) ring artefact; b) metal artefact. Furthermore, Figure 2 depicts the images already placed in the model before applying the learning algorithm to the model. These images are a representation of an image with either a ring artefact or metal artefact.

4.1. Review of image recognition and learning techniques for medical image systems

In modelling of this system, the following libraries and algorithms were used:

- Tensorflow™ – this software is utilised as a machine learning software on PyCharm IDE
- OpenCV – for image processing and detection of features
- Keras library – is a library interface for Tensorflow™ and is utilised as a supporting library for machine vision

Furthermore, these algorithms utilises a CUDA-based Graphical Processing Unit (GPU) that allows for parallel computing provided by the GPU. The system model setup was then outlined as indicated in Figure 3.

- Image data collection and preparation
- Dataset creation and data model training
- Image testing
- Model evaluation

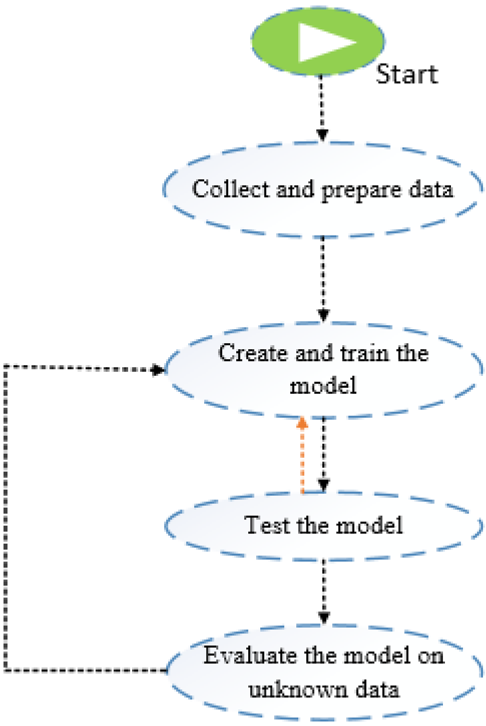

Figure 3. Model setup framework.

Figure 3 depicts the model task overview outlining the model setup framework. This setup is made out of four key components namely 1) collect and prepare data; 2) Create and train the model; 3) Evaluate the model using unknown and known data; 4) test the model.

- Collect and prepare presents the start of the project and how the data is collected for the model. The data is collected by scanning an image with Toshiba equipment and manually checking the images against the scanner datasheet to identify the type of artefact. Upon noting the type of an artefact, a folder is created and images are multiplied to reach 50 image samples, then copied into a listed folder per artefact type i.e. metal artefact. However, no scientific model or principle was utilised for image sampling number per dataset, and it was the prerogative of the researcher to estimate the image sample number. It is noted that the sample number might affect the results output.
- A train and test model was created utilising the feature learning model that relies on the following: a) input data; b) convolution; c) pooling and classification model. The

system is trained by inputting a dataset into the model and the 19 iterations are executed in PyCharm IDE for data training. Upon the completion of the iterations, an unknown dataset with the same image dataset is inputted and the output is observed.

- The input of a known image dataset is to evaluate the accuracy of the model and the results are observed and evaluated against the initial dataset. Each dataset has notes aligned with it containing possible solutions.
- The sample code below depicts the directory for datasets. Furthermore, Figure 4 depicts the data structure of the datasets and modelling assets directory.

```
train_data_dir='Dataset/train'
validation_data_dir='Dataset/test'
```

Figure 4. Data modelling structure.

Figure 4 depicts the data modelling structure for locating the datasets for both the training data and the validation data. Upon locating the data, the feature learning model is applied to the data by first resizing the image`s width and height before the convolution is applied.

The application of convolution is to differentiate the two artefacts based on their features. The system is trained by inputting a labelled dataset into the model and testing is performed by inputting an unknown dataset into the model and the output results are evaluated against a set of reconstructed image datasets and solutions. The system is trained with 19 iterations using machine learning techniques. Upon the completion of the iteration, the model is tested and evaluated against the unknown data to test for accuracy. The system model is then evaluated on the unknown data and this data is then used to determine the artefact type and possible solution.

Additionally, Figure 5 further explains the “collect and prepare data” with references to the image sizes. The image size used was 512x512 pixels. Additionally, in most CT scanners, the gantry`s bore size used in simulations of radiation therapy is bigger to accommodate situations in which the overall diameter of imaging volume is large owing to immobilisation devices [58]. However, this resonates with the physical development of the CT scanner, while this article focuses on reconstructing the captured images in a form of a dataset.

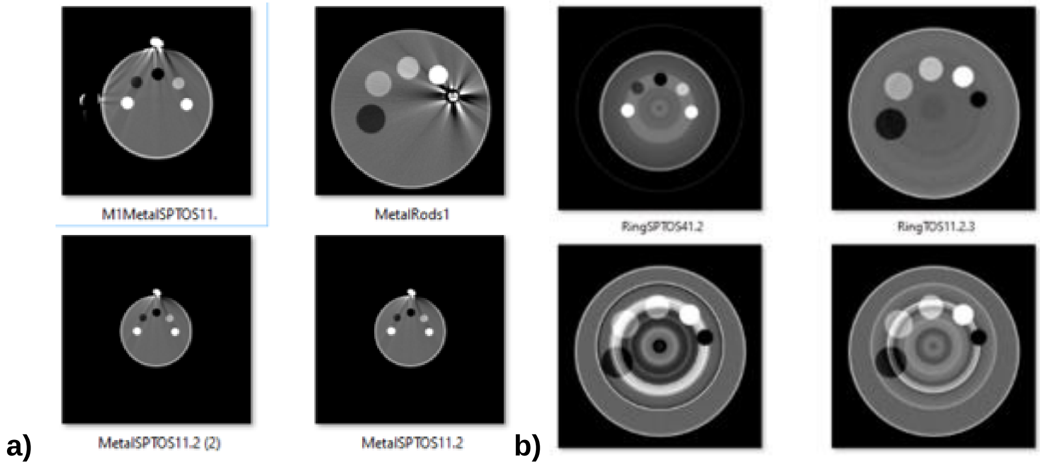

Figure 5. a) Metal artefact images 512X512 pixels; b) Ring artefact images 512X512.

Figures 5 a) and b) depict the original captured image artefacts for both metal and ring artefacts. Since these images are taken from the same source, they are manually sorted by placing them into a master folder and a dataset is created for both the metal and ring artefact and is labelled as such per artefact.

Each data collected contains 100 images in the dataset that is organised as follows:

- Ring artefact - training 50 images for data testing with 19 iterations
- Metal artefact - training 50 images for data testing with 19 iterations

The training of the model is created to allow the model to learn by identifying the different features as outlined in Figure 7 a) and b). Figure 7 a) outlines the feature detection for a metal artefact while Figure 7 b) outlines the feature detection for the ring artefact.

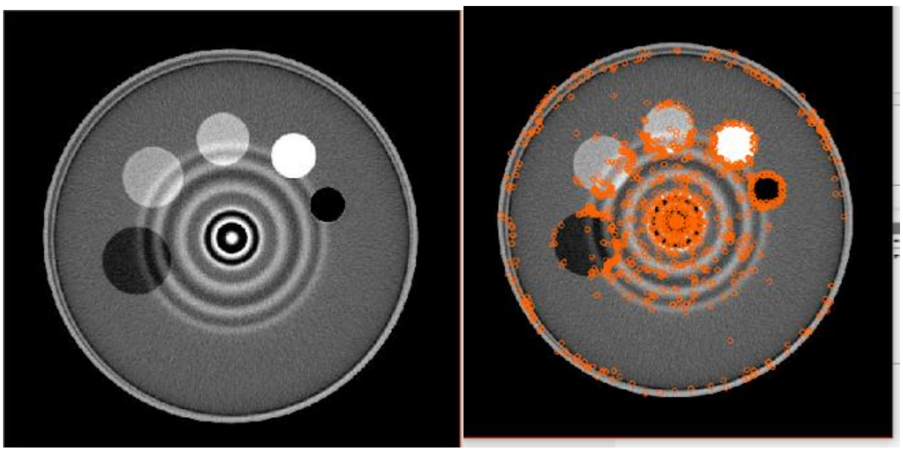

Figure 6a). Original image and b) feature detection ring artefact.

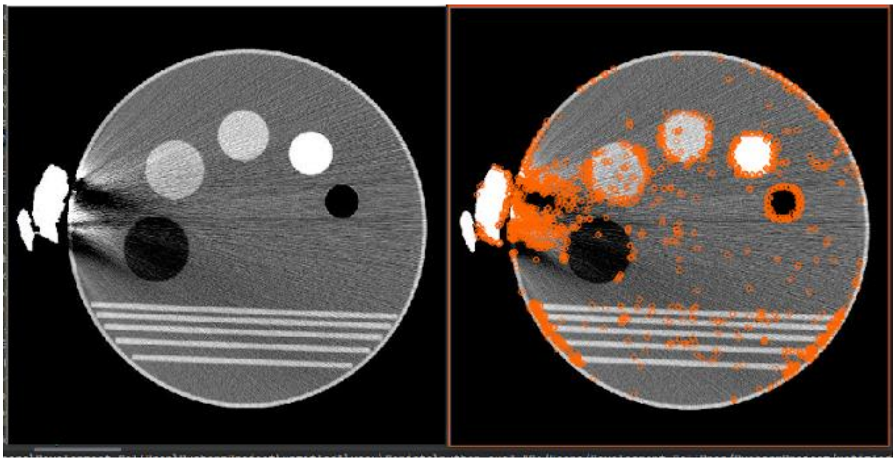

Figure 6b). Original image and b) feature detection metal artefact.

Figures 6 a) and b) depict the test application of the datasets in the model. Figures 6a) and b) depict both the metal and ring artefact dataset that is placed in the model for training and validation. Figures 6 a) and b) further present the difference between the original image and feature detected image for both ring and metal artefact. This is pivotal as the recognition is dependent on these features for accuracy testing. This model is fully automated and once the input image or dataset is applied into the model, the model analyses the image and provides the output as per the defined procedure above.

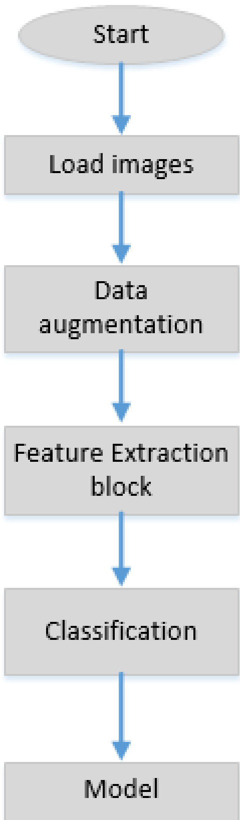

Figure 7. Model flow diagram.

Figure 7 presents the algorithm flow diagram. The two datasets (ring and metal artefact) are loaded into the model. The data is then augmented to increase the training datasets. This is pivotal because it has been seen that the fewer the images in the dataset, the higher the possibilities of inaccuracy. This was conducted in a trial and error method and no scientific approach was applied as machine learning prediction depends primarily on the dataset dimensions.

The dataset data parameter generation is then applied as follows:

- rescale —Each digital image is created by a pixel with a value between 0 and 255. 0 in black, 255 in white. So the rescale of the scaled array of the original image pixel values should be between [0,1] which makes the images contribute more equally to the overall loss. Otherwise, higher pixel range image results in greater loss and a lower learning rate should be used, lower pixel range image would require a higher learning rate.

- shear_range — The shape of the image is the transformation of the shear range. Its function is to fix one axis and stretch the image at a certain angle known as the angle of the shear.

- zoom_range — the image is enlarged by a zoom of less than 1.0. and when the image is more than 1.0 then the image zoomed out.

- horizontal_flip — some images are then flipped horizontally at random to have a full view of the images in both the horizontal and vertical positions.

Upon successful execution of this process, CNN architecture is applied on a model, however, the CNN model needs to adhere to the following process as follows:

- Always begin with a lower filter value such as 32 and begin to increase it layer-wise.

- Construct the model with a layer of Conv2D followed by a layer of MaxPooling.

- The kernel_size is preferred to be an odd number like 3x3.

- Relu was used for activating the function

- Input_shape takes in image width & height with the last dimension as colour channel.

- Flattening the input after CNN layers and adding ANN layers.

- Use activation function as softmax for the last layer if the problem is more than 2 classes, define units as the total number of classes and use sigmoid for binary classification and set the unit to 1.

A 22 layer 2D CNN design was developed which consisted of five 2D convolution layers, with the second layer comprising 32 filters and the third layer of 64 layer filters all with a kernel size of 3x3. Each convolution (Conv) layer is followed by a ReLu activation layer and it ends with a max-pooling (MAXPOOL) layer with a stride of 2. The feature extraction block consists of CONV-ReLu-MAXPOOL modules and the output from the extraction block is then flattened and passed to a fully connected layer with 475,746 parameters.

In the early days of image processing development, linear filters were used as the primary tools for image enhancement and restoration. However, due to the advancements in technology, other algorithms such as supervised learning multi-class classification logistic regression algorithm and linear regression algorithm are currently in use in the market. In this article, the logistic regression algorithm is utilised citing the difference between the two algorithms as outlined in Table 1.

Table 1: Difference between linear and logistic regression algorithms in machine learning

Linear regression algorithm	Logistic regression algorithm
Predicts the continuous dependent variable using a given set of independent variables	Predicts the categorical dependent variable using a given set of independent variables
Solves regression problems	Solves classification problems
Predicts the value of continuous variables	Predict the values of categorical variables
Easily predict the output	Find the S-curve by which we can classify the samples
The least-square estimation method is used for the estimation of accuracy	The maximum likelihood estimation method is used for the estimation of accuracy
Continuous value	Categorical value i.e. 0 or 1

Additionally, the correction and origin are depicted in both medical and industry. However, the use of logistic regression is aligned with the proposition for addressing the artefacts problem that is seen in medical facilities. Additionally, the brightness of an image is altered with distance in either the horizontal or vertical direction of the image by checking the high spatial frequency. When the brightness changes slowly or at a constant rate, the image is said to have a low spatial frequency. Spatial frequency filtering can alter an image by sharpening, smoothing, blurring, and applying noise reduction and feature extraction.

5. Results

Based on the model output sequencing and accuracy testing. The accuracy testing was based on two image datasets with 50 sample images per dataset. This test was evaluated utilising an unknown image dataset that was not part of trained data. This allowed for the model to predict the model accuracy with a dataset of 50 images each. However, to optimally get conclusive results a weight or benchmark of 80% was added and the model output was supposed to obtain this threshold with the given datasets.

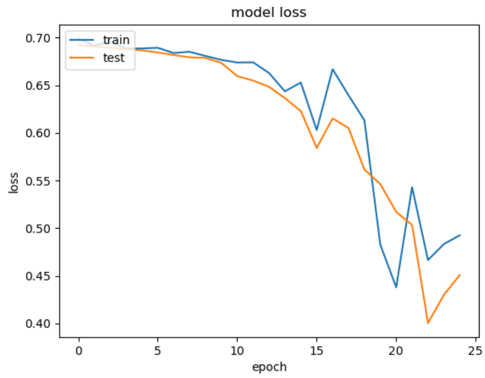

(a) (b)

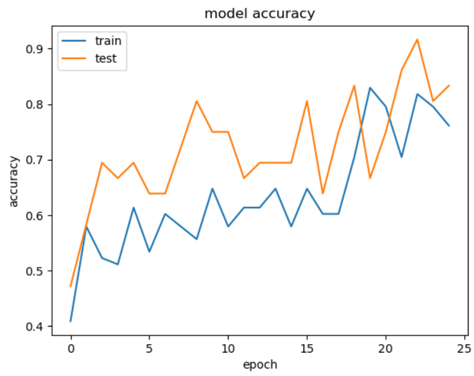

Figure 9 a) Model data loss; **6b).** Model accuracy.

However, the model required data augmentation to provide conclusive results. As this was not part of the study, the results were then based on the 50 images per dataset. Figure 9 a) depicts the model results for data loss or inaccuracy for 35 epoch iterations. Figure 9 a) depicts that as the model epoch counts increase the data loss reduces and this is due to the number validation conducted, with data loss being 0.49 on the 24th epoch as compared to 0.70 on the 0th epoch test. Subsequently, in Figure 9 b), as the data model training increases, the model accuracy increases with the system producing 0.4 accuracy test at epoch 0 and 0.8 accuracy test and epoch 25. This incremental accuracy is due to multiple data training applications.

6. Conclusion

This paper observed the modelling of a system for the detection and identification of two kinds of artefacts mainly ring and metal artefact. However, using machine learning and image processing techniques such as Keras library and OpenCV the system was deemed efficient, and effectiveness was measured against the accuracy results based on the number of image samples within the dataset. The results do prove that the system is efficient and effective in identifying the different artefacts based on the features. However, the accuracy of the model is deemed not as effective, hence the need for data augmentation is required. This thus concludes the study that the model`s accuracy is not 100%, therefore an optimization algorithm needs to be added to the model for the model to provide over 80% accuracy despite the number of image samples.

7. Acknowledgements

Acknowledgement for academic and financial assistance from the Central University of Technology, Free-State (CUT, FS), Mr Lepekola Lenkoe with code test testing and optimization and Dr Tshepo Kukuni for language editing, code remodelling, and unending support.

8. References

[1] B. Zheng, "Computer Aided Diagnosis in Mammography Using Content-Based Image Retrieval Approaches: Current Status and Future Perspectives," 2009.

[2] T. Kukuni and B. Kotze, "Industrial augmented reality as an approach for device identification within a manufacturing plant for property alteration purposes," Four international conferences on applications and systems of visual paradigms, p. 15, 2019.

[3] M. v. d. Glas, "Principles in Computer Tomographic Imaging," 2000.

[4] G. Dougherty, "Digital Image Processing for Medical Applications," 2007, pp. 1-459.

[5] D. Bell, "Rapiopaedia," 16 February 2021. [Online]. Available:

https://radiopaedia.org/articles/computed-tomography. [Accessed 27 January 2022].

[6] D. A. Pollacco, "Magnetic Resonance Imaging," p. 1, 22 March 2016.

[7] K. Mollenhoff, A.-M. Oros-Peusquens and J. N. Shah, "Introduction to the basics of magnetic resonance imaging," pp. 1-25, 2012.

[8] A. Filler, "The History, Development and Impact of Computed Imaging in Neurological Diagnosis and Neurosurgery: CT, MRI and DTI," p. 3, 2009.

[9] M. Eldib, M. Hegazy, Y. Mun, M. Hye, M. Cho, M. Cho and S. Lee, "A Ring Artefact Correction Method: Validation by Micro-CT Imaging with Flat-Panel Detectors and a 2D Photon-Counting Detector," p. 269, 30 January 2017.

Authors

Joe-Herve Bonkondo Benganga

Joe-Herve Bonkondo Benganga holds B-Tech: Engineering: Electrical, N.Dip: Computer Systems Engineering from Central University of Technology, Free State and Medical Equipment Certificates in Anaesthetic Machine from Spacelabs Healthcare, CT scanner from Canon Medical Systems and Ulrich Injector CTMotion from Ulrich Medical. He is currently studying towards a Master of Engineering in Electrical Engineering with the Central University of Technology, Free State.

Joe-Herve Bonkondo Benganga is a technical representative in Tecmed Africa, specialising in technical services for CT, MRI scanners and contrast injectors.

Benganga`s skills professionally and academically are in electronics, medical equipment, design and modelling, C#, C, and MySQL databases. Benganga has an interest in the development of medical systems and evaluation applications such as machine learning and AI being implemented in medicine specifically in radiology. He is a follower of Aunt Minnie journals and webinars.

Ben Kotze

Ben Kotze holds a Masters and Doctoral degrees in Electrical Engineering.

He is professionally registered with the Engineering Council of South Africa (ECSA) and several associations of which the oldest South African Institute of Electrical Engineers (SAIEE est. 1904) where he is a fellow.

With seven years, industry experience and over thirty years of tertiary education experience in Electrical Engineering of which he lectured more than 23 subjects. He is still actively involved with industry and work integrated learning (WIL).

He is currently doing research on vision, several different AGV’s, renewable energy systems, simulation and control, augmented reality systems, IoT security, smart farming, and prediction methods. Several undergraduate students, masters and doctoral students passed by his mentorship. He attended several international and national conferences in engineering and education and have published in accredited journals on these topics. He is currently the assistant dean teaching and learning in the Faculty of Engineering, Built Environment and Information Technology at the Central University of Technology, Free State. Also actively involved in the Centre for Sustainable Smart Cities.

Annexure C: Application of Machine Learning for Image Artefact Detection based on Computed tomography Scanner

At The 8th International Conference on Green Computing and Engineering Technologies

Application of Machine Learning for Image Artefact Detection based on Computed tomography Scanner

J.H.B Benganga[1#], B. Kotze[1*], T.G. Kukuni1[**]

[1]*Department of Electrical, Electronic and Computer Engineering*

Central University of Technology, Free State

Bloemfontein, South Africa

[#]*hervebenganga@gmail.com*, [*]*bkotze@cut.ac.za*, [**]*tgkukuni@gmail.com*

Abstract

The application of machine learning in solving complex medical and non-medical challenges keeps growing. The use of CT scanners is very crucial in saving lives hence the need to investigate alternative approaches for solving artefacts found in Computer Tomographic images. In some instances, such faults take a while to figure out the types of artefacts and their causes due to large datasheets. It is, therefore, against this background that such a study needs to be investigated. This paper makes use of 180 image datasets and feature detection is applied on each dataset (ring and metal) and both datasets are trained for both 25 and 50 epoch tests. After completion of both epochs, unknown datasets are inputted into the model. This research results thus concluded that the model is efficient with an accuracy of 87% and 91% respectively for both 25 and 50 epochs based on 170 image datasets. Furthermore, for 88 image dataset, the results shows the model accuracy of 80% and 90% respectively for both 25 and 50 epochs. As a result, these results demonstrates the stability of the model and shows that the more images with higher resolutions are in a dataset, the higher the accuracy.

Keywords: *Artefact, Machine Learning, CT scanner, Image Processing, Datasets.*

1. Introduction

In a contemporary healthcare approach, Computed tomography (CT) images are widely used for medical diagnosis and treatment purposes [59]. However, in the past few years, the world has seen many different approaches developed with the primary aim of improving CT image quality. This development has also spiked interest in Medical Imaging System (MIS) amongst the researchers within the computer vision community [60]. However, the term “artefact “in the context of this research paper, refers to any discrepancy or anomaly that is found within the captured CT image. This paper thus focuses on the two types of artefacts namely; Ring and Metal artefact.

This research paper presents a machine learning-based approach for detecting image artefacts on CT images captured from Toshiba equipment. The final objective of this study is, therefore, to; 1) present an automated approach model for artefact detection; 2) To develop a machine learning-based model with capability to distinguish between metal and ring artefacts. To summarise, this article proposes an automated machine learning model developed on Keras for artefact detection and providing distinction between metal and ring artefact without any human interaction required.

The remainder of this paper is as follows. Section 2 provides the problem statement elaborating on the research question. Section 3 provides a discussion on the literature review on types of approaches already conducted in addressing artefact detection in medical imaging. Section 4 presents the systems modelling and development technique as well as the platform and application of machine learning techniques for data training. The results are outlined in Section 5 with accuracy testing between the trained data and tested data and the paper is concluded in Section 6.

2. Problem statement

Both medical and research institutions make use of standard-based troubleshooting procedures based on the equipment type and model. In most instances, technicians are prone to manufacturer-specific CT scanners and this results in a costly and time-consuming exercise that delays the medical attention to the patients.

It is for such reasons, that an automated artefact detection model with capabilities for artefact image detection and distinguishment model based on machine learning needs to be investigated, developed, and implemented to evaluate the feasibility and reliability of such a system in a live environment setup.

3. Literature review

In general, artefacts are caused by a range of sources and can degrade the quality of a CT image to varying degrees. However, the trend towards using machine learning is not only being driven by the need to increase diagnostic confidence but essentially by new clinical applications that create the potential for further academic and technical research.

This research paper makes mention of two types of commonly known artefacts namely ring and metal artefact. These artefacts have been investigated by a number of researchers such as Jin et al [61]. Subsequently, Dougherty et al. [9] present the medical imaging system for constructing an image in response to signals from diverse types of objects namely bodies and phantoms. Dougherty further highlights that medical imaging systems can be classified according to the radiation, and academic field of use. However, such applications are important in reducing the response time to save lives [62].

Huang et al. [63] presents a residual learning approach based on Convolution Neural Network (CNN) to reduce metal artefact in a cervical CT scans. Furthermore, Ghani et al [64] presents the data projection model utilising a self-supervised sinogram framework. In contrast, Safdari et al [65] presents a technique for a new algorithm to reduce the metal artefact challenge by deploying five key steps in the algorithm namely a) extraction of metal region; b) filtration of the extracted metallic region; c) Segmentation and accurate extraction; d) utilisation of interpolation and 3) insertion of the corrected metallic section of the image to the original image. Additionally, Kyme et al [66] also investigate the best method to estimate and correct Single-Photon Emission Computed Tomography (SPECT), Positron Emission Tomography (PET) and CT images. In this study, Kyme makes use of motion fields within the modified reconstruction framework to obtain motion-corrected images.

3.1. CT scanner basics

Figure 1 illustrates the operation of the third and fourth-generation scanners.

Figure 1. Test equipment being aligned (prepared for scanning) in the gantry aperture of a CT scanner.

Figure 1 depicts the preparatory scanning process for third and fourth-generation scanners. As indicated in Figure 1, the third-generation scanners are still in practice in most of the medical institutions of South Africa. Furthermore, the CT scanner in Figure 1 further illustrates the classification of a digital imaging system due to its use of computers to process images. This is important as a basis for radiographers and technicians to familiarise themselves with the functions and parts involved in making a CT scanner work.

4. Methodology

In the early days of image processing development, linear filters were used as the primary tools for image enhancement and restoration. However, due to the advancements in technology, other algorithms such as supervised learning multi-class classification logistic regression algorithm and linear regression algorithm are currently in use in the market. In this research study, the logistic regression algorithm is utilised.

4.1. Algorithm modelling approach

In the modelling process of the algorithm, two datasets are loaded into the model. Once this process has been completed, is important to augment the training dataset artificially by applying image augmentation to ensure stable results output. Augmentation code sneak peek is outlined below.

```
# this is the augmentation configuration we will use for training
train_datagen = ImageDataGenerator(
   rescale=1. / 255,
   shear_range=0.2,
   zoom_range=0.2,
   horizontal_flip=True)
```

Image dataset augmentation is accomplished by defining the image data generator parameters within the algorithm. The parameter settings are set as follows:

- Rescale —Each digital image is created by a pixel with a value between 0 and 255. 0 = black, 255 = white. So rescale the scales array of the original image pixel values to be between [0,1] which makes the images contribute more equally to the overall loss. Otherwise, higher pixel range image results in greater loss and a lower learning rate should be used, lower pixel range image would require a higher learning rate.
- Shear_range — The shape of the image is the transformation of the shear. It fixes one axis and stretches the image at a certain angle known as the angle of the shear.
- Zoom_range — The image is enlarged by a zoom of less than 1.0. The image is more than 1.0 zoomed out of the picture.
- Horizontal_flip —Some images are flipped horizontally at random.

Furthermore, an approach making use of CNN is applied. CNN is designed for images that contain convolution layers that compare overlapping rectangular patches of the input to small learnable weight metrics “kernels/ filters” that encode features [67].

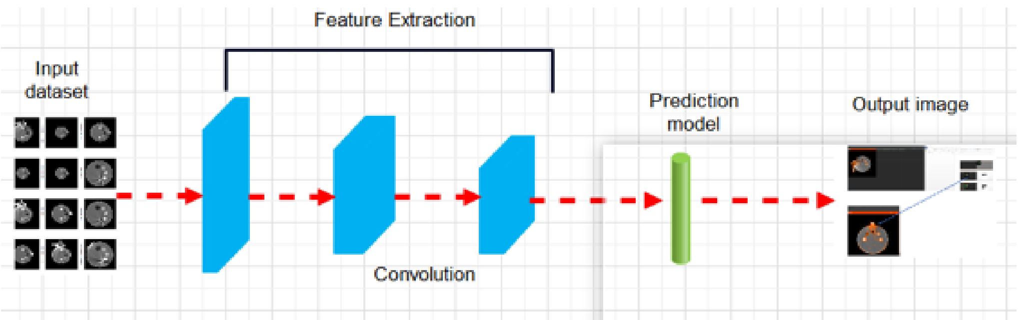

Figure 2. Convolution network layer output.

Figure 2 depicts the convolution network. The full convolution network comprises of the input dataset (metal and/or ring artefact). CNN architecture in the context of this research paper is based on layers of convolution. The convolution layers receive input and transform the input data from the image and pass it as input to the next layer. The transformation is known as the operation of convolution. However, it is critical to define the number of filters for each convolution layer. These filters detect patterns such as edges, shapes, curves, objects, textures, or even colors. The more sophisticated patterns or objects it detects are more deeply layered.

4.2. Implementation of image recognition and learning techniques for medical image systems

Machine learning algorithm was implemented using the python programming language integrated with the following machine learning and computer vision-based algorithms and libraries such as 1) Keras; 2) TensorFlow, and 3) OpenCV.

- Tensorflow^{TM} – this software is utilised as a machine learning software
- OpenCV – for image processing and detection
- Keras library – is a library interface for Tensorflow^{TM} and is utilised as a supporting library for machine vision

These algorithms utilises a CUDA-based Graphical Processing Unit (GPU) that allows for parallel computing power provided by the GPU. The system implementation algorithm relied on the following system parts:

- AMD Ryzen 5 1600 3.4 GHz six-core processor
- NVIDIA GeForce GTX 1660 Ti 1.86GHz, 6 GB GPU
- 16GB DDR4 RAM

The model framework describes the research project and how the data is collected. The data is collected by scanning image quality test equipment known as a phantom with Toshiba Medical Systems CT scanners. Upon noting the type of artefact, a folder is created and images are multiplied to reach 85 image samples, then copied into the folder per artefact type i.e. (metal artefact and ring artefact). In this research paper, the researchers took 85 image samples per investigated artefact.

The system is trained and tested against a set of reconstructed image datasets. The system is trained on both 25 and 50-epoch tests using machine learning techniques. Upon the completion of the iteration, the system or model is tested and evaluated against the unknown data. The system model is evaluated on the unknown data and this data is then used to determine the artefact type.

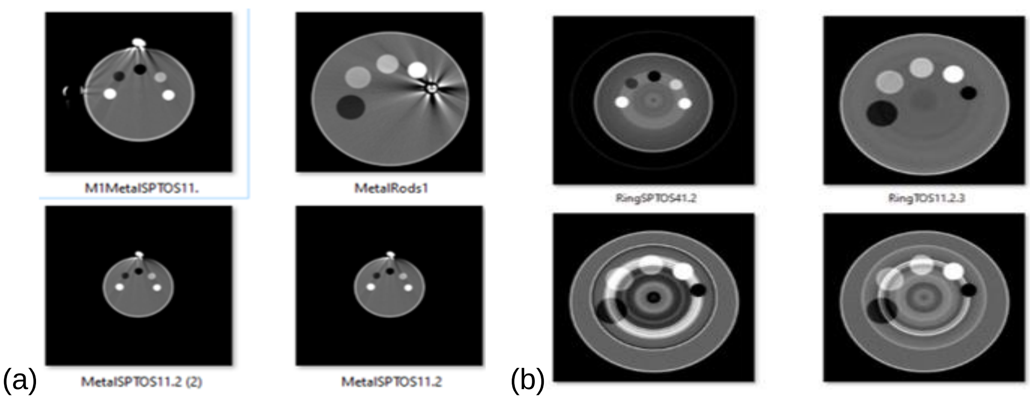

Figure 3. (a) Metal artefact images 512x512 pixels; (b) Ring artefact images at 512x512 pixels.

In the collect and prepare data phase, the two images as outlined in Figures 3 (a) and (b) are copied into a single folder to create an image dataset. This image dataset comprises of raw data in which no filtering has been applied apart from enhancing the image brightness.

The enhancement is done to allow for machine vision application for artefact detection without any system optimisation.

The training of the model is created to allow the model to learn by identifying the different features within an image and to automatically detect the artefacts. Figures 4 (a) and (b) presents the feature detection model for both metal and ring artefact.

(a) 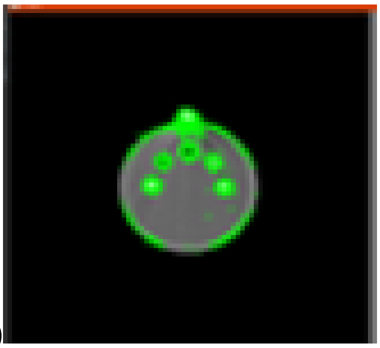 (b) 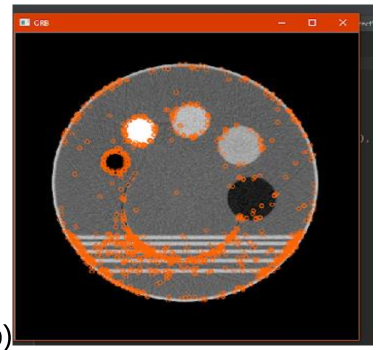

Figure 4. (a) Metal artefact detection; (b) Ring artefact detection.

Figures 4 (a) and (b) depicts the metal and ring artefact detection in a model based on a feature detection algorithm. Furthermore, ring artefact is seen by circles that formulate a smile-like face. Upon applying feature detection on the dataset for image detection purposes, convolution is then applied to both image datasets as indicated in Figure 5.

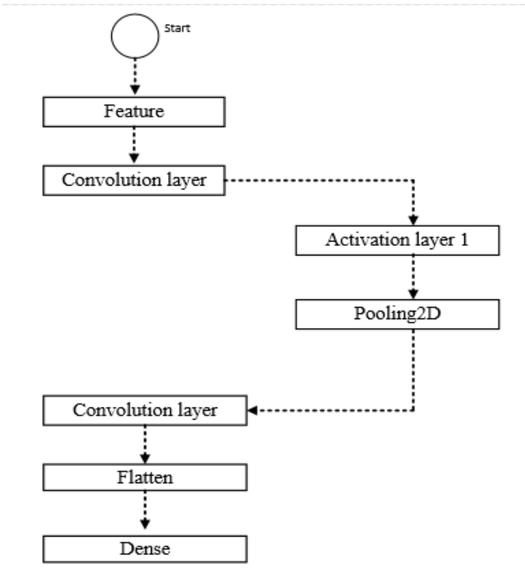

Figure 5. Model flow diagram.

Figure 5 depicts the model flow diagram. The features are applied to the model in the convolution layer. Upon the successful application of features, the process is highlighted at the activation layer and Pooling2D. Additionally, the features are also applied in the convolution layer, and the layer is placed at the flattening and dense mode and as a result, the modelling is achievable.

5. Results

Artefacts can seriously degrade the quality of CT images and in some instances to the point of making diagnostics unusable. However, to optimize image quality, it is necessary to understand why artefacts occur and how they can be prevented or suppressed. Hence the use of machine learning-based applications is necessary for such applications.

However, the general approach in artefact evaluation makes use of analytic clinical data (patient scan). This approach is recommended to try to reproduce the artefact using a test phantom or just air in the scan field. However, this approach has let the conduction of this research paper that aimed at developing an automated model that will be used to identify and detect different artefacts without any human intervention.

Table 1 presents the results of the paper based on the number of images within the dataset and also the epoch number.

Table 1. Model accuracy results based on 25 epochs for 170 and 88 image datasets.

Model accuracy results	Model loss graph	Results at 25 epoch
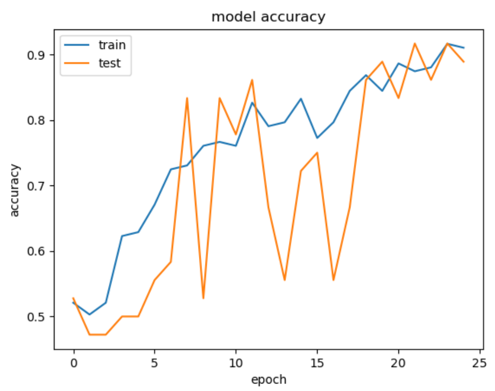		Trained Model 89% accuracy 21% Loss Testing model on test data 87% accuracy 49% loss
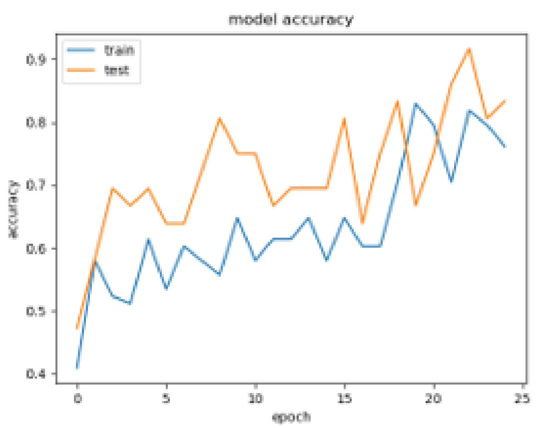	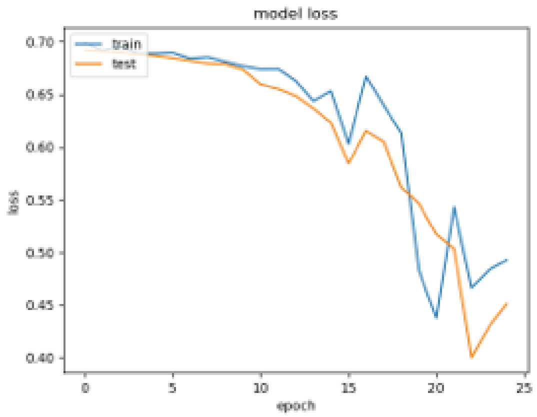	Trained Model 75% accuracy 47% Loss Testing model on test data 80% accuracy 45% loss

Table 1 depicts model accuracy results for 25 epoch tests based on 170 and 88 image datasets. The results demonstrate that for a 25 epoch with 170 image dataset, the trained model the accuracy is 89% with 21% loss experienced. The testing model output results shows that the accuracy test is 87% with 49% loss. Furthermore, for 88 image dataset, the results demonstrates that the trained model accuracy is 75% with 47% loss, while the test model demonstrates 80% accuracy with 45% loss. Table 1 does demonstrate the stability of the proposed model for higher image datasets.

Table 2. Model accuracy results based on 50 epoch for 170 and 88 image datasets.

Model accuracy results	Model loss graph	Results at 50 epoch
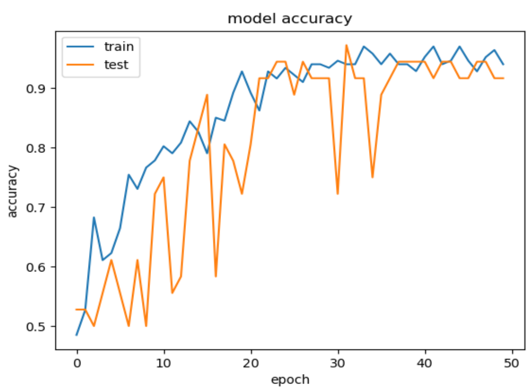	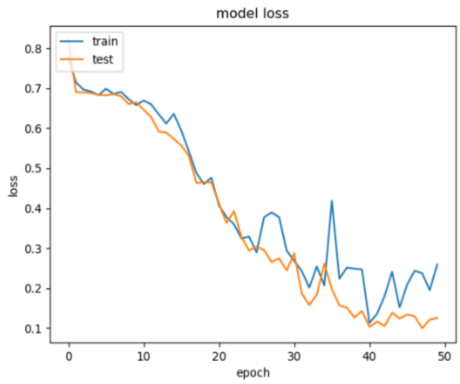	Trained model 94% accuracy 21% Loss Testing model on test data 91% accuracy 15% loss
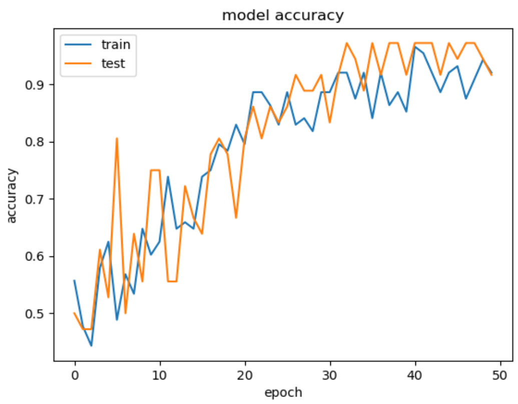	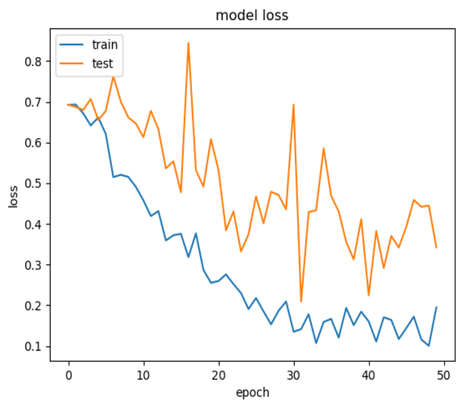	Trained Model 91% accuracy 21% Loss Testing model on test data 90% accuracy 31% loss

Table 3 depicts model accuracy results for 50 epoch test based on 170 and 88 image datasets. The results demonstrates that for a 50 epoch with 170 image dataset, the trained model the accuracy is 94% with 21% loss experienced. The testing model output results shows that the accuracy test is 91% with 15% loss. Furthermore, for 88 image dataset, the results demonstrates that the trained model accuracy is 91% with 21% loss, while the test model demonstrates 90% accuracy with 31% loss. Table 2 does demonstrate the stability of the proposed model for 88 image datasets with higher epoch tests.

6. Conclusion

The main goal of this research paper was to develop an automated machine learning-based model with the capabilities for artefact detection by comparing data from the trained model against the actual data from the testing model. This model was developed by capturing a total of 170 images comprising of 85 ring artefact and 85 metal artefact datasets. These image datasets were captured from Toshiba CT scanner and then a folder was created where the images were stored to create datasets. The machine learning model was then developed in python with each image having 512x512 pixels.

This research result has thus concluded that the model is efficient with an accuracy of 87% and 91% respectively for both 25 and 50 epochs based on 170 image datasets. Furthermore, for 88 image dataset, the results show the model accuracy of 80% and 90% respectively for both 25 and 50 epochs. Thes results demonstrate the stability of the model and also indicate that the more images with higher resolutions are in a dataset, the higher the accuracy.

6. References

[1] L. Yu, Z. Zhang, X. Li, H. Ren, W. Zhao and L. Xing, "Metal Artefact Reduction in 2D CT images with Self-supervised Cross-Domain Learning," p. 1, 28 September 2021.

[2] J. B. Benganga and B. Kotze, "Image Learning and Correction as a Means of Evaluating and Fault Finding Computer Scanner Image Artefact," vol. 19, no. 3, p. 2813, July 2022.

[3] K. Jin, T. McCann, E. Froustey and M. Unser, "Deep convolution neural network for inverse problems in imaging," *IEEE Transactions on image processing,* vol. 26, no. 9, pp. 4509-4522, 2017.

[4] G. Dougherty, "Digital Image Processing for Medical Applications," 2007, pp. 1-459.

[5] T. Kukuni, B. Kotze, W. Hurst and L. Lenkoe, "Augmented Reality In Smart Manufacturing: A user Experience Evaluation," *Webology,* vol. 19, no. 3, pp. 2405-2406, 2022.

[6] X. Huang, J. Wang, F. Tang, T. Zhong and Y. Zhang, "Metal artefact reduction on cervical ct images by deep residual learning," *biomedical engineering ,* vol. 17, no. 1, p. 175, 2018.

[7] M. Ghani, W. Karl, "Fast accurate ct metal artefact reduction using data domain deep learning," *IEEE Transactions on Computational Imaging,* 2019.

[8] M. Safdari, A. Karimiam, M. Yazdchi, "Metal artefact reduction in CT images of head by image processing techniques," in *International Conference on Physics Science and Technology*, 2011.

[9] A. Kyme, R. Fulton, "Motion estimation and correction in SPECT, PET and CT," *Physics in Medicine and Biology,* p. 1, 2021.

[10] P. Cheng, E. Montagnon, R. Yamashita, I. Pan, A. Chenevert, F. Romero, G. Chartrand, S. Kadoury and A. Tang, "Deep Learning: An Update for Radiologists," *Informatics,* vol. 41, no. 5, pp. 1430-1431, 2021

Authors

Joe-Herve Bonkondo Benganga

Joe-Herve Bonkondo Benganga holds a B-Tech: Engineering: Electrical and an N.Dip: Computer Systems Engineering from the Central University of Technology, Free State. Joe-Herve further possesses Medical Equipment Certificates in Anaesthetic Machine from Spacelabs Healthcare, CT scanner from Canon Medical Systems, and Ulrich Injector Pump CT Motion from Ulrich Medical. He is currently studying towards a Master`s degree of Engineering in Electrical Engineering at the Central University of Technology, Free State.

Joe-Herve Bonkondo Benganga is a technical representative in Tecmed Africa, specialising in technical services for CT, MRI scanners and contrast injectors.

Benganga`s skills professionally and academically are in electronics, medical equipment, design and modelling, C#, C, and MySQL databases. Benganga has an interest in the development of medical systems and evaluation applications such machine learning and AI being implemented in medicine specifically in radiology. He is a follower of Aunt Minnie radiology journals and webinars.

Dr Ben Kotze

Ben Kotze holds a master's and Doctoral degrees in Electrical Engineering.

He is professionally registered with the Engineering Council of South Africa (ECSA) and several associations of which the oldest South African Institute of Electrical Engineers (SAIEE est. 1904) where he is a fellow.

With seven years of industry experience and over thirty years of tertiary education experience in Electrical Engineering of which he lectured more than 23 subjects. He is still actively involved with industry and Work Integrated Learning (WIL).

He is currently researching vision, several different AGVs, renewable energy systems, simulation and control, augmented reality systems, IoT security, smart farming, and prediction methods. Several undergraduate students, masters, and doctoral passed by his mentorship. He attended several international and national conferences in engineering and education and has published in accredited journals on these topics. He is currently the assistant dean of teaching and learning in the Faculty of Engineering, Built Environment, and Information Technology at the Central University of Technology, Free State. Also actively involved in the Centre for Sustainable Smart Cities.

Dr Tshepo Kukuni

Tshepo Godfrey Kukuni holds master's and Doctoral degrees in Electrical Engineering, and he has worked both in industry and tertiary education. He is currently employed as an Open Innovation Specialist and his also a Director at Rea Thusa Consulting Engineers (PTY) LTD. Dr Kukuni has published papers in different journals both nationally and internationally. Dr Kukuni is also currently working on research on Network Intrusion Detection applications, Augmented Reality Applications, Free-Piston Engines, Image Processing, Computer vision, Design and modelling, and Machine Vision. Dr Kukuni is also a registered member of the South African Association of PhDs (SAAPhDs) and his also on the Advisory Committee on Innovation at the Institute for the Study of Legislature in South Africa (ISLSA).

Annexure D: Code algorithm

Code algorithm was used on both datasets in the form of trained datasets and test dataset. The datasets are called from the directory to the Tensorflow^{TM} where the code is simulated using machine learning.

```
img_width,img_height=224,224

train_data_dir='Dataset/train'
validation_data_dir='Dataset/test'

nb_train_samples=170
nb_validation_samples=38

epochs=50
batch_size=64
# this is the augmentation configuration we will use for training
train_datagen = ImageDataGenerator(
    rescale=1. / 255,
    width_shift_range=0.1,
    height_shift_range=0.1,
    shear_range=0.2,
    zoom_range=0.2,
    horizontal_flip=True,
    vertical_flip=True)


test_datagen = ImageDataGenerator(rescale=1. / 255)

train_generator = train_datagen.flow_from_directory(
    train_data_dir,
    target_size=(img_width, img_height),
    color_mode='grayscale',
    batch_size=batch_size,
    class_mode="categorical")

validation_generator = test_datagen.flow_from_directory(
    validation_data_dir,
    target_size=(img_width, img_height),
    color_mode='grayscale',
    batch_size=batch_size,
    class_mode="categorical")


input_shape=(img_width,img_height)
model=Sequential()
model.add(Conv2D(64,(3,3),input_shape=(img_width,img_height,1)))
model.add(Activation('relu'))
model.add(MaxPooling2D(pool_size=(2, 2)))

model.add(Conv2D(64,(3,3),input_shape=(img_width,img_height,1)))
model.add(Activation('relu'))
model.add(MaxPooling2D(pool_size=(2, 2)))

model.add(Conv2D(128,(3,3),input_shape=(img_width,img_height,1)))
model.add(Activation('relu'))
```

```
model.add(MaxPooling2D(pool_size=(2, 2)))

model.add(Conv2D(254,(3,3),input_shape=(img_width,img_height,1)))
model.add(Activation('relu'))
model.add(MaxPooling2D(pool_size=(2, 2)))

model.add(Conv2D(512,(3,3),input_shape=(img_width,img_height,1)))
model.add(Activation('relu'))
model.add(MaxPooling2D(pool_size=(2, 2)))



model.add(Flatten())
model.add(Dense(1024))
model.add(Activation('relu'))
model.add(Dense(64))
model.add(Activation('relu'))
model.add(Dense(10))
model.add(Activation('softmax'))

print("Modeling Summary")
print(model.summary())
from keras.optimizers import Adam
opt=Adam(lr=0.001)

model.compile(loss='categorical_crossentropy',
            optimizer=opt,
            metrics=['accuracy'])
```

Annexure E: Toshiba/Canon causes of, and solutions for metal and ring artefacts.

Artefact Type	Causes	Solutions
Soft Ring 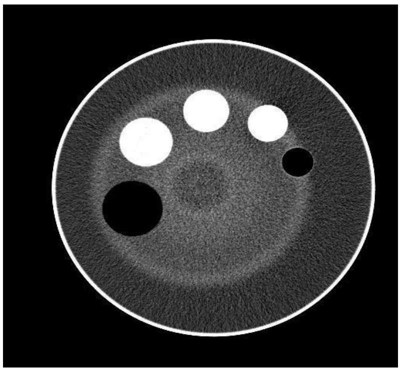	• Medical contrast on mylar • Medical contrast on detector panel • Hardened clothing in the scan field • Loose power supply connections • Morning mis-calibration • Faulty power supply • Faulty reference detector	• Cleaning and reseating detector power boards and connections • Calibrations • Replace power supply. • Adjust detector power supplies. • Replace reference detector.
Hard Ring 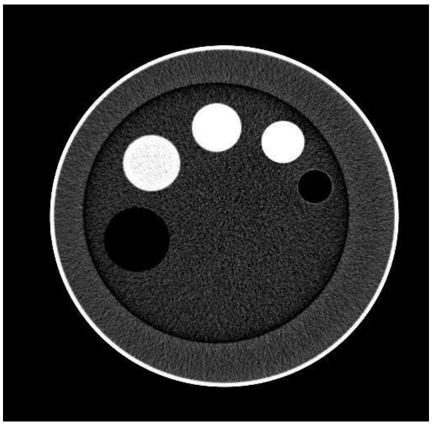	• Faulty power supply • Faulty detector control board • Faulty detector	• Replacement of detector power board • Replace detector control board. • Replace detector power supplies. • Replace entire detector.

Multiple Rings 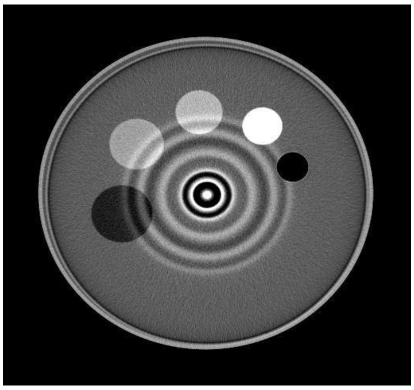	• Faulty power supply • Faulty detector control board • Loose detector connections • Loose gantry • Reconstructio n fault	• Replace detector control board. • Replace detector power supplies. • Replace entire detector.
Metal Artefact 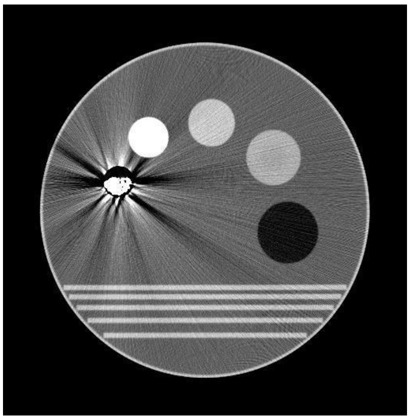	• Incorrect patient positioning • Incorrect scanning protocol selection • Metal objects on patient • Mis-calibration	• Repositioning of patient • Tilting of the gantry • Remove metals. • Reconstruct scan (The issue is applications related. The use of incorrect scan and reconstructio n settings yields image artefacts.)
Beam hardening and scatter	• Metal objects in the scan field	• Clean detector and mylar ring • Scan on

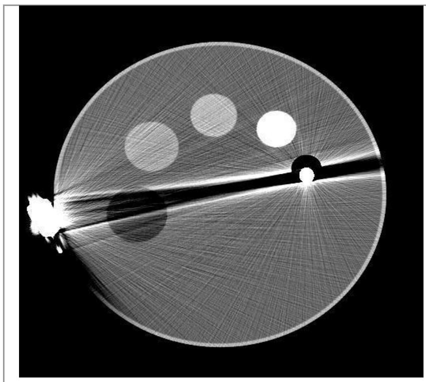	• Mis-calibration • Metal objects on patient • Reconstructio n error • Software faults • Medical contrast on mylar or detector panel • Faulty power supply • Incorrect protocol selection	higher kV • Scan on two different energies • Replace detector boards. • Replace entire detector. • Software reinstallation

Annexure F: Code transfer learning code

CNN Code

```
import os
from tensorflow import keras
from tensorflow.keras.layers import Dense,  Input, InputLayer, Flatten,GlobalAveragePooling2D
from tensorflow.keras.models import Sequential, Model
from keras.preprocessing.image import ImageDataGenerator
from keras.models import Sequential ,load_model
from keras.layers import Conv2D, MaxPooling2D
from keras.layers import Activation, Dropout, Flatten, Dense
from keras.utils import  normalize,to_categorical


from keras import models
from keras import layers
from keras.preprocessing import image
from keras.utils.vis_utils import plot_model
import matplotlib.pyplot as plt
import numpy as np
from keras import backend as K
from keras.applications.inception_v3 import InceptionV3
from tensorflow.keras.optimizers import Adam
from pathlib import Path


train_data_dir='Dataset/train'
test_data_dir='Dataset/test'

#data agumanetatiom
train_datagen=ImageDataGenerator(rescale=1./255,
                                 rotation_range=40,
                                 width_shift_range=0.2,
                                 height_shift_range=0.2,
                                 shear_range=0.2,
                                 zoom_range=0.2,
                                 horizontal_flip=True,
                                 vertical_flip=True)
#test data has no agumentation
test_datagen=ImageDataGenerator(rescale=1./255)

train_generator=train_datagen.flow_from_directory(train_data_dir,
                                                  batch_size=32,
                                                  class_mode='categorical',
                                                  target_size=(150,150))
test_generator=test_datagen.flow_from_directory(test_data_dir,
                                                  batch_size=32,
                                                  class_mode='categorical',
                                                  target_size=(150,150))

pre_trained_model=InceptionV3(input_shape=(150,150,3),include_top=False,weights='imagenet')

for layer in pre_trained_model.layers:
    layer.trainable=False

pre_trained_model.summary()
#adding the last layer to the pre-trained model
x=layers.Flatten()(pre_trained_model.output)
```

```
x=layers.Dense(50,activation='relu')(x)
x=layers.Dense(20,activation='relu')(x)
x=layers.Dense(2,activation='softmax')(x)

model=Model(pre_trained_model.input,x)

print(model.summary())
#hyperparameters
model.compile(optimizer=Adam(lr=0.0001),loss='categorical_crossentropy',metrics=['acc'])

history=model.fit_generator(train_generator,
                            validation_data=test_generator,
                            steps_per_epoch=4,
                            epochs=40)
model.save_weights('iception_transfer.h5')
model.save('JHB_iception_tranfer_model.h5')

plt.plot(history.history['acc'])
plt.plot(history.history['val_acc'])
plt.title('model accuracy Inceptionv3')
plt.ylabel('accuracy')
plt.xlabel('epoch')
plt.legend(['train', 'test'], loc='upper left')
plt.show()

plt.plot(history.history['loss'])
plt.plot(history.history['val_loss'])
plt.title('model loss Iceptionv3')
plt.ylabel('loss')
plt.xlabel('epoch')
plt.legend(['train', 'test'], loc='upper left')
plt.show()
```

Resnet50

```
import os
from tensorflow import keras
from tensorflow.keras.layers import Dense,  Input, InputLayer, Flatten,GlobalAveragePooling2D
from tensorflow.keras.models import Sequential, Model
from keras.preprocessing.image import ImageDataGenerator
from keras.models import Sequential ,load_model
from keras.layers import Conv2D, MaxPooling2D
from keras.layers import Activation, Dropout, Flatten, Dense
from keras.utils import  normalize,to_categorical


from keras import models
from keras import layers
from keras.preprocessing import image
from keras.utils.vis_utils import plot_model
import matplotlib.pyplot as plt
import numpy as np
from keras import backend as K
from keras.applications.resnet50 import ResNet50
from tensorflow.keras.optimizers import Adam
from pathlib import Path

train_data_dir='Dataset/train'
```

```
test_data_dir='Dataset/test'

#data agumanetatiom
train_datagen=ImageDataGenerator(rescale=1./255.,
                                 width_shift_range=0.2,
                                 height_shift_range=0.2,
                                 shear_range=0.2,
                                 zoom_range=0.2,
                                 horizontal_flip=True,
                                 vertical_flip=True)
#test data has no agumentation
test_datagen=ImageDataGenerator(rescale=1./255.)

train_generator=train_datagen.flow_from_directory(train_data_dir,
                                                  batch_size=32,
                                                  class_mode='categorical',
                                                  target_size=(224,224))
test_generator=test_datagen.flow_from_directory(test_data_dir,
                                                  batch_size=32,
                                                  class_mode='categorical',
                                                  target_size=(224,224))

pre_trained_model=ResNet50(include_top=False,input_shape=(224,224,3),weights='imagenet')

for layer in pre_trained_model.layers:
    layer.trainable=False

pre_trained_model.summary()

model=models.Sequential()
model.add(pre_trained_model)
model.add(layers.Flatten())
model.add(layers.Dense(50,activation='relu'))
model.add(layers.Dense(20,activation='relu'))
model.add(layers.Dense(10,activation='softmax'))

print(model.summary())

model.compile(optimizer=keras.optimizers.Adam(lr=0.0001),loss='categorical_crossentropy',metrics=[
'acc'])

history=model.fit_generator(train_generator,validation_data=test_generator,
                            steps_per_epoch=6,
                            epochs=25)

model.save_weights('resnet50_transfer.h5')
model.save('JHB_resnet50_transfer_model')

plt.plot(history.history['acc'])
plt.plot(history.history['val_acc'])
plt.title('model accuracy Resnet50')
plt.ylabel('accuracy')
plt.xlabel('epoch')
plt.legend(['train', 'test'], loc='upper left')
plt.show()

plt.plot(history.history['loss'])
plt.plot(history.history['val_loss'])
plt.title('model loss ResNet50')
plt.ylabel('loss')
```

```
plt.xlabel('epoch')
plt.legend(['train', 'test'], loc='upper left')
plt.show()
```

VGG16 code

```
from tensorflow import keras
from tensorflow.keras.layers import Dense,  Input, InputLayer, Flatten
from tensorflow.keras.models import Sequential, Model
from keras.preprocessing.image import ImageDataGenerator
from keras.models import Sequential ,load_model
from keras.layers import Conv2D, MaxPooling2D
from keras.layers import Activation, Dropout, Flatten, Dense
from keras.utils import  normalize,to_categorical


from keras import models
from keras import layers
from keras.preprocessing import image
from keras.utils.vis_utils import plot_model
import matplotlib.pyplot as plt
import numpy as np
from keras import backend as K

img_width,img_height=224,224

train_data_dir='Dataset/train'
test_dir='Dataset/test'

nb_train_samples=170
nb_validation_samples=38

from keras.applications import VGG16
vgg16_base=VGG16(weights='imagenet',include_top=False,input_shape=(224,224,3))
vgg16_base.trainable=False




epochs=25
batch_size=32

#Data argumentation
train_datagen = ImageDataGenerator(
    rescale=1. / 255,
    width_shift_range=0.1,
    height_shift_range=0.1,
    shear_range=0.2,
    zoom_range=0.2,
    horizontal_flip=True,
```

```
    vertical_flip=True)


test_datagen = ImageDataGenerator(rescale=1. / 255)

train_generator = train_datagen.flow_from_directory(
    train_data_dir,
    target_size=(img_width, img_height),
    batch_size=batch_size,
    class_mode="categorical")

validation_generator = test_datagen.flow_from_directory(
    test_dir,
    target_size=(img_width, img_height),
    batch_size=batch_size,
    class_mode="categorical")

vgg16_base.summary()
model=models.Sequential()
model.add(vgg16_base)
model.add(layers.Flatten())
model.add(layers.Dense(50,activation='relu'))
model.add(layers.Dense(20,activation='relu'))
model.add(layers.Dense(10,activation='softmax'))

print(model.summary())
from keras.optimizers import Adam
opt=Adam(lr=0.001)

model.compile(loss='categorical_crossentropy',
              optimizer=opt,
              metrics=['accuracy'])

print("Fit model on training data")
history=model.fit_generator(
    train_generator,
    steps_per_epoch=6,
    epochs=epochs,
    validation_data=validation_generator)

model.save_weights('first_transfer.h5')
model.save('JHB_tranfer_model.h5')


plt.plot(history.history['accuracy'])
plt.plot(history.history['val_accuracy'])
plt.title('model accuracy VGG16')
plt.ylabel('accuracy')
plt.xlabel('epoch')
plt.legend(['train', 'test'], loc='upper left')
plt.show()
```

```
plt.plot(history.history['loss'])
plt.plot(history.history['val_loss'])
plt.title('model loss VGG16')
plt.ylabel('loss')
plt.xlabel('epoch')
plt.legend(['train', 'test'], loc='upper left')
plt.show()
```

Central University of Technology, Free State

Annexure G: Algorithm 2D CNN

```
Input: input_shape=(img_width,img_height)
Model Conv2D:
            Sequential()
(Conv2D(32,(3,3),input_shape=(img_width,img_height,1)))
(Activation('relu'))(MaxPooling2D(pool_size=(2, 2)))

(Conv2D(32,(3,3),input_shape=(img_width,img_height,1)))
(Activation('relu'))
(MaxPooling2D(pool_size=(2, 2)))

(Conv2D(32,(3,3),input_shape=(img_width,img_height,1)))
(Activation('relu'))
(MaxPooling2D(pool_size=(2, 2)))

(Conv2D(64,(3,3),input_shape=(img_width,img_height,1)))
(Activation('relu'))
(MaxPooling2D(pool_size=(2, 2)))

(Conv2D(64,(3,3),input_shape=(img_width,img_height,1)))
(Activation('relu'))
(MaxPooling2D(pool_size=(2, 2)))

Model Flatten: (Flatten())
Model Dense (32)
(Dense(32))
Model (Relu)
(Activation('relu'))

Model(Dropout)
(Dropout(0.5))
Model(Dense)
(Dense(2))
Model(Softmax)
(Activation('softmax'))
```

Annexure H: Code setup

```
mg_path='Dataset/metal_artifact/MetalSPTOS50mA11.jpg'

img=image.load_img(img_path,color_mode='grayscale',target_size=(img_width,img_height))
img_array=image.img_to_array(img)
img_batch=np.expand_dims(img_array)

predicting_class=model.predict_classes(img_batch)

if predicting_class==[0]:
    predicting='Ring_artifact'
else:
   predicting='Metal_artifact'

print(predicting)

img = cv2.imread('Dataset/metal_artifact/MetalSPTOS50mA11.jpg')
gray_img = cv2.cvtColor(img, cv2.COLOR_BGR2GRAY)

orb = cv2.ORB_create(nfeatures=2000)
kp, des = orb.detectAndCompute(gray_img, None)

kp_img = cv2.drawKeypoints(img, kp, None, color=(0, 255 ,255), flags=0)

cv2.imshow('Crey',gray_img)
cv2.imshow('ORB', kp_img)
cv2.waitKey()
```

Annexure I: Data Augmentation

```
train_datagen = ImageDataGenerator(
    rescale=1. / 255,
    shear_range=0.2,
    zoom_range=0.2,
    horizontal_flip=True)

test_datagen = ImageDataGenerator(rescale=1. / 255)

train_generator = train_datagen.flow_from_directory(
    train_data_dir,
    target_size=(img_width, img_height),
    subset='training',
    batch_size=batch_size,
    class_mode="categorical")

validation_generator = test_datagen.flow_from_directory(
    validation_data_dir,
    target_size=(img_width, img_height),
    subset='validation',
    batch_size=batch_size,
    class_mode="categorical")
```

Central University of Technology, Free State

Annexure J: Output prediction code

```
img_path='Dataset/metal_artifact/MetalSPTOS50mA11.jpg'

img=image.load_img(img_path,color_mode='grayscale',target_size=(img_width,img_height))
img_array=image.img_to_array(img)
img_batch=np.expand_dims(img_array)

predicting_class=model.predict_classes(img_batch)

if predicting_class==[0]:
    predicting='Ring_artifact'
else:
   predicting='Metal_artifact'

print(predicting)
```